In situ Fabricated Polymer-Metal Nanocomposite Thin Films: 'Dip Catalysts' and SERS Substrates

A Thesis Submitted for the Degree of
DOCTOR OF PHILOSOPHY

by

Ellendula Hariprasad

School of Chemistry
University of Hyderabad
Hyderabad 500 046
INDIA

October 2013

Dedicated To

Amma (Guna Prabha), Nanna (Ramulu)

CONTENTS

DECLARATION

I hereby declare that the matter embodied in this thesis is the result of investigations carried out by me in the School of Chemistry, University of Hyderabad, Hyderabad under the supervision of Prof. T. P. Radhakrishnan.

In keeping with the general practice of reporting scientific observations, due acknowledgements have been made wherever the work described is based on the findings of other investigators.

Ellendula Hariprasad

CERTIFICATE

This is to certify that the work described in this thesis entitled "***In situ* Fabricated Polymer-Metal Nanocomposite Thin Films: 'Dip Catalysts' and SERS Substrates**" has been carried out by Ellendula Hariprasad, under my supervision and the same has not been submitted elsewhere for any degree.

Prof. T. P. Radhakrishnan
(Thesis Supervisor)

DEAN
School of Chemistry
University of Hyderabad
Hyderabad 500 046

ACKNOWLEDGEMENTS

I take this opportunity to express my profound respect and deep sense of heartfelt gratitude to Prof. T. P. Radhakrishnan, my research supervisor and well wisher, for his constant guidance, encouragement, care and for the freedom he gave me in carrying out my research. His innovative thoughts, commitment to the work with a great sense of discipline and patience are highly admirable and motivating which I always have aspired to imbibe. My association with him is a memorable one.

I would like to thank present and former Deans and faculty members of the School of Chemistry for their support and help on various occasions. My sincere thanks to all the teachers for their excellent teaching during my masters course. From their inspired and dedicated teaching, I have benefited much in my career. My special thanks to Prof. M. Durgaprasad and Prof. G. R. Desiraju for the excellent teaching and inspiration they gave in my M.Sc days. I thank Prof. D. Basavaiah, Prof. S. Mahapatra, Prof. T. Jana, Prof. Lalitha Guruprasad and Prof. A. K. Sahoo Prof. P. K. Panda for care and concern. I thank all the faculty members for their cooperation whenever required.

I would also like to thank Prof. D. Narayana Rao (physics), Prof. Rajaram (physics), Prof. M. Laxman (ANGRAU) Dr. B. Sridhar (IICT), Dr. B. L. V. Prasad (NCL, Pune), and Prof. Chandrabhas Narayana (contacted for SERS) for their support and help in my doctoral research.

I thank all non-teaching staff, School of Chemistry for their cooperation. I would like to express my sincere gratitude to Dr. Raghavaiah (XRD), Mr. Venkata Ramana (GC-MS), Mr. Durgaprasad Muvva (TEM, CFN), Mr Laksmi narayana (FESEM, School of Physics), Mr. Pavan (SEM, CIL), Mr. Kumar (PXRD), Mrs. Deepti (Raman, School of Physics), Ms. Suneetha (AFM, School of Physics), Ms. Fatima (IR), Ms. Sandya (Profilometer), Mr. Bhaskar Rao (LC-MS), Mr. Venkatesh (FESEM, ARCI) for their assistance in various instruments is greatly appreciated.

I thank UGC-CAS and CSIR for providing the fellowship. I also thank DST for funding and supporting the visit to University of Bari to attend the international symposium on Polymer/Metal nanocomposites.

I am deeply indebted to all my teachers right from my school to the university, for the excellent training I received throughout my academics. My special thanks to my teachers Raju, Zakir during my school days, Jaiguru, Syam sundar reddy, Purna chandar rao during my intermediate Dr. Narsimha reddy, Dr. Pulla reddy, Dr. Bhavani, Dr. Swathi, during my B. Sc and Dr. Dharma teja, Dr. Madhumathi and Dr. Mrunalini during B. Ed.

It is a great pleasure to thank my seniors Dr. Shatabdi porel and Dr. Jaya Prakash, Dr. Abhijit Patra, Dr. Rajesh and Dr. Ramesh for their help and cooperation. I am extremely thankful to Gupta for his help, support and encouragement during my M. Sc and Ph. D. I am also thankful to Raja (Durgaprasad), Balaswamy for their support. My special thanks to Kesav, Lasya, and srujana for their affection and support during the last few years and maintaining a lively environment in the lab. I also acknowledge project students worked with me; Dama, Navya, Armita, Sagitha and chaitanya. I also acknowledge the project students worked in lab; Rajendra, Arun, Aleem, Durgadas, Dijo, Amar, Shaik, Pravisha, Anuradha, Srinivas, Radhakrishna, Tejaswi, Mubarak, balu, Raju Francisco, and Pragnesh.

It is happy to me to remember all my childhood friends, Amruth, ganganna, Maha Raju, Praveen, Govi, Swamy goud, Rajesh, Sankeerth, Inter friends; Visu, Kodi (padala santhu), Yella reddy, Shiva Srinu, Gundu (nagraj), Srinu (chityala), Shilpa, Shirisha, Degree friends; Shiva ram reddy, Kishore, Anjanna, kadari, shravan, shiva, shekar reddy, Ravi, satyajit, chaitanya, santosh (army), Madhu sudhan, Anil, Hari, Ramesh, kamal B. Ed friends; Swapna, Swaroopa, Sridevi, Sushma, Tejendra Prasad, Madhu, Venkatesam, Aparanjini, Jalaja, Master minds friends; Upendar, Ramesh, Veeranna, Annapurna, Sharada, Aruna, Naseem M.Sc friends; Rajesh, Gopi, Bizzy, Guppi, Dandu, Katta, Murthy, Reddy sab, venu, Guruji, Manoj, Tirunagari, raju chowhan, dargaiah, Manoranjini, Rosmin, Durga rao (Telugu), Shankar (ls), bhattu, thodeti, Ifrahim, venky, venky, immi, srinu, Praveen, koona, venu (anthro), rajendra, Ph. D friends; Soumya, Tridib, Dinesh, Santhosh,

Chandu, Ashok, Surya, Bhanu, Malli, Bharath, Kishore, Vanaja, Vikranth, Srinivas (ls), Chakri (ls), Geetha (ls), Aswani (ls), Kumari (ls), Niveditha, Denise erb, who are a great support to me all through the life. It's my pleasure to acknowledge my lovable roommates; karunakar, DP, satti pandu, guruji, Srinu, Yasin for their support and love during the Ph. D.

I thank all research scholars of School of chemistry and friends for the cheerful and enlivening atmosphere they maintained and for making my stay in the campus unforgettable. Anji, Siva, Jagadish, Ramesh Reddy, Sekhar Reddy, Phani, Venu, Ram Suresh, D.K., Viji, Ramu, Chaitanya, Rambabu, GDP, Srinivas, Arun Babu, Sandip, Tanmoy, Ravi, Rajeswar, Satpal, Ranjith, Sanjiv, Naren, gnanavel, Nandu, Brahmam, Ramesh, Nagarjuna reddy, Srinu, Sashi, Babu, Pavan, Tirupati, Sudheer, Kishore, Shiva, Ramu, Sheshu, Chandu, Monima, Sridevi, Poulomi, Ramesh, Potti bava, Pilli, Shekar, Haneesh, Ganesh, Vignesh, Naidu, Praveen, Dharavath, Balu, swamy, Krishna chary, Bhargavi, Rajendra, Gopi, Rafia, Shuvra, Malkappa, Sudhanshu, Raju, Obayya, Ritwik, Brijesh, Koppolu, Ganesh, Naveen, Venky, Madhava chary, Shakti devi, Murali, Shiva, Bharani, from life science; rajsheel, kishore nalam, kishore, rama krishna, venky, syppy, from physics; suresh, Ravi, Yasasvini, Abhilash, Ali, Shekar, Balu, Sriramulu, Sriram, and kuldeep, Naresh (sest) require a special mention.

Above all it is the endless sacrifice, support and motivation from my Father (Ramulu) and Mother (Guna prabha) which has brought me to the position where I am. I am at a loss of words to express gratitude to them. I am grateful to my family members Geetha, Hari bava, Spandana, Saikrishna (late), Bharath, Dileep, Saijyothi, Saiteja, Sarithakka, Ramesh bava for their love, care and moral support.

E. Hariprasad

COMMON ABBREVIATIONS

AFM	atomic force microscope
EF	enhancement factor
EDXS	energy dispersive X-ray spectroscopy
FESEM	field emission scanning electron microscope
FOM	figure-of-merit
ICP-OES	inductively coupled plasma - optical emission spectroscopy
kDa	kilo dalton
kW	kilo watt
LOD	limit of detection
mL	milliliter
µL	microliter
µm	micrometer
nm	nanometer
M_w	weight average molecular weight
ppb	parts-per-billion
pmol	picomol
PVA	poly(vinyl alcohol)
PVVV	poly(vinyl butyral-*co*-vinyl alcohol-*co*-vinyl acetate)
PS	polystyrene
PSAA	poly(styrene-*co*-allyl alcohol)
RPM	revolutions per minute
SEM	scanning electron microscope
LSPR	localized surface plasmon resonance
SERS	surface enhanced Raman scattering
TEM	transmission electron microscope
TON	turn-over-number
TOF	turn-over-frequency
GC-MS	gas chromatography-mass spectrometer
4NP	4-nitrophenol
4ATP	4-aminothiophenol
R6G	rhodamine 6G
x	metal to polymer weight ratio
t	time
T	temperature

CHAPTER 1

Introduction

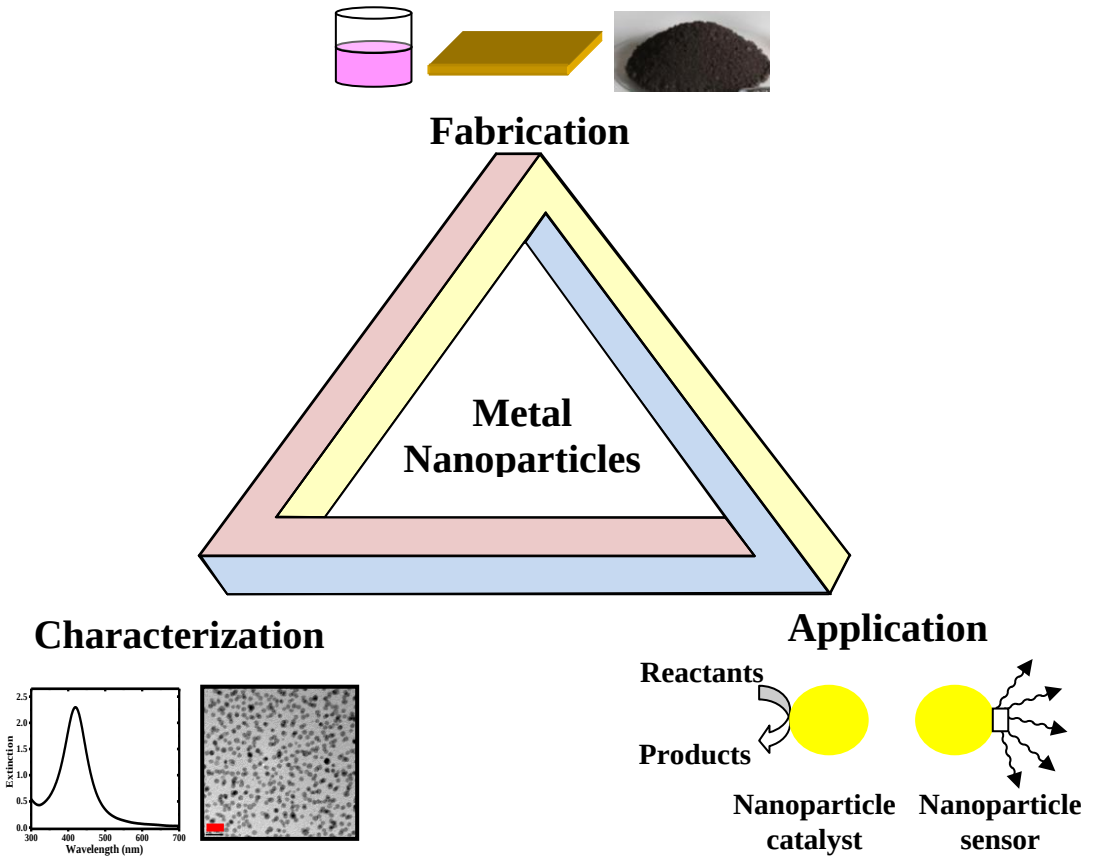

Fabrication, characterization and application of metal nanoparticles are discussed in this chapter.

Scope

In recent years there has been an explosive growth in the field of metal nanoparticles in terms of development of novel fabrication methodologies, investigation of the unique characteristics and deployment in a wide range of applications from electronics and photonics, to catalysis and sensing, to biology and medicine. Polymer-metal nanoparticle composites are versatile materials, which combine the unique characteristics of the components in synergetic manner, leading to the emergence of novel characteristics and functions. In situ generation of the nanoparticles is the most convenient and attractive route to the fabrication of metal nanoparticle-embedded polymer thin films, which involves the reduction or decomposition of appropriate precursors inside the solid film. The environment-friendly soft-chemical protocol we have optimized for the fabrication of noble metal nanostructures inside polymer thin films, uses aqueous medium for the synthesis and the polymer acts simultaneously as the reducing as well as stabilizing agent. Effective control provided by the in situ fabrication route on various aspects of the nanostructures and significant applications of these nanocomposite thin films in areas such as chemical catalysis and surface enhanced Raman scattering (SERS) are presented in this thesis.

In this chapter we present an appraisal of the uniqueness of nanomaterials, followed by a brief commentary on their historical development and a general overview of the various classes of nanomaterials (Sec. 1.1). In Sec. 1.2, we focus on metal nanoparticles, describing their unique properties, synthesis and range of applications. The methodologies developed for the fabrication of polymer thin films embedded with in situ generated metal nanoparticles and the unique features and applications that highlight the versatility of these nanocomposite materials are presented in Sec. 1.3. Sec.1.4 and 1.5 present overviews of the topics of special interest in this thesis, namely metal nanoparticles in catalysis and surface enhanced Raman scattering. The layout of the thesis is outlined in Sec. 1.6.

1.1 Nanomaterials

Materials are substances that are characterized by specific and generally useful physical attributes or functions. The materials characteristics are determined by the elemental composition, bonding and structure, presence of impurities, surface structure and so on. Understanding the relationship between these factors and the properties of materials is crucial to many of the technological breakthroughs. Materials play an important role in day-to-day life. The advances in materials is a reflection of the evolution of mankind and the increasing demands for a higher quality of life. We associate the historic ages with the materials used at different stages as the development of civilization is directly related to them. People used only natural materials like stone and wood in the early stages of human life in the Stone Age. The Bronze Age started around 3000 BC, when copper was discovered and its properties could be altered by alloying. Development of the use of iron and the distinct advantage in terms of manufacturing weapons marked the Iron Age starting around 1200 BC. The Silicon Age beginning with the invention of the transistor in the 1950's and the electronics revolution enabled by the advances in materials have dramatically and irreversibly changed our lives. Realization of the unusual properties of materials in the nanometric size regime (approximately 1 to 100 nm at least in one dimension)[1] and the use of size as a new parameter to control and manipulate materials characteristics, have ushered in the age of nanoscience and nanotechnology, with potentially strong impact on the evolution of human civilization.

1.1.1 *Uniqueness*

Materials are often classified as electronic, magnetic, optical, etc. based on their prominent properties. Another useful classification could be based on their chemical composition, structure or function - metals, semiconductors, ceramics, glasses, organics, polymers and composites. Impact of chemical composition and structure on the properties of materials can generally be understood using the basic laws of classical physics and chemistry. The unique effects of size on the properties of materials

possessing the same composition and structure, specifically in the size range of a few nanometers, can be understood in terms of quantum mechanical principles governing confinement effects and distinct surface features. Nanoscience and nanotechnology deal with nano-sized materials, by manipulating them at the atomic, molecular and supramolecular levels, to achieve the desired properties and create devices and systems with fundamentally new functionality.[2]

Several methodologies have been developed for the fabrication of nanomaterials and along with the advances in the characterization methods, a wide range of applications have arisen in different fields. A case in point is metal nanoparticles for which many varied technological applications have been demonstrated. In the nanoscale regime, gold can act as a catalyst[3] and silver as a bactericide.[4] Gold and silver nanoparticles are used in ultra sensitive detection of molecules (even single molecule) through surface enhanced Raman scattering (SERS).[5] These unique properties can be attributed to the enhanced surface-to-volume ratios as the size of particles decreases, and the confinement of electrons to distances that are small compared to their scattering length scales. Electron energy states alter due to the confinement of electrons to small distances, giving rise to unique size-dependent properties. Particles at the nanoscale show depression in melting point due to the increased proportion of surface atoms that posses fewer neighbouring atoms than those in the bulk.

Nanomaterials are playing an important role in textile, paints/coatings, and chemical industries. Textiles (anti staining, self cleaning, medical), wear-resistant coatings, cosmetics and paints and fog-free mirror coatings are some of the remarkable materials that have been developed based on nanotechnology. Renewable energy sources such as solar cells, fuel cells and reforming catalysts are also made using nanomaterials. Nanomaterials have permeated almost every field of science as seen from the terms such as nanochemistry, nanophotonics, nanoelectronics and nanomedicine. The unique features and functions of nanomaterials are exploited in all these areas.

1.1.2 *History*

Nanoparticles have been used in different fields from ancient times without a detailed knowledge of their specific role. The Vedas, believed to be the oldest writings in the world, propound an alternative medicine (ayurveda) that uses colloidal gold named "swarna bhasma" in the treatment of various ailments. Soluble gold nanoparticles were used in ancient days as pigments for aesthetic and curative purposes. An example is the famous Lycurgus cup[6] from the 4th century A.D in Rome; the optical properties of the embedded gold and silver nanoparticles make it appear greenish under reflected light, but red when illuminate from inside (Fig. 1.1a). Colloidal particles of coinage metals such as copper, gold and silver were used in the stained-glass windows of many medieval cathedrals around tenth century (Fig. 1.1b). Incorporation of colloidal gold into molten silica to create Ruby glass (Fig. 1.1c) is a process known from around 1600s.[7]

However first scientific study was made by Michael Faraday who fabricated colloidal gold (which he described as 'finely divided gold') by the reduction of gold chloride using phosphorus as the reducing agent in CS_2.[8] After about half a century, J. C. Maxwell-Garnett attempted a quantitative theoretical description of light scattering by metal nanoparticles, assuming the size of the particle to be negligible compared to the wavelength of the light.[9] In 1908, the first rigorous theoretical treatment by Gustav Mie provided the basic understanding of the optical properties of spherical metallic nanoparticles.[10]

A major development that played a crucial role in the escalation of nanoscience and nanotechnology is the invention of the transmission electron microscope (TEM). From the concept developed by Max Knoll and Ernst Ruska in 1931(visible light replaced by electron beam to image at a resolution higher than that permitted by the diffraction limit of visible light), the first practical TEM was built by Albert Prebus and James Hiller in 1938. As the wavelength of electron beam can be tuned by controlling the accelerating voltage and can be reduced to atomic dimensions at high voltage, nanostructures can be imaged with sufficient resolution. In 1959,

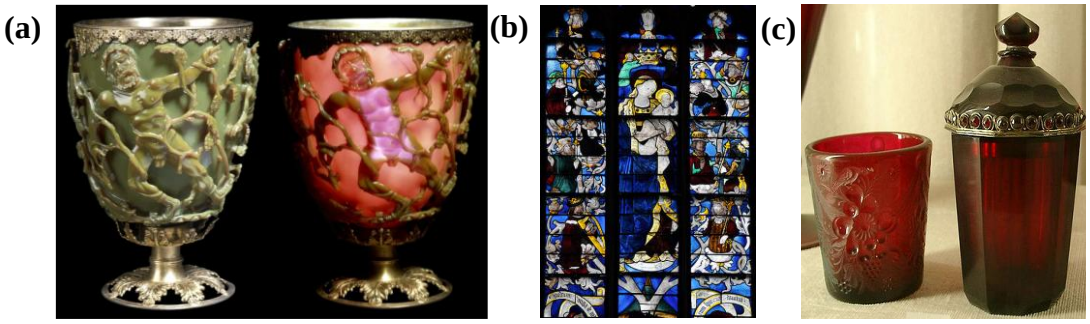

Figure 1.1. *(a) The Lycurgus cup in reflected light (green) and transmitted light (red) (Ref. 6b). (b) Stained glass window at Evreux Cathedral (France) (http://www.en.wikipedia.org/wiki/stained-glass). (c) Gold Ruby glass (or) Cranberry glass (http://www.en.wikipedia.org/wiki/Cranberry_glass).*

Richard Feynman, a Nobel laureate in physics, forecast the vast application potential of nanoscale materials, in his famous lecture at the American Physical Society meeting entitled "There's Plenty of Room at the Bottom"; he pointed out the possibility of designing, observing and manipulating materials at the atomic scale and the new phenomenon that can be exploited. The first use of the term "nanotechnology" was by Norio Taniguchi at the International Conference on Precision Engineering (ICPE) in 1974.

The remarkable growth of nanotechnology research started in the 1990's. It was facilitated by the inventions of the scanning tunnelling microscope (STM) in 1981 by Gerd Karl Binning and Heinrich Rohrer and the atomic force microscope (AFM) in 1986 by Binning, Quate and Gerber. In these techniques, the sample is scanned using a very fine tip, measuring the tunnelling current or the van der Waals forces.[11] Together with electron microscopy these new developments significantly expanded the number and type of materials that could be imaged on a nanometer scale.

The basic strategy developed by Michael Faraday for the synthesis of metal nanoparticles has evolved with the replacement of phosphorus by other reducing agents such as citrate and borohydride, use of stabilizers such as thiols and biphasic organic solvent-water system together with phase-transfer reagent.[12] Discovery of novel materials such as carbon nanotube, fullerene and graphene have further enriched the field of nanoscience and nanotechnology.

1.1.3 *Classification*

A wide range of nanomaterials are known today and are used in various fields based on their composition and properties. Even though a rigorous classification of nanomaterials is difficult and perhaps pointless, some broad classifications are sometimes useful to provide an understanding of the field. One kind of terminology used in nanoscience is roughly based on the size - clusters, nanoparticles/nanocrystals, and colloids.[13] A cluster is the collection of few atoms/molecules (typically less than 100) stabilized by a ligand shell which makes them isolable and soluble in appropriate solvents. Colloids are the stable suspension of particles with sizes less than a micron in a liquid. Nanoparticles are the particles with sizes up to few tens of nanometers, which can be either solid/hollow, amorphous/crystalline or polycrystalline. The crystalline solid particles can be called as nanocrystals.

H. Gleiter in 1995 proposed a systematic classification of nanomaterials based on the growth habit and morphology which was further extended by V. Skorokhod in 2000. According to them nanostructures were classified into 2-, 1- and 0-dimensinal[14] as shown in Fig. 1.2. Plates and discs with polygonal shapes and size greater than 100 nm in 2 dimensions are classified as 2-dimensional nanostructures. Cylinders, wires, rods etc. with size greater than 100 nm in only one dimension are classified as 1-dimensional nanostructures. Spherical particles, cubes, icosahedrons etc. which are less than 100 nm in all directions are described as 0-dimensional. However, some of the interesting structures like bipods, tripods and multipods will not fit into this classification.

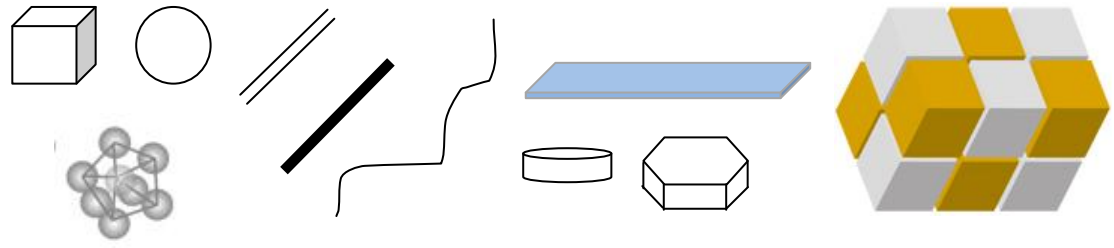

Figure 1.2. *Classification of nanostructured materials based on morphology and growth habit (figure is adapted from ref. 14).*

3-D nanomaterials include powders and fibers, multilayer and polycrystalline materials in which the 0-D, 1-D and 2-D structural elements are in close contact with each other and form interfaces.[14]

1.2 Metal Nanoparticles

Metals occupy 2/3 fraction of the periodic table and form the major component in several devices and technologies. Due to their specific electronic structure, they show interesting properties like electropositivity, high electrical and thermal conductivity and magnetism, leading to many applications in various fields of science and engineering. The remarkable contrast between the properties of bulk and nano forms of metals makes metal nanoparticles especially interesting. The major factors that are responsible for the special attributes are the high surface-to-volume ratio, quantum size effects and electrodynamic interactions.[15,16] The unique properties and applications of metal nanoparticles and the general methodologies developed for their synthesis are briefly reviewed in the following sections.

1.2.1 *Optical Properties*

Most metals are opaque in their bulk state and exhibit the so-called 'metallic' appearance due to the total reflection of the incident light. In the case of finely dispersed metals, the total absorption of light makes them appear dark brown or black (example palladium black). However at the nanoscale regime, as the particle size approaches the mean free path of electrons, they show different colors depending on the size and shape. For example bulk silver is shiny white ('silvery'), whereas 5 nm silver particles are yellow. This is due to the collective coherent oscillation of free electrons with respect to the positive metallic lattice in the metal nanoparticle, in the presence of the oscillating electromagnetic field of the light incident on it, [17-20] as shown in Fig. 1.3. When this oscillation resonates with a specific frequency of the light, it leads to strong absorption, and is termed as localized surface plasmon resonance (LSPR). Mie has shown

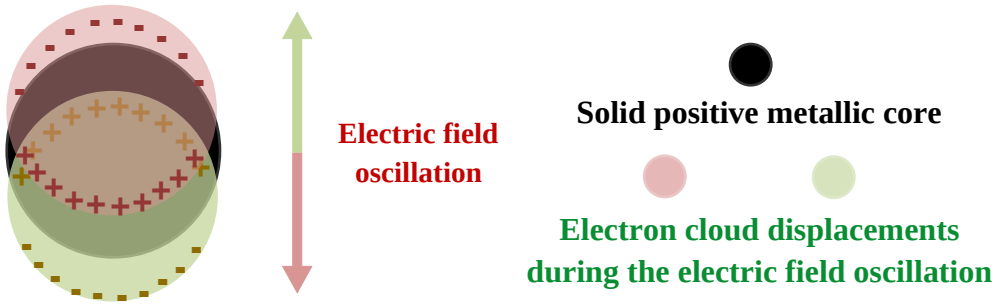

Figure 1.3. *Schematic representation of the electron cloud displacements in nanoparticles under the effect of an oscillating electric field. Direction of the electric field and the corresponding displacement of electron cloud are indicated with the same color.*

that scattering and absorption of incident light by the isolated spherical particles follows the equation,[10]

$$C_{ext}(\lambda) = \frac{24\pi^2 R^3 \varepsilon_m^{3/2}(\lambda)}{\lambda} \frac{\varepsilon''(\lambda)}{[\varepsilon'(\lambda) + 2\varepsilon_m(\lambda)]^2 + \varepsilon''^2(\lambda)}$$

where C_{ext} (λ) is the extinction cross-section at wavelength λ, R is the radius of the particle, and ε is the dielectric constant; subscript m denotes the medium surrounding the particle and $\varepsilon'(\lambda)$ and $\varepsilon''(\lambda)$ denote the real and imaginary parts of the dielectric function of the material of the particle. C_{ext} becomes extremely large when $\varepsilon'(\lambda) = -2\varepsilon_m$, which shows that at this wavelength the optical absorption and scattering would be very strong, indicating the resonance condition. The resonance for silver, copper and gold occur in the visible region. The size, shape, composition, inter-particle interactions of the nanoparticles and dielectric properties of the surrounding medium affect the LSPR spectra.[16,21,22]

LSPR of metal nanoparticles can be exploited in a wide range of applications in fields such as photonics,[23] medical diagnostics[24] and sensing.[25] Another important application is in the area of surface enhanced Raman scattering (SERS), which is surface phenomenon associated mostly with metal nanoparticles that has significant application potential in ultrasensitive detection of molecules; this will be discussed in detail in Sec. 1.5.

1.2.2 *Catalytic Activity*

Combining the advantage of homogeneous and heterogeneous catalytic processes harmoniously is a continuing goal in catalysis. Metal nanoparticles are important candidates with the added ability to achieve new reactivity and selectivity. Metal nanoparticles are efficient catalysts, their large surface area-to-volume ratio and specific surface structure being key factors.[26] Noble metal nanoparticles in particular combine many of the advantages of homogeneous and heterogeneous catalysts.[27-30] Several methodologies have been developed for the fabrication of noble metal nanoparticles with varying sizes and shapes, that can be used to tailor their catalytic activity.[31-34] The particles having sharp edges and sharp corners or rough surfaces often exhibit strong catalytic activity.[35]

Typical examples of reactions in which colloidal metal particles of about 3 nm size have shown high activity and selectivity are the hydrogenation of olefins and dienes,[36-38] hydration of acrylonitrile,[39] and light-induced hydrogen generation from water.[40] Palladium nanoparticles serve as highly efficient catalysts for carbon-carbon coupling reactions.[41-45] Platinum and gold nanoparticles catalyze oxidation reactions.[46,47] Silver nanoparticles were also found to be good catalysts for oxidation reactions.[48,49] An important problem pertains to the recycling of nanoparticle catalysts. We take up this issue in greater detail in Sec. 1.4.

1.2.3 *Biological Activity*

Living organisms are built of cells with size in the range of micrometers and proteins within the cells have sizes of a few nanometers that are comparable to the dimensions of nanoparticles. Understanding of biological processes at the nanoscale level is a strong driving force behind the development of nanotechnology in this field.[50] Because of this, one can ideally probe the cellular machinery using nanoparticles without introducing violent perturbations.[51] Over the wide range of size-dependant physical properties available, optical[52] and magnetic[53] effects are often used for biological applications. LSPR extinction of metal nanoparticles can be shifted from the

visible to the near-infrared (NIR) wavelengths by tuning the size and shape of the nanoparticles; gold is a particularly successful case in this regard. As the tissues are relatively transparent to NIR signals, such nanoparticles are a convenient imaging tool.[54] Gold and silver nanoparticles can be used as fluorescent tracers in immuno and DNA probe assays as well as in cell and molecular biology studies due to their large light-scattering power. They are advantageous over standard organic dyes in terms of low cost, simplicity of use, flexibility in tuning the color of scattered light, and ultra-sensitivity.[55]

Metal nanoparticles are used in applications such as cancer cell diagnostics,[56,57] gene and drug delivery[58,59] and therapeutics.[60] The low cytotoxicity of gold and silver nanoparticles is an important advantage.[61,62] The light absorbed and scattered by them can be converted to heat to induce effects like hyperthermia.[63] Photothermal therapy using the absorption properties of antibody-conjugated gold nanoshells[64] and solid gold nanospheres[65] has been demonstrated to selectively kill cancer cells, leaving the healthy cells unaffected. Metal nanoparticles are also used as bactericidal agents,[66] and in tissue engineering.[67]

1.2.4 *Other Properties*

Melting point is an intensive property of materials. However, when the particle size decreases down to nanometric dimensions, reduction in the melting point by several hundreds of degrees is observed. This phenomenon was first demonstrated by Takagi in 1954,[68] using TEM. Careful monitoring of the electron diffraction from particles of different sizes over a wide temperature range can provide information on the size-dependant melting point.[69] The Gibbs-Thomson equation,

$$\Delta T_m = T_m(bulk) \times \frac{4\sigma_{sl}}{H_f \rho_s d}$$

provides the quantitative relationship between the melting point depression ΔT_m and the diameter of the particle, d, and involves quantities such as σ_{sl} (solid–liquid interface energy per unit area), H_f (bulk enthalpy of fusion per gram) and ρ_s (density of solid).

In magnetic materials, novel properties can be realized when the particle size becomes smaller than the average size of the magnetic domains. In this regime, the intrinsic magnetic properties are strongly influenced by the particle size and give rise to phenomena such as superparamagnetism and quantum tunneling of magnetization.[70,71] These magnetic nanoparticles have many potential applications in magneto-optical switches,[72] magnetically controllable single electron transistor devices[73] and toxic waste (including removal of heavy metals[74]) remediation from ground water.[75]

Bulk metals are insoluble in water and organic solvents, but metal nanoparticles stabilized by appropriate capping agents are generally soluble in various solvents. This solubility arises from the enhanced interaction of the surface atoms and/or capping agents with the solvent molecules. Gold metal is insoluble but gold nanoparticles can be solubilized in water and organic solvents such as alcohol, acetone and acetonitrile through suitable choice of capping agents.[76]

Coulomb blockade is an important electrical effect observed in metal nanoparticles.[77] Nanoparticles can effectively function as miniature electrical devices.[78] Due to the nanometric size, many of the mechanical properties of the nanomaterials become different from that of the bulk material; these include the hardness, elastic modulus, fracture toughness, scratch resistance, wear resistance and fatigue strength.[79,80] Copper with ultra-fine grain size has been shown to exhibit higher tensile yield strength and ductility than that of layer particles.[81,82]

1.2.5 *Synthesis*

The wide application potential of metal nanoparticles has resulted in an increasing demand for the development of novel fabrication methodologies. Metal nanoparticles are fabricated in various formulations such as aqueous or organic solutions, composites, powders, organized assemblies and thin films. The various approaches involved in the fabrication can be broadly classified into ‘top-down’ and ‘bottom-up’ approaches. Top-down approach refers to the creation of nanoscale

particles from larger/bulk metal through various methods including mechanical methods such as cutting, grinding, and milling, in controlled manners in appropriate atmosphere that prevent oxidation of the metal during the process. This approach generally requires sophisticated machinery, high energy and harsh conditions. High energy ball milling is a commonly used top-down approach. Avoiding imperfections in surface structures and crystallographic defects is a challenging problem in these approaches. In spite of such problems, they are suitable for the large scale synthesis in industry. The size, shape and inter-particle spacing of metallic nanostructures can be efficiently controlled on suitable surfaces using lithography, such as electron beam lithography (EBL)[83,84] and focused ion beam (FIB) lithography.[85]

'Bottom-up' approach involves the controlled aggregation of atomic/molecular building blocks to form nano sized particles. These techniques of synthesis and assembly of nanoparticles are in general, energetically and economically cheaper manner. Hence they are widely used for the fabrication of metal nanoparticles. The process involves the reduction or decomposition of metal precursors by using a suitable reagent/treatment in the presence of appropriate capping agent to get metal atoms which assemble to form nanoparticles. This idea is employed in numerous wet chemical methods to fabricate nanoparticles of various sizes and shapes. The explosive growth in such soft chemical routes facilitates the synthesis of metal nanoparticles with great flexibility.

Bottom-up approaches can be broadly classified into chemical and physical methods as shown in Fig. 1.4. The physical methods of formation of nanoscale metals often involve the deposition of metal nanosturctures on suitable substrates. Physical vapor deposition (PVD) and chemical vapor deposition (CVD) are two general modes of deposition. Evaporation or sputtering of metals in vacuum followed by condensation on a suitable substrate is a method of physical vapor deposition. In chemical vapor deposition, the source gases are introduced into a reaction chamber and energy is provided in the form of heat or high frequency electric field (RF power) to decompose and deposit the products of the reaction on the substrate, forming a thin film.

In chemical methods, synthesis of nanoparticles proceeds via chemical reduction or decomposition by external stimuli depending on the metal precursor. Some precursors break down into metal atoms by a variety of methods including photochemical, thermal, radiolytic and microwave/ultrasound irradiation. The rate of reaction in a photochemical synthesis can be enhanced by increasing the intensity of light.[86] Thermolysis of organometallic complexes can produce uniform-sized metal nanocrystals.[87] Synthesis of metallic/bimetallic nanoparticles by radiolysis provide efficient control over the size distribution.[88] Metal oxides have been converted to metal nanoparticles by the use of ultrasound.[89] Another approach in chemical method is the reduction of metal ions to atoms in presence of stabilizing agent. Reducing agents used includes molecular hydrogen, hydrides, citrate, ascorbic acid, glucose and alcohols,

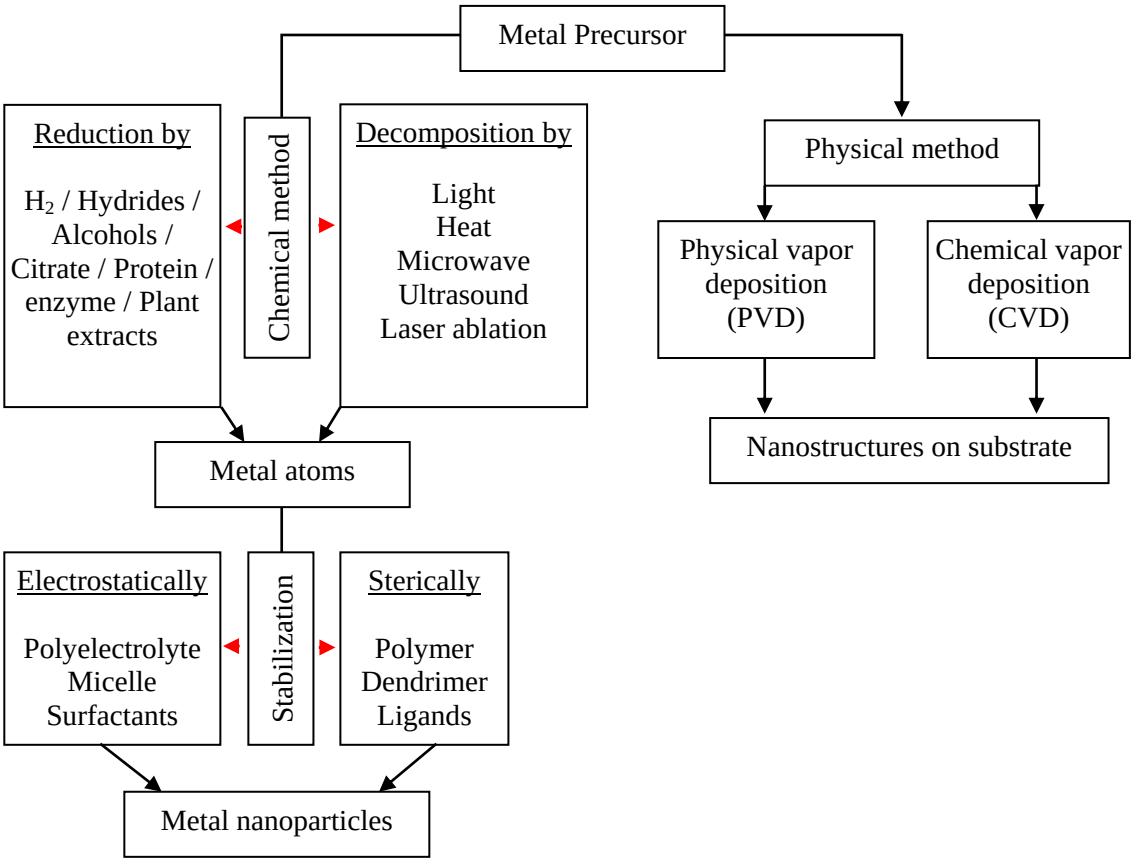

Figure 1.4. *Schematic illustration of the steps involved in the fabrication of metal nanostructures via bottom-up approaches through chemical and physical methods. General reagents/processes used are listed.*

protein/enzyme, plant extracts[90] and oxidizable solvents like alcohol.[91] Due to high surface area, nanoparticles tend to aggregate in order to reduce the surface free energy. Capping agents are used to stop the agglomeration, by protecting them electrostatically and/or sterically.

Choosing the suitable capping agent is a crucial part of the synthesis as well as application. Thiols, amines, carboxylates, cyclodextrins, citrates, quaternary ammonium salts and phosphines are some of the widely used stabilizing agents. Polymers are also commonly used for capping metal nanoparticles; by choosing the polymer with the suitable functional group one can reduce the metal ion as well. Polymers provide simplicity in the synthesis and convenience in handling of nanoparticles through *in situ* generation techniques. Polymer-metal nanoparticle composite thin films are particularly interesting because of their utility in technological applications.

1.3 Polymer-Metal Nanocomposite Thin Films

Polymers and metals are two different kinds of materials with contrasting characteristics in their individual bulk states. However, formation of a polymer-metal nanocomposite provides a versatile route to harmonize the two and harness unique benefits. The polymer matrix can facilitate the stabilization and organization of the metal nanoparticles and exhibits novel characteristics and functions. Optical and electronic responses of metal nanoparticles can be significantly altered by the dielectric environment provided by the polymer matrix.[92] On the other hand, the mechanical properties and thermal behavior of the polymer can be affected by the presence of nanoparticles.[93,94] The synergy between the properties of metal nanoparticles and the characteristics of polymers lead to the uniqueness of polymer-metal nanocomposites and emergence of various applications.

1.3.1 *Fabrication*

Thin films of these nanocomposite materials are particularly advantageous in terms of the ease of fabrication as well as the use in a wide range of applications. In this thesis, we are particularly interested in thin films. Several methods have been developed for the fabrication of polymer-metal nanocomposite thin films in recent times[95] including sputtering and co-deposition of metal nanoparticles with polymer.[96] However, *in situ* methods have become very popular because they are easy to carry out and yield a homogeneous distribution of nanoparticles in the polymer matrix. One approach is to fabricate the composite material by carrying out the polymerization of the monomers simultaneously with the *in situ* generation of nanoparticles.[97] Homogeneous distribution of nanoparticles in the film may not be guaranteed in this method because of the possibility of phase separation. In another approach, the metal nanoparticles can be generated from suitable precursors within the polymer matrix. Several closely related approaches have also been developed, and they generally facilitate a homogeneous distribution of nanoparticles and removal of undesirable byproducts while ensuring negligible potential health hazards associated with nanomaterials.

Incorporation of the metal precursor in the solid polymer film can be achieved mainly through two approaches as shown in Fig. 1.5; approach 1 involves incorporation of the metal precursor into a prefabricated polymer thin film through various methods (treatment with metal precursor solution[98-101] or vapor[102], plasma treatment[101]) and approach 2 involves the coating of polymer solution containing the metal precursor. Approach 2 is generally simpler than 1 to implement and mixing the polymer and the precursor in solution would ensure homogeneous distribution of the metal ions, leading to homogeneous particle distributions under optimised conditions. This composite films can be treated in several ways including photoirradiation,[98-100] **c**hemical reduction[101] electrochemical reduction[103] and thermal treatment[102] to generate the nanoparticles *in situ* inside the film. Thermal treatment is probably the simplest procedure, which can cause either decomposition of the precursor or reduction by the polymer itself; polymers with functional groups like alcohols and amines can act as the reducing agents.

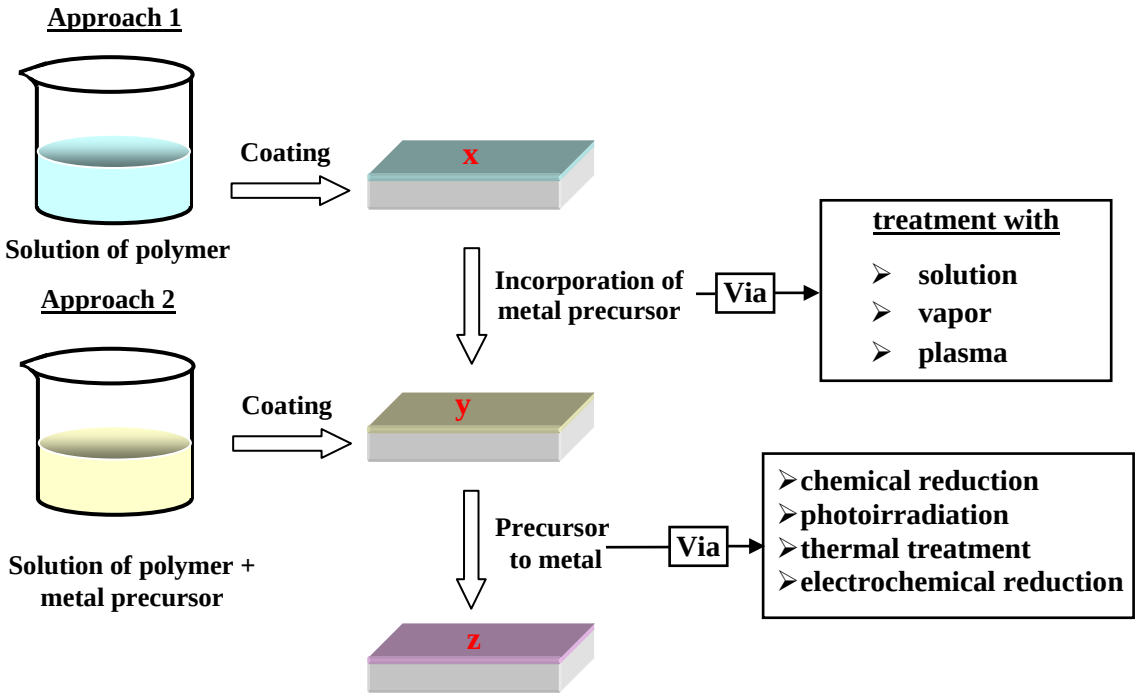

Figure 1.5. *Schematic diagram of the two approaches generally employed for the in situ synthesis of metal nanoparticles inside a polymer thin film on substrate (x = thin film of polymer, y = thin film of polymer +metal precursor, z = thin film of polymer + metal nanoparticles); dimensions are not to scale.*

Rational choice of biodegradable polymers with suitable functional groups and the use of aqueous medium for the process would make the methodology interesting from green chemistry considerations. Careful choice of the precursor and polymer and simple methods such as spin-coating followed by thermal annealing or photoirradiation allows the generation of a homogeneous distribution of metal nanoparticles within the polymer thin film. Generation of silver nanoparticles inside poly(vinyl alcohol) (PVA) films by thermal treatment was demonstrated several years ago,[104] and a detailed protocol was developed later in our laboratory, to fabricate noble metal nanoparticle-embedded polymer thin film including a procedure for making free-standing films.[105]

The environmentally benign nature; mostly involving aqueous medium, the facile spin-coating process used to form thin films and the mild conditions required for the soft chemical synthesis of the nanoparticles are important features of the protocol developed in our laboratory. The procedure ensures that the potentially hazardous metal

nanoparticles are formed within the polymer film and therefore never exposed to the environment. PVA is a water soluble polymer with several hydroxyl groups; it facilitates the fabrication of several noble metal nanoparticles through the reduction of the metal precursor by the hydroxyl groups under mild thermal annealing/photoirradiation. The progress of the nanoparticle production inside the film can be monitored using spectroscopy and microscopy techniques. An additional sacrificial support layer of polystyrene (PS) enables the fabrication of free-standing films and also production of extremely thin films for monitoring/imaging the nanostructures directly through a TEM without additional microtoming or other sample preparation procedures. This is a major advantage of the protocol developed for the metal nanoparticle-embedded polymer thin film.

The general protocol is schematically represented in Fig. 1.6. A film of PS is spin-coated first on the substrate, followed by a film of polymer containing the metal salt; typical thicknesses of the two layers are ~3 µm and ~0.05-0.3 µm respectively. When the film is heated, the metal nanostructures are generated inside the film. The chemistry (reduction process) happening inside the polymer followed by significant

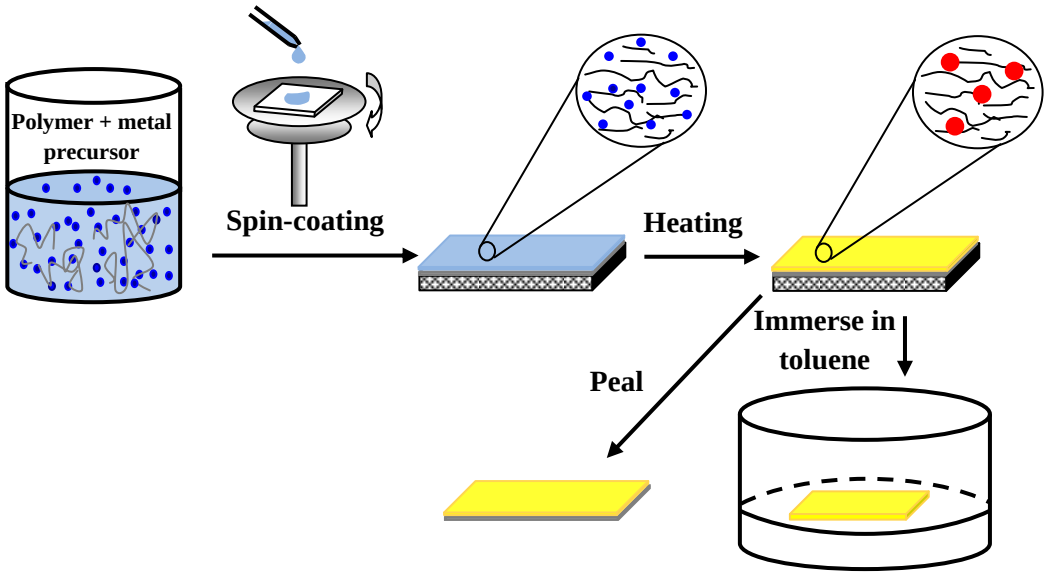

Figure 1.6 *In situ fabrication of polymer-metal nanocomposite thin film: spin coating of the solution of polymer and metal precursor on a PS-coated substrate, followed by thermal annealing to get thin film of polymer with embedded metal nanoparticles. Formation of free-standing film is also indicated.*

chemical changes in the polymer such as the cross-linking can be described using the typical reaction sequences shown in Fig. 1.7. Size, shape and density of the metal nanoparticles formed *in situ* inside the polymer thin film can be tuned by varying the metal-to-polymer ratio, viscosity of the solution mixture, spin-coating conditions and the thermal annealing time and temperature. Fabrication of silver,[105] gold,[106] palladium[107] and mercury[69] nanostructures inside polymer thin films and the impact of the various experimental parameters on their characteristics have been investigated.

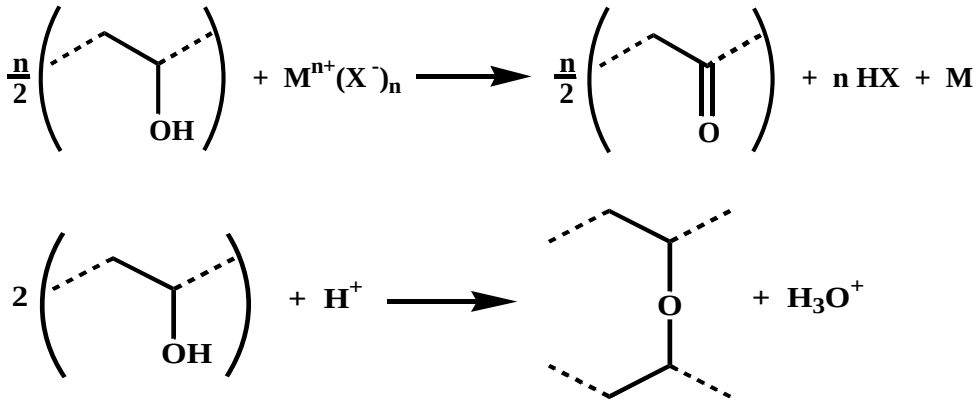

Figure 1.7 *Schemes showing the reduction of metal ion by PVA and a possible polymer cross-linking pathway.*

1.3.2 *Characterization*

A wide range of spectroscopy and microscopy techniques can be used for monitoring the formation of metal nanoparticles and their structural and compositional characterization. The most convenient way to monitor the formation of nanoparticles is to measure the electronic absorption/extinction spectrum of the nanocomposite film. The characteristic LSPR spectra of nanostructures of noble metals such as silver, gold, copper and palladium appearing in the visible and ultraviolet wavelength ranges provide a convenient tool to monitor their growth and gain insight into the size, shape and distribution. Reduction of the metal precursor to metal nanostructures and formation of the nanoparticles with different shapes in the PVA thin films as a function of processing time is reflected in these spectra.[105-107]

X-ray photoelectron spectroscopy (XPS) can provide valuable information about the formation of metal nanostructures inside the polymer film by monitoring the oxidation state changes of the metal. XPS spectra have been effectively used to confirm the formation of metal nanoparticles of silver, gold, copper and palladium in polymer films[93, 94, 100, 107]

Atomic force microscopy (AFM) is a scanning probe technique that can be employed easily to observe the film morphology and also the structural features of nanoparticles.[100,107-108] In this technique a tip is brought in close proximity of the sample surface and scanned, measuring different forces such as mechanical contact force, van der Waals forces, electrostatic forces and magnetic forces depending on the nature of the sample. Typically, the deflection is measured using a laser spot reflected from the top surface of the cantilever into an array of photodiodes. *In situ* growth of nanostructures in a polymer film in real time and organization of nanoparticles induced by stretching of polymer film, have been explored using AFM.[109,110]

Detailed characterization can be achieved using electron microscopes, scanning electron microscope (SEM) and transmission electron microscope (TEM), together with energy dispersive X-ray scattering (EDXS), wavelength dispersive X-ray scattering (WDXS) and selected area electron diffraction. Nanostructures formed inside the polymer films can be imaged and characterized directly; this is a distinct advantage over the imaging of nanostructures synthesized in a fluid medium due to the chances of aggregation of such particles during the sample preparation process. One approach to the preparation of the thin film sample is by microtoming the film fixed inside a resin matrix to a sufficiently thin slice. [110-115] In the methodology we have developed (Fig. 1.6), the free-standing film floating on the surface of toluene after the sacrificial layer of PS has been dissolved, can be collected on a TEM grid and imaged directly.[69, 105-107, 112] This technique is of considerable practical value.

X-ray diffraction techniques are commonly used to characterize the size and structure of crystalline metal nanoparticles, and simultaneously the structure of the polymer. Small and wide angle x-ray scattering technique is well suited for this.

Production of gold nanoparticles inside PVA films by photoirradiation has been followed using X-ray diffraction.[110] Growth of the nanoparticles as well as the lamellar structure of the polymer matrix in the Ag-PVA film were studied using small angle X-ray scattering.[116]

Spectroscopic ellipsometry has been shown to be an effective tool for monitoring the formation of silver nanoparticles inside PVA film.[117] Real time ellipsometry was also used to evaluate the process of evaporation of the polymer from the composite film accompanied by shifts in the plasmon resonance of the silver nanoparticles.

The distribution of particles across the thickness of the film is important for characterization of metal nanoparticle-embedded polymer films. Rutherford backscattering spectrometry was used together with AFM and TEM imaging to investigate the formation of silver nanoparticles inside Poly(methyl methacrylate) (PMMA) film.[108] Dynamic secondary ion-mass spectroscopy was successfully employed to determine the depth profile of gold nanoparticles inside PS thin films and correlated to the glass transition temperature of the nanocomposite material.[94]

1.3.3 *Applications*

Metal nanoparticle-embedded polymer thin films formed through the *in situ* approach possess unique attributes that effectively enhance their application potential. While the solubility of the precursor and the polymer in the same solvent like water or alcohol are advantageous in terms of making the film formation facile and environmentally benign as noted above, the likelihood of the polymer chain cross-linking (Fig. 1.7) concomitant with the nanoparticle production reduce the solubility of the final nanocomposite thin film, enhancing its application potential in aqueous media. At the same time, the hydrogel character of polymers like PVA is critically important, as it leads to the swelling of the thin film facilitating contact between the external medium and the metal nanoparticles embedded within the film. These aspects are

especially important in various applications such as catalysis and sensing. We described below, some of the applications explored mainly using noble metal-PVA thin films fabricated using the *in situ* method.

Optical limiter

Intensity of the light transmitted through a material scales linearly with intensity of the incident light. However, in the case of some special materials and appropriate light wavelengths, the output intensity can get clamped at a constant value, beyond a threshold. This phenomenon is known as optical limiting and can arise due to a number of processes including nonlinear absorption and scattering by the medium of high intensity light such as that from short pulse lasers. As metal nanoparticles in colloidal medium are known to show strong optical limiting responses, the nanocomposite thin films have been investigated in this context. Ag-PVA films exhibit appreciable optical limiting characteristics for ns and fs-pulsed lasers;[105,118,119] a notable point is the high transparency of these films in the linear regime. Studies on free-standing PVA/Ag-PVA/PVA films allowed the estimation of accurate nonlinear coefficients without any error due to contributions from the substrate.[118] Optical limiting capability of Au:Ag-PVA,[120] Pd-PVA[107] and Pt-PVA[121] thin films have also been explored.

Microwave absorber

Microwaves are used extensively in wide-ranging applications in different contexts like radar technology, defense industry, cooking ovens and semiconductor processing. Ag-PVA thin films show appreciable microwave absorption in the frequency range of 8-12 GHz which is of interest in telecommunication applications.[122]

Random lasing with coherent feedback

An interesting discovery with great application potential is the random lasing with coherent feedback observed in Ag-PVA films containing a dye molecule like Rhodamine-6G.[123] The authors attribute the random lasing with coherent feedback to

the effect of highly localized light modes caused by surface plasmon resonance interaction between the silver nanoparticles and light.

Surface enhanced Raman scattering substrates

The surface plasmon field of metal nanoparticles is known to enhance the intensity of Raman scattering bands by several orders of magnitude. *In situ* synthesized Ag-PVA film containing poly(γ-glutamic acid) has been shown to be an efficient substrate for surface enhanced Raman scattering.[124] SERS response of 4-aminothiophenol on Ag-polycarbonate films showed ~10^7 enhancements in the signal;[125] further enhancements observed with plasma etching of the film demonstrates the versatility of nanoparticle-embedded polymer films in terms of their post-fabrication tunability. A unique advantage of these nanocomposite films is demonstrated in Chapter 4 by fabricating them as a thin coating inside glass capillaries and using these disposable SERS substrates for the sensitive detection of probe molecules.

Electron beam lithography and patterning

In situ generation of silver and gold nanoparticles inside a PVA thin film with concomitant polymer cross-linking has been induced by electron beam lithography patterning.[126,127] This allows the generation of negative tone polymer nanocomposite resists which are of interest in plasmonic technologies.

Sensor

The LSPR absorption of metal nanoparticles is an effective tool commonly used in sensor applications. Ag-PVA thin film has been shown to be a highly efficient sensor for mercury in all its stable oxidation states, 0, +1 and +2, in aqueous medium, in both *in situ* and *ex situ* modes.[128] Sensitive changes in the LSPR absorption of the Ag-PVA film both in terms of reduction of the intensity and a unique blue shift of the λ_{max} have been exploited for detecting mercury down to ppb levels.

Antibacterial

Silver nanoparticles are well-known antibacterial agents.[129] An exploratory study on *E. Coli* showed that Ag-PVA film can act as a potent and reusable bactericide.[130] The minimum inhibitory and bactericidal concentrations (of silver in the nanocomposite film used to treat unit volume of the *E. coli* bacterial medium) were found to be 4.5 and 6.5 μg/ml respectively, indicating the high efficacy of the Ag-PVA. It was also found that one piece of film can be used to repeatedly and efficiently kill the bacteria in several samples of water, with simple washing in between the usages. Examination of the film between uses, by AFM and LSPR absorption demonstrated that it remained intact throughout.

Catalyst

Catalytic applications of the polymer-metal nanocomposite thin films in hydrogenation[131] and C-C coupling[112] reactions, developed as part of this thesis work, are described in detail in Chapters 2 and 3.

Miscellaneous

Nanocomposite thin films fabricated by the *in situ* technique have also been shown to exhibit significant dichroic properties upon uniaxial drawing[132] and to act as efficient membranes for selective gas transport.[133]

1.4 Metal Nanoparticles as Catalyst

In the majority of reactions in chemical industry, high product yields are realized through the involvement of catalytic processes. Catalysts play a crucial role in the fabrication of a wide range of products such as fine chemicals, plastics and fertilizers, and in the reduction of environmental pollution, for example through cleaning up automotive exhaust gases in three-way catalytic converters. Catalysts operate in homogeneous or heterogeneous fashion. While the homogeneous mode is usually very

efficient, it suffers from the problems of catalyst loss, reducing recycle capacity. Heterogeneous catalysis offers a more convenient separation of products and catalyst, and enables recycling. However, this mode limits the catalyst activity as only the surface atoms are exposed to the reactants and involved in the catalysis.

Nanoparticles are well known in the field of catalysis for a very long time. However, tuning the characteristics of metal nanoparticles for catalytic application has progressed considerably only in recent times. Metal nanoparticles form an important class of catalysts. Several reactions of great interest in organic synthesis including cross coupling, hydrogenation, electron transfer, oxidation and reduction use metal complexes or metal nanoparticles as catalysts. A major goal in the field of nanocatalysis is to combine the advantages of homogeneous and heterogeneous catalytic processes. Nanoparticles represent a new frontier in catalysis, where this unification can be achieved in addition to the development of new or divergent reactivity and selectivity. Several formulations including non-supported and supported metal nanoparticles were developed to realize ideal catalyst design as discussed above. Some of the basic designs are colloidal metal nanoparticles, supported metal catalysts, encapsulated porous materials, and polymer-metal composites. Relevant concepts and typical examples for these methodologies are presented below.

1.4.1 *Colloidal Metal Nanoparticles*

Nanostructured metal colloids consist of isolable particles of sizes 1 to 50 nm that are prevented from agglomeration by protecting shells.[134] Colloidal nanoparticles can be used as homogeneous and heterogeneous catalysts. As a result of this, they are used in several reactions, which are of general and industrial importance.[135] Beller et al. showed that palladium colloids are effective and active catalysts for the Heck reaction of aryl bromides.[136] Palladium nanoparticles synthesized by Ding and Gin via ion exchange of Pd(II) into a cross linked lyotropic liquid crystal polymer and subsequent reduction to Pd(0) with hydrogen gas, exhibits high catalytic activity in hydrogenation and Heck coupling reactions.[137] Colloidal gold nanoparticle solutions shows catalytic

activity in the aerobic oxidation of alcohols, oxidation of CO, homocoupling of phenylboronic acid, as well as borohydride reduction of nitro groups.[138]

The effect of size and shape of the metal nanoparticles on catalytic activity was studied by various research groups.[31-34] The particles which are having sharp edges, sharp corners, or rough surfaces are the most active catalysts.[35] It has been shown that catalysis happens at the surface of these metal nanoparticles. Due to their high surface energy, nanoparticles tend to rapidly sinter into larger clusters, especially under the conditions typically used in catalysis. This sintering process leads to the reduction of the active surface area, and also to the loss of the unique properties of the nanostructured catalysts.[139]

1.4.2 *Core-Shell, Yolk-Shell and Hollow Nanostructures*

Core-shell nanoparticles may be composed of a single, two or multiple metal elements. Core-shell nanoparticles with two or more metal components are typically made by sequential reduction of metal salt precursors in solution phase.[140] Core-shell nanostructures exhibit improved catalytic properties relative to their single-component counterparts. For example Au@Pd nanoparticles can catalyze effectively the Suzuki-Miyaura coupling between chlorobenzene and phenylboronic acid than mono metallic palladium.

Another kind of core-shell nanostructure is composed of a metallic core (catalytic) and a porous oxide shell that facilitates the passage of the reactants to the catalyst core, while preventing sintering of the metallic nanoparticles. Metal nanoparticles in the form of metal core (Pt, Co)@oxide shell (SiO_2) were found to exhibit exceptional thermal stability and thus were well suited to perform catalytic reactions at high temperatures.[141] Ag-CeO_2 core-shell nanostructures have been shown to be high-temperature stable catalysts for reactions such as CO oxidation and cyclohexene hydroconversion.[142]

Yolk-shell structures are core-shell structures with a mobile core. This can be achieved by partially etching the metal core while keeping the shell intact. A unique aspect of the yolk-shell catalyst is that the catalytic core has minimum hindrance from the support and thus one may investigate the intrinsic catalytic properties of the core. Wang et al. prepared a yolk-shell type of catalyst; Au nanoparticles inside a porous shell of SiO_2.[143] Song and co-workers fabricated Au@SiO_2 yolk-shell nanoreactors, which showed good performance in the reduction of o-nitroaniline by sodium borohydride.[144]

Metal nanostructures with hollow interior and special structural properties such as high specific surface area and low density have attractive applications in catalysis. Hollow nanoparticles are often made by chemical etching methods; for example, silver nanoparticles used as a sacrificial template are etched by Au^{3+} ions, the galvanic replacement reaction giving rise to porous gold nanostructures.[145] Pt nanotubes and Pt hollow spheres can exhibit higher activity than its solid particles in oxygen reduction reaction and methanol oxidation reaction.[146] Hollow ruthenium nanoparticles show enhanced catalytic activity in dehydrogenation of ammonia borane.[147]

1.4.3 *Metal Nanoparticles in Ionic Liquids*

Ionic liquids (ILs) are suitable medium for the synthesis of transition metal nanoparticles; the products can be regarded as soluble forms of heterogeneous catalysts. IL's can act as solvent, stabilizer, ligand, and support for metal nanoparticles. It appears that nanoparticles in IL's behave as homogeneous catalysts for the hydrogenation of alkenes, but as heterogeneous catalysts for the reduction of arenes or in Fischer-Tropsch synthesis.[148] Several catalytic systems based on transition metal nanoparticles immobilized in IL's have been developed in recent years for hydrogenation,[149] C−C coupling reactions,[150] methoxycarbonylation,[151] borylation,[152] hydrosilylation[153] and hydrodehalogenation,[154] under both single-phase and multi-phase conditions.

1.4.4 *Supported Metal Catalysts*

Supported metal catalysts in the chemical industry are known from more than a century. Metal nanoparticles supported on oxides like alumina (Al_2O_3), silica (SiO_2), titanium dioxide (TiO_2) and ceria (CeO_2) are the active catalysts for many reactions. Several industrial processes apply catalysts consisting of metal nanoparticles supported on oxides to a variety of important reactions.[155] The most widely used conventional method for preparing metal catalysts is the wet impregnation method.[156] In this method supports are soaked in the metal salt solution, followed by drying, calcination and reduction by hydrogen gas treatment to activate the surface of metal nanoparticles formed. Many variations and new methods have been developed in the past decades, including co-precipitation, which involves simultaneous precipitation of the active metal and the support, deposition precipitation,[157] sol-gel method,[158] and deposition of colloids.[159]

Even though the reaction usually takes place on the surface of metal particles; their interaction with the support is thought to be crucial for some systems. For example oxides of cerium acts as support for metal nanoparticles, due to the relative ease with which the oxide can be reduced and the generated oxygen can be used in the catalytic processes taking place on the metal nanoparticles.[160] Hence these supported nanoparticles have potential applications in the autocatalytic converters used in automobiles.

The oxide support not only provides a platform to prevent the nanoparticles from washing away during the reaction, and to inhibit sintering and growth, but also alters the catalytic properties by changing the shape or electronic structure of the metal nanoparticle. In few cases, the region where the metal and oxide are in contact is believed to be the active site for catalysis.[161] Somorjai et. al. provided the clearest evidence for this by producing a material where each platinum metal particle is in contact with two oxides (SiO_2 and CeO_2) simultaneously, leading to the catalysis of two reactions at the same time, one at each metal-oxide interface.[162]

Many other types of support materials have been used for adsorption of noble metal nanoparticles, including biological supports, magnetic nanostructures, carbon nanotubes[44,45,163] and polymers.[41,164] Bio-generated palladium nanoparticles that are formed on the surface of Gram-negative bacteria have been used as catalysts in Suzuki-Miyaura and Mizoroki-Heck cross-coupling reactions.[165] Palladium nanoparticles loaded onto the magnetic nanoparticle supports have also been used as catalysts for these reactions.[166] Palladium nanoparticles immobilized onto functionalized multi-walled carbon nanotubes have been used in cross-coupling reactions.[167]

1.4.5 *Encapsulation in Porous Materials*

Metal organic frameworks (MOF) are porous crystalline compounds consisting of metal ions or clusters coordinated to mostly rigid organic molecules, to form one-, two-, or three-dimensional structures. Nanoparticle-MOF composites can be prepared either by using MOF's as templates to generate nanoparticles within their cavities[168] or by encapsulating pre-synthesized nanoparticles in MOF's.[169] Platinum nanoparticles entrapped in mesoporous metal–organic framework show catalytic role in the asymmetric hydrogenation of ethyl pyruvate and ethyl 2-oxo-4-phenylbutyrate.[170] Palladium nanoparticles encapsulated in mesoporous metal-organic framework have been shown to be effective for the direct C2 arylation of various indoles with aryl boronic acids.[171] Copper nanoparticles embedded in metal-organic framework act as a high performance catalyst for the reduction of aromatic nitro compounds.[172]

Hybrid materials formed from polyoxometalates (POM) and metal nanoparticles are interesting in terms of the acidic and redox properties of the POM's at the molecular or atomic level. POM's stabilise nanoparticles via their high anionic charge and large size, preventing particle aggregation by electrostatic repulsion. POM-stabilised nanoparticles have been investigated and found to be effective and more selective catalysts for several liquid phase catalytic reactions.[173] Maayan and Neumann hypothesised that the complimentary combination of metal nanoparticles and POM's would produce superior catalysts for the oxidation of non-activated secondary

alcohols.[174] PdO nanoparticles supported on a protonic ionic liquid–POM hybrid material was reported to be a new heterogeneous catalyst for Heck reaction.[175]

1.4.6 *Polymer-Metal Nanocomposites*

Polymeric materials including biopolymers[176] have been widely used for the immobilization of metal nanoparticles. These hybrid materials can be used as catalysts in the form of fibres, resins, gels, capsules and thin films and a wide range of reactions have been investigated including oxidation, hydrogenation, carbon-carbon coupling and carbon-hetero atom cross-coupling. Polystyrene-gold and polystyrene-platinum nanocomposites were prepared via polymer incarceration method and used in multiphase redox reactions using molecular hydrogen and molecular oxygen under mild conditions.[177] Palladium/Nafion nanocomposites revealed a high activity in oxygen reduction and hydrogen oxidation reactions.[178] Silver and gold nanoparticles incorporated into polyurethane foams or polyacrylonitrile/polyamide fibers were successfully employed in the reduction of 4-nitrophenol by $NaBH_4$.[179]

Resins are cross-linked polymers which are not soluble in commonly used organic solvents. Platinum nanoparticles in poly(*N*-isopropylacrylamide) based resins show higher activity and reusability compared to the conventional Pt/C catalyst in the hydrogenation of allyl alcohol.[180] Stereoselectivity of resin-supported metal catalysts in the hydrogenation of 1,2-dimethylcyclohexene was investigated using Pd/resin catalysts; different ratios of *cis*- and *trans*-isomers were achieved depending on the pressure of hydrogen gas used.[181]

Microgel-stabilized metal nanoparticles exhibit the advantages of both homogeneous and heterogeneous catalysts, such as high activity and easy separation for reuse.[182] Metal nanoparticles supported on microgel can efficiently catalyze the aerobic oxidation of benzyl alcohol at room temperature and are used in the catalytic hydrogenation of 4-nitrophenol.[183]

Honeycomb-like thin films of polystyrene-block-poly(2-vinylpyridine) embedded with gold or silver nanoparticles,[184] and free-standing films of platinum nanoparticle embedded in poly(2-vinylpyridine) (P2VP)[185] were employed in the reduction of 4-nitrophenol. Utilization of metal nanoparticle-embedded polymer thin films in various organic transformations will be discussed in Chapters 2 and 3.

1.5 Surface Enhanced Raman Scattering

We describe in this section, the basic concepts of Raman spectroscopy, the different approaches used to enhance the Raman signals, in particular surface and tip enhanced Raman scattering (SERS and TERS) and finally, the use of metal nanoparticles as efficient SERS substrates.

1.5.1 *Raman Spectroscopy*

When light interacts with matter, some of the intensity gets absorbed and some scattered, and the remaining gets transmitted. Raman spectroscopy deals with the vibrational and rotational transitions by examining the frequencies present in the radiation scattered by molecules. Among the incident photons that collide with the

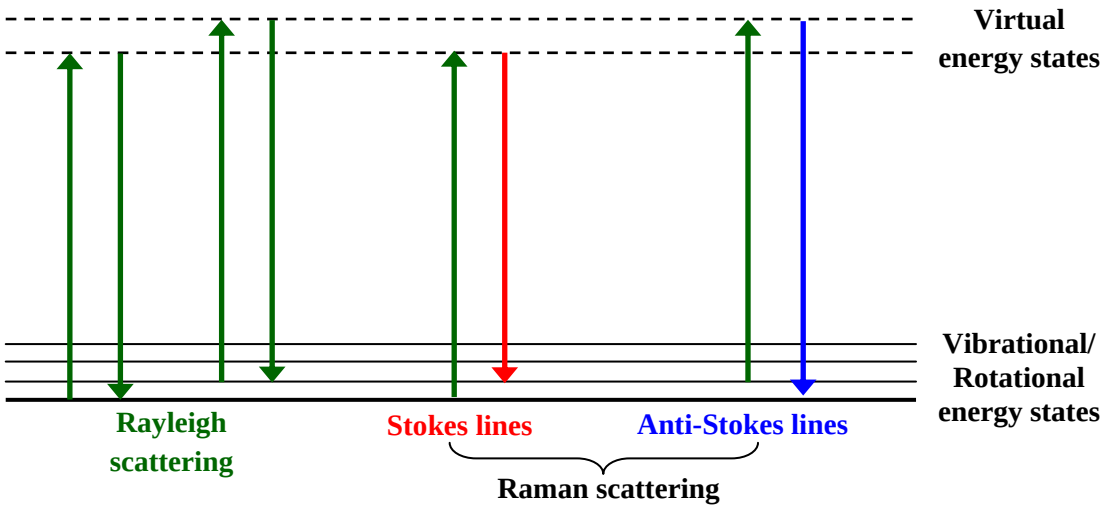

Figure 1. 8 *A schematic illustration of different cases of light scattering by molecules.*

molecules, most are scattered back without change in their energy (Rayleigh scattering); only a very small number of photons exchange their energy with the molecules leading to inelastic scattering or Raman scattering. The light can give up or take up some of the energy from the molecules on which it is incident and emerge with a lower (Stokes radiation or Stokes shift) or higher frequency (anti-Stokes radiation or anti-Stokes shift) (Fig. 1.8). As SERS mostly deals with vibrational Raman spectroscopy rather than rotational Raman spectroscopy, further discussion is focused on the former.

The basic requirement for vibrational Raman transition is that the polarizability (α) should change as the molecule vibrates. The selection rule according to classical physics is derived in Box 1.1. The molecules which are in the vibronic ground state (ν_0) shows Stokes shift and the molecules in the excited vibronic states show anti- Stokes shift; even though both the shifts are equal with opposite sign, the higher intensity Stokes shifts were usually measured experimentally.

As only a very small fraction of the incident photons get Raman scattered, the Raman signal is generally very weak and difficult to detect. Hence several techniques of sample preparation, sample illumination and scattered light detection have been developed for enhancing the intensity of the Raman signal.

Stimulated Raman scattering is an example of non-linear Raman spectroscopy. Very strong laser pulses with an electric field strength $>10^9$ Vcm^{-1} are used. The strongest mode in the regular Raman spectrum is amplified about four-to-five orders of magnitude, while the weaker Raman-active modes are not observed.

Coherent anti-Stokes Raman spectroscopy (CARS) is another type of non-linear Raman spectroscopy. It uses two coherent laser beams in order to produce an anti-Stokes frequency signal. Frequency of the first laser ν_1 is usually fixed and the frequency of the second one is tuned. When the frequency difference between the two lasers ν_2-ν_1 exactly equals the frequency of some Raman active mode of interest ν_m, then a strong light with frequency $\nu_1+\nu_m$ is emitted. This particular mode will be the only strong mode in the Raman signal.

Box 1.1

The electric field strength (E) of the electromagnetic wave (incident light or laser beam) fluctuates with time (t) as shown in Eq. (1):

$$E = E_o \cos 2\pi\nu_o t \qquad (1)$$

where, E_o is the amplitude and ν_o the frequency of the light. If a molecule is irradiated by this light, an electric dipole moment P is induced in it, as shown in Eq. (2):

$$P = \alpha * E$$

from equation (1) $P = \alpha * E_o \cos 2\pi\nu_o t \qquad (2)$

Here, α is the proportionality constant and is called the polarizability. If the molecule is vibrating with a frequency ν_m, the nuclear displacement q (assuming harmonic vibration) is given by

$$q = q_o \cos 2\pi\nu_m t \qquad (3)$$

where, q_o is the vibrational amplitude. For small amplitude of vibration, α is a linear function of q. Thus, we can write

$$\alpha = \alpha_o + [\partial\alpha/\partial q]_o\, q + \ldots\ldots \qquad (4)$$

Here, α_o is the polarizability at the equilibrium position, and $[\partial\alpha/\partial q]$ is the rate of change of α with respect to the change in *q*, evaluated at the equilibrium position.

Combining (2) with (3) and (4), we obtain

$$P = \alpha * E_o \cos 2\pi\nu_o t$$

$$= \alpha_o * E_o \cos 2\pi\nu_o t + [\partial\alpha/\partial q]_o\, q * E_o \cos 2\pi\nu_o t$$

$$= \alpha_o * E_o \cos 2\pi\nu_o t + [\partial\alpha/\partial q]_o * q_o \cos 2\pi\nu_m t * E_o \cos 2\pi\nu_o t$$

$$= \alpha_o * E_o \cos 2\pi\nu_o t + (\tfrac{1}{2})[\partial\alpha/\partial q]_o\, q_o\, E_o\, [\cos\{2\pi(\nu_o + \nu_m)t\} + \cos\{2\pi(\nu_o - \nu_m)t\}]$$

The first term represents an oscillating dipole that radiates light of frequency ν_o (Rayleigh scattering), while the second term corresponds to the Raman scattering of frequencies $\nu_o + \nu_m$ (anti-Stokes) and $\nu_o - \nu_m$ (Stokes). If $[\partial\alpha/\partial q]_o$ is zero, the vibration is not Raman-active. In other words, a mode is Raman-active, only if the polarizability (α) changes as the molecule vibrates.

Resonance Raman (RR) scattering is used to acquire very specific information about the molecule by exciting at an energy that corresponds to an electronic transition of the chromophoric group in the molecule. Under these conditions, the intensities of

Raman bands originating in this chromophore are selectively enhanced three-to-five orders of magnitude. This selectivity is important not only for identifying vibrations of this particular chromophore in a complex spectrum, but also for locating its electronic transitions in an absorption spectrum. This is particularly advantageous in vibrational studies of large biological molecules containing chromophoric groups.

1.5.2 *Surface-enhanced Raman Scattering (SERS)*

This is one of the most popular methods of enhancing the intensity of a Raman spectrum. The intensity of Raman scattering from molecules adsorbed on rough metal surfaces or on nanostructures is considerably enhanced. SERS offers significant improvement of the signal-to-noise ratio in Raman experiments. Intensity of the Raman signal is proportional to the square of the electric dipole moment P (= α * E). Hence, the enhancement of polarizability (α) or electrical field (E) or both can lead to the SERS phenomenon. The enhancement of polarizability may arise because of charge-transfer or bond formation between the metal surface and the probe molecule; this is commonly called the chemical enhancement. The second one takes into account the interaction of the incident laser beam with the rough metal surface or metal micro/nano particles. The electromagnetic wave excites the conduction electrons at the metal surface giving rise to a surface plasma resonance. This is believed to be the reason for the strong enhancement of the electric field in the vicinity of the probe molecule and hence the intensity of the Raman signal; this effect is known as the electromagnetic enhancement. SERS has wide application potential in various fields of research including surface sciences, electrochemistry, analytical chemistry, biological and biomedical sciences and forensic science.[186]

Raman signals that are generally very weak and unnoticeable in the normal Raman spectrum can often be clearly observed through the SERS. However, some of the peaks which appear in the conventional Raman spectrum may not be present in SERS, due to specific chemical interactions with the metal surface. The non-linear character of signal intensity as a function of concentration is another issue to be

considered. Surface enhanced resonance Raman spectroscopy (SERRS) technique utilizes both the surface enhancement effect and the Raman resonance effect, so that the resulting enhancement in the signal intensity can be very high and the resemblance to the regular resonance Raman spectra, makes it much easier to interpret.

Tip enhanced Raman spectroscopy (TERS) is a near-field optical technique that uses a metallic (usually silver-/gold-coated AFM or STM) tip, which is illuminated with a focused, diffraction-limited excitation beam to enhance the Raman signals of molecules situated in its vicinity. The tip can be scanned across a sample surface and acts as a near-field light source. In TERS the enhancement originates from a single enhancing metallic nanostructure at the end of the SPM tip, whereas in SERS several "hot spots" contribute, leading to an averaged spectrum. The spatial resolution in TERS is approximately the size of the tip apex (20-30 nm). TERS has been shown to have sensitivity down to the single molecule level and holds great promise for bioanalysis applications.[187] However, due to the high reactivity, chemical degradation of the tip over time is quite possible.[188] Degradation due to mechanical factors[189] and local heating by laser[190] are also practical problems. Cost and sophistication of the instrumentation and difficulty involved in using liquid samples are some of the other drawbacks of TERS.

SERS is a simple, cost effective, efficient and widely explored technique. While various nanostructures have been used as SERS substrates, metal nanoparticles is one of the favourite. A wide range of metal nanoparticle based SERS substrates have been developed in recent years.

1.5.3 *Metal Nanoparticles as SERS Substrates*

Noble metals such as silver and gold in the form of nanoparticles are well suited for the preparation of SERS substrates as we can excite their localised surface plasmons at visible wavelengths. The first observation of enhanced Raman signal was on pyridine molecules adsorbed on a silver electrode roughened by means of successive oxidation and reduction cycles.[191] This enhancement effect was studied independently by

Jeanmaire et al.[192] and Albrecht et al.[193] in 1977; they proposed different mechanisms. While the former invoked an electromagnetic effect as the cause of the enhancement, the latter involved a chemical enhancement factor, due to the electronic coupling of molecules adsorbed on the roughened metal surface. The issue continues to be debated.

The Raman signal enhancement is maximized when the metal grains with optimised structure are smaller than the incident laser wavelength.[194] Such plasmonic nanostructures have a very high local optical field in the vicinity of sharp edges and corners; these are called SERS hotspots and cause tremendous enhancement in the Raman signals.[195] An important aspect of single molecule SERS is the localization of molecules in SERS hot-spots leading to high sensitivity.

Nanostructures with various shapes have been prepared as SERS substrates. The traditional substrates used for SERS were primarily based on chemically synthesized spherical gold and silver nanoparticles.[196,197] The inter particle junction is essentially a SERS hot-spot.[198] Even single molecules can be detected with these nanosphere junctions, and the associated hot-spots.[197,199,200] Silver nanosphere dimers generated by a simple chemical synthesis are well-defined systems to study SERS hot-spots.[200] Another important category of nanoparticles used are the core-shell nanostructures, or the nanoshells.[201] Plasmonic structures such as cubes or truncated cubes, triangles, pyramids, rods and wires have been developed for SERS. Isolated silver nanocubes with sharp and truncated edges[202] was studied using 1,4-benzenedithiol as the probe molecule and a linearly polarized 514 nm laser as the excitation source. SERS hot-spots can be isolated and probed by bringing two silver nanocubes close to each other.[203] Nanotriangles or nano-triangular patterns having sharp edges at their vertices with strong localized fields can be harnessed for SERS applications.[204] Gold nanopyramids and their assemblies produce efficient SERS substrates.[205] SERS properties of individual nanorods and their assembly have been investigated.[206] Nanowire based substrates allow remote excitation of Raman scattering.[207] Nanowires have also been utilized to create SERS hotspots by forming junctions between the nanowires[208] or between the nanowire and another plasmonic nanostructure.[209]

Transition metal nanoparticles generally show lower activity compared to noble metal nanoparticles. A strategy based on "borrowing SERS" was proposed in the 1980's, either by depositing SERS-active metals onto inactive substrates[210] or by depositing inactive materials over SERS-active substrates.[211] Transition metals themselves are also used as SERS substrates. Studies on Raman signals from adsorbates on porous Nickel, Titanium, and Cobalt films have been reported.[212] Iron nanoparticles have also been reported to be SERS active.[213] SERS active metal surfaces can be created by methods such as roughening[214] and chemical etching.[215]

SERS substrates based on nanoparticles can be prepared by a variety of methods including drop-casting/spin-coating the solutions, lithographic (electron, ion beam) embedding in polymer matrices,[216] adsorbing on filter paper and ink-jet printed cellulose paper.[217]

The important parameters that characterizes the efficiency of a SERS substrates is the enhancement factor it provides for the Raman signal from the probe molecule.[218] From an application point of view, the critical requirement is to prepare substrates with high enhancement factors and good reproducibility. The SERS intensity depends significantly on the optical properties of the substrate/nanostructures. This can be tuned by varying the size, shape and spacing of the nanostructures. Additional issues such as the lifetime and stability of the substrate, target molecule compatibility and the facility of performing SERS in varied chemical environments need to be addressed. Depending on the nature of the applications, either good reproducibility or high enhancement may be required. In the case of isotropic structures the enhancement across the structure is uniform, however, the enhancement may not be high. In the case of anisotropic structures, the signal produced is strongly nonlinear and hence the enhancement is high, but this normally comes at a cost of non uniform responses. This situation has been referred to as the 'SERS uncertainty principle', and expressed as: 'substrate reproducibility' × 'enhancement factor' = constant.[219] In view of this, when SERS is applied to real analytical problems, a balance between reproducibility and enhancement needs to be optimised.

The ideal characteristics of a SERS substrate for practical applications has been discussed by Natan et.al.[220] The substrate size should be at least 10 mm^2 with the spot-to-spot reproducibility across the whole area better than 20%. Signals measured for at least three non-resonant analytes over a month should show less than 20% variation. The enhancement factor should be better than 10^5 and additional criteria such as the cost, ease of preparation and ease of use of the substrate should be considered. Polymer-metal nanocomposites promise some of the ideal characteristics of SERS substrates as discussed in Chapter 4.

1.6 Layout of the Thesis

The main objectives of this thesis is to optimize the protocol developed in our laboratory for the *in situ* generation of metal nanoparticles inside polymer films and explore the utility of these metal nanoparticle-embedded polymer thin films in catalytic applications and as SERS substrates. Our fabrication protocol is simple, convenient and environmentally benign. We use aqueous or alcoholic medium and mild thermal annealing or photochemical methods for the soft chemical processes involved. Poly(vinyl alcohol) (PVA) or poly(vinyl butyral-co-vinyl acetate-co-vinyl alcohol) (PVVV) are the preferred polymers; they have excellent film forming capability, are hydrogels and biodegradable, and capable of acting as the reducing agent for noble metal ions and stabilizers for the generated nanoparticles. We present our investigations on the use of Ag-PVA and Pd-PVA multilayer films as efficient 'dip catalysts' in several organic transformations and Ag-PVA and Ag-PVVV films as efficient SERS substrates. The thesis is organized into five chapters. Following the introductory material presented in the previous sections of this chapter, we outline the salient features of the subsequent chapters below.

Chapter 2:

This chapter describes the development of a simple multilayer-film design and a convenient protocol for its fabrication through the *in situ* formation of silver

nanoparticles inside PVA film for application as a 'dip catalyst' in the reduction of 4-nitrophenol by sodium borohydride. An efficient, robust and recyclable catalyst was developed by careful selection of the polymer and optimization of the silver-polymer ratio. The catalyst composition and parameters such as the ratio of reactants were optimized in order to realize efficient catalysis. The kinetics of the catalytic reaction under different conditions was investigated. The unique advantage of convenient catalyst monitoring is illustrated by the periodic spectroscopy and microscopy studies of the thin film, which revealed the basis of its durability. A plausible mechanism for the action of catalyst is proposed in the last part of the chapter.

Chapter 3:

Extension of the methodology developed in chapter 2 to the development of a 'dip catalyst' based on palladium nanoparticle for the Suzuki−Miyaura reaction is presented in this chapter. The fabrication parameters for the Pd-PVA film were optimized for enhanced catalyst efficiency, and the thin film was characterized in detail through spectroscopy, and microscopy. The thin film 'dip catalyst' was gainfully employed in the Suzuki−Miyaura reaction of iodobenzene with phenylboronic acid providing a very high yield, TON and TOF, and the possibility of scale up. Extensive recycling capability and the unique advantage of convenient catalyst monitoring between reuse cycles could be demonstrated. In order to integrate the various significant and quantifiable parameters related to the catalyst performance we defined a figure-of-merit (FOM) and a quantitative appraisal of the present catalyst in the context of the others reported in the literature is presented on the basis of the FOM.

Chapter 4:

This chapter is focused on the utility of easily fabricated polymer-metal nanocomposite thin films with *in situ* generated silver nanoparticles, as inexpensive and convenient substrates for SERS. A new silver-polymer nanocomposite thin film was developed by photoirradiation based *in situ* fabrication of the nanoparticles inside

PVVV film. Raman scattering experiments with analyte molecules such as 4-aminothiophenol and rhodamine 6G were investigated on Ag-PVA and Ag-PVVV. A unique utility of these materials as SERS substrates was demonstrated by fabricating glass capillaries with their inner walls coated with the nanocomposite thin film that can be used to pick up extremely small volumes of highly dilute analyte solutions and directly recording their Raman spectra.

Chapter 5:

The final chapter presents a brief overview of the various investigations in this thesis and highlights the significant achievements of the new explorations. The highlights of the work include: (i) the development of the concept of a 'dip catalyst' based on polymer-metal nanocomposite thin films, (ii) the specific design of multilayer thin films with *in situ* generated silver and palladium nanoparticles and the optimization of a simple, convenient and environmentally benign protocol for their fabrication, (iii) the demonstration of the reusability of these catalysts in organic reactions and the unique advantage of the films in catalyst monitoring and (iv) the exploration of the applications of the *in situ* fabricated nanocomposite thin films as substrates and coatings for SERS.

The new directions in which the present studies can be expanded and evolved are also discussed in this chapter.

References:

1. Lövestam, G.; Rauscher, H.; Roebben, G.; Klüttgen, B. S.; Gibson, N.; Putaud, J.-P.; Stamm, H. *Considerations on a Definition of Nanomaterial for Regulatory Purposes*, JRC Reference Reports, **2010**.

2. (a) Pitkethly, M. J. *Nano Today* **2004**, *20*. (b) Mansoori, G. A.; Soelaiman, T. A. F. *J. ASTM Int.* **2005**, *2*. (DOI: 10.1520/JAI13110)

3. Valden, M.; Lai, X.; Goodman, D. W. *Science* **1998**, *281*, 1647.

4. Morones, J. R.; Elechiguerra1, J. L.; Camacho, A.; Holt, K.; Kouri, J. B.; Ramirez, J. T.; Yacaman, M. J. *Nanotechnology* **2005**, *16*, 2346.

5. (a) Sharma, B.; Frontiera, R. R.; Henry, A.; Ringe, E.; Van Duyne, R. P. *Mater. Today* **2012**, *15*, 16. (b) Graham, D. *Angew. Chem. Int. Ed.* **2010**, *49*, 9325. (c) Lombardi, J. R.; Birke, R. L. *Acc. Chem. Res.* **2009**, *42*, 734. (d) Li, L.; Hutter, T.; Steinerc, U.; Mahajan, S. *Analyst* **2013**, *138*, 4574.

6. (a) Daniel, M.-C.; Astruc, D. *Chem. Rev.* **2004**, *104*, 293. (b) Freestone, I.; Meeks, N.; Sax, M.; Higgitt, C. *Gold Bull.* **2007**, *40*, 270.

7. Moore, N. H. *Old glass*, Tudor, New York, **1935**.

8. Faraday, M. *R. Phil. Trans. R. Soc. Lond.* **1857**, *147*, 145.

9. Maxwell-Garnett, J. C. *Phil. Trans. R. Soc. Lond. A* **1904**, *203*, 385.

10. Mie, G. *Ann. d. Physik* **1908**, *25*, 377.

11. Binnig, G. K.; Quate, C. F.; Gerber. Ch. *Phys. Rev. Lett.* **1986**, *56*, 930.

12. (a) Brust, M.; Walker, M.; Bethell, D.; Schiffrin, D. J.; Whyman, R. J. *J. Chem. Soc. Chem. Commun.* **1994**, 801. (b) Daniel, M.-C.; Astruc, D. *Chem. Rev.* **2004**, *104*, 293.

13. Klabunde, K. J. *Nanoscale Materials in Chemistry*, John Wiley: New York, **2001**.

14. (a) Gleiter, H. *Nanostruct. Mater.* **1995**, *6*, 3. (b) Gleiter, H. *Acta Mater* **2000**, *48*, 1. (c) Gusev, A. I.; Rempel, A. A. *Nanocrystalline Materials*, Cambridge International Science Publishing, **2004**.

15. Schmid, G. *Clusters and Colloids - From Theory to Applications*, VCH: Weinheim, Germany, **1994**.

16. Ghosh, S. K.; Pal, T. *Chem. Rev.* **2007**, *107*, 4797.

17. (a) Kreibig, U.; Vollmer, M. *Optical Properties of Metal Clusters*, Springer: New York, **1995** (b) Jain, P. K.; Lee, K. S.; El-Sayed, I. H.; El-Sayed, M. A. *J. Phys. Chem. B* **2006**, *110*, 7238.

18. Kelly, K. L.; Coronado, E.; Zhao L. L.; Schatz, G. C. *J. Phys. Chem. B* **2003**, *107*, 668.

19. Kreibig, U.; Vollmer, M. *Optical Properties of Metal Clusters*, Springer, Berlin, **1995,** *25*.

20. Link, S.; El-Sayed, M. A. *Annu. Rev. Phys. Chem.* **2003**, *54*, 331.

21. Jain, P. K.; Huang, X.; El-Sayed, I. H.; El-Sayed, M. A. *Plasmonics* **2007**, *2*,107.

22. Berciaud, S.; Cognet, L.; Tamarat, P.; Lounis, B. *Nano Lett*. **2005**, *5*, 515.

23. (a) Mitsuishi, M.; Ishifuji, M.; Endo, H.; Tanaka, H.; Miyashita, T. *Polym. J.* **2007**, *39*, 411. (b) Barnes, W. L.; Dereux, A.; Ebbesen, T. W. *Nature* **2003**, *424*, 824.

24. (a) Haes, A. J.; Van Duyne, R. P. *Expert Rev. Mol. Diagn.* **2004**, *4*, 527.

25. Homola, J.; Yee, S. S.; Gauglitz, G. *Sensors and Actuators B* **1999**, *54*, 3.

26. Heiz, U.; Landman, U. *Nanocatalysis*, Springer, Berlin, **2007**.

27. Witham, C. A.; Huang, W.; Tsung, C.; Kuhn, J. N.; Somorjai G. A.; Toste, F. D. *Nat. Chem.* **2010**, *2*, 36.

28. Schmid, G. *Chem. Rev*. **1992**, *92*, 1709.

29. Roucoux, A.; Schulz, J.; Patin, H. *Chem. Rev*. **2002**, *102*, 3757.

30. Shylesh, S.; Schnemann, V.; Thiel, W. R. *Angew. Chem. Int. Ed.* **2010**, *49*, 3428.

31. Samim, M.; Kaushik, N. K.; Maitra, A. *Bull. Mater. Sci.* **2007**, *30*, 535.

32. Isaifan, R. J.; Ntais, S.; Baranova, E. A. *Appl. Catal. A* **2013**, *464*, 87.

33. Bratlie, K. M.; Lee, H.; Komvopoulos, K.; Yang, P.; Somorjai, G. A. *Nano Lett.* **2007,** *7*, 3097.

34. Xiong, Y.; Wiley, B. J.; Xia, Y. *Angew. Chem. Int. Ed.* **2007**, *46*, 7157.

35. Mahmoud, M. A.; Narayanan, R.; El-Sayed, M. A. *Acc. Chem. Res.* **2013**, *46*, 1795**.**

36. Bönnemann, H.; Brijoux, W.; Siepen, K.; Hormes, J.; Franke, R.; Pollmann, J.; Rothe, J. *Appl. Organomet. Chem.* **1997**, *11*, 783.

37. Chen, C. W.; Serizawa, T.; Akashi, M. *Chem. Mater.* **1999**, *11*, 1381.

38. Hirai, H.; Nakao, Y.; Toshima, N. *J. Macromol. Sci. Chem.* **1978**, *A12*, 1117.

39. Hirai, H.; Chawanya, H.; Toshima, N. *React. Polym.* **1986**, *3*, 127.

40. Toshima, N.; Takahashi, T.; Yonezawa, T.; Hirai, H. *J. Macromol. Sci. Chem. A* **1988**, *25*, 669.

41. Li, Y.; Hong, X. M.; Collard, D. M.; El-Sayed, M. A. *Org. Lett.* **2000**, *2*, 2385.

42. Li, Y.; El-Sayed, M. A. *J. Phys. Chem. B* **2001**, *105*, 8938.

43. Li, Y.; Boone, E.; El-Sayed, M. A. *Langmuir* **2002**, *18*, 4921.

44. Astruc, D. *Inorg. Chem.* **2007**, *46*, 1884.

45. Balanta, A.; Godard, C.; Claver, C. *Chem. Soc. Rev.* **2011**, *40*, 4973.

46. Fukuoka, A.; Kimura, J.-I.; Oshio, T.; Sakamoto, Y.; Ichikawa, M. *J. Am. Chem. Soc.* **2007**, *129*, 10120.

47. Mallat, T.; Baiker, A. *Annu. Rev. Chem. Biomol. Eng.* **2012**, *3*, 11.

48. Verykios, X. E.; Stein, F. P.; Coughlin, R. W. *Catal. Rev. Sci. Eng.* **1980**, *22*, 197.

49. Shiraishi, Y.; Toshima, N. *Colloids Surf. A* **2000**, *169*, 59.

50. Whitesides, G. M. *Nat. Biotechnol.* **2003**, *21*, 1161.

51. Taton, T. A. *Trends Biotechnol.* **2002**, *20*, 277.

52. Parak, W. J.; Gerion, D.; Pellegrino, T.; Zanchet, D.; Micheel, C.; Williams, C. S.; Boudreau, R.; Le Gros, M. A.; Larabell, C. A.; Alivisatos, A. P. *Nanotechnology* **2003**, *14*, R15.

53. Pankhurst, Q. A.; Connolly, J.; Jones, S. K.; Dobson, J. *J. Phys. D: Appl. Phys.* **2003**, *36*, R167.

54. Huang, X.; El-Sayed, I. H.; Qian, W.; El-Sayed, M. A. *J. Am. Chem. Soc.* **2006**, *128*, 2115.

55. Yguerabide, J.; Yguerabide, E. E. *Anal. Biochem.* **1998**, *262*, 137.

56. Alivisatos, A. P. *Nat. Biotechnol*. **2004**, *22*, 47.

57. Sokolov, K.; Aaron, J.; Hsu, B.; Nida, D.; Gillanwater, A.; Follen, M.; Macaulay, C.; Adler-Storthz, K.; Korgel, B.; Discour, M.; Pasqualini, R.; Arap, W.; Lam, W.; Richartz-Kortum, R. *Technol. Cancer Res. Treat.* **2003**, *2*, 491.

58. Shan, Y.; Luo, T.; Peng, C.; Sheng, R.; Cao, A.; Cao, X.; Shen, M.; Guo, R.; Tomás, H.; Shi, X. *Biomaterials* **2012**, *33*, 3025.

59. McBain, S. C.; Yiu, H. HP.; Dobson, J. *Int. J. Nanomedicine* **2008**, *3*, 169.

60. Hirsch, L. R.; Stafford, R. J.; Bankson, J. A.; Sershen, S. R.; Rivera, B.; Price, R. E.; Hazle, J. D.; Halas, N. J.; West, J. L. *Proc. Natl. Acad. Sci.* **2003**, *100*, 13549.

61. Goodman, C. M.; McCusker, C. D.; Yilmaz, T.; Rotello, V. M. *Bioconjugate Chem.* **2004**, *15*, 897.

62. Lee, K. J.; Nallathamby, P. D.; Browning, L. M.; Osgood, C. J.; Xu, X. H. N. *ACS Nano* **2007**, *1*, 133.

63. (a) Govorov, A. O.; Richardson, H. H. *Nano Today* **2007**, *2*, 30. (b) Yoshida, J.; Kobayashi, T. *J. Magn. Magn. Mater.* **1999**, *194*, 176.

64. Loo, C.; Lowery, A.; Halas, N.; West, J.; Drezek, R. *Nano Lett.* **2005**, *5*, 709.

65. El-Sayed, I. H.; Huang, X.; El-Sayed, M. A. *Cancer Lett.* **2006**, *239*, 129.

66. Marambio-Jones, C.; Hoek, E. *Journal of Nanoparticle Research* **2010**, *12*, 1531.

67. Ma, J.; Wong, H.; Kong, L. B.; Peng, K. W. *Nanotechnology* **2003**, *14*, 619.

68. Takagi, M. *J. Phys. Soc. Jpn*. **1954**, *9*, 359.

69. Ramesh, G. V.; Prasad, M. D.; Radhakrishnan, T. P. *Chem. Mater.* **2011**, *23*, 5231.

70. Chen, Q.; Zhang, Z. J. *Appl. Phys. Lett.* **1998**, *73*, 3156.

71. Zhang, X. X.; Tejata, J.; Hernandez, J. M.; Ziolo, R. F. *Nanostruct. Mater.* **1997**, *9*, 301.

72. (a) Menendez, J. L.; Bescos, B.; Armelles, G.; Serna, R.; Gonzalo, J.; Doole, R.; Petford-Long, A. K.; Alonso, M. I. *Phys. Rev. B* **2002**, *65*, 205413. (b) Shemer, G.; Markovich, G. *J. Phys. Chem. B* **2002**, *106*, 9195.

73. (a) Fiete, G. A.; Zarand, G.; Halperin, B. I.; Oreg, Y. *Phys. Rev. B* **2002**, *66*, 024431. (b) Weymann, I.; Barnas, J.; Martinek, J. *J. Supercond. Novel Magn.* **2003**, *16*, 1.

74. Ponder, S. M.; Darab, J. G.; Mallouk, T. E. *Environ. Sci. Technol.* **2000**, *34*, 2564.

75. Elliott, D. W.; Zhang, W. X. *Environ. Sci. Technol.* **2001**, *35*, 4922.

76. (a) Johnson, S. R.; Evans, S. D.; Brydson, R. *Langmuir* **1998**, *14*, 6639. (b) Chen, S.; Murray, R. W. *Langmuir* **1999**, *15*, 682. (c) Ganguli, M.; Jayachandran, K. N.; Maiti, S. *J. Am. Chem. Soc*. **2004**, *126*, 26.

77. (a) Aslam, M.; Mulla, I. S.; Vijayamohanana, K. *Appl. Phys. Lett.* **2001**, *79*, 689. (b) Doty, R. C.; Yu, H.; Shih, C. K.; Korgel, B. A. *J. Phys. Chem. B* **2001**, *105*, 8291.

78. (a) Stewart, D. R.; Ohlberg, D. A. A.; Beck, P. A.; Chen, Y.; Williams, R. S.; Jeppesen, J. O.; Nielsen, K. A.; Stoddart, J. F. *Nano Lett.* **2004**, *4*, 133. (b) Lau, C. N.; Stewart, D. R.; Williams, R. S.; Bockrath, M. *Nano Lett.* **2004**, *4*, 569.

79. Cheng, S.; Spenser, J. A.; Milligan, W. W. *Acta Mater.* **2003**, *51*, 4505.

80. Ma, E. *JOM* **2006**, *58*, 49.

81. Youssef, K. M.; Scattergood, R. O.; Murty, K. L. *Appl. Phys. Lett.* **2005**, *87*, 091904.

82. Zhao, Y.-H.; Bingert, J. F.; Liao, X.-Z.; Cui, B.-Z.; Han, K.; Sergueeva, A. V.; Mukherjee, A. K.; Valiev, R. Z.; Langdon, T. G.; Zhu, Y. T. *Adv. Mater.* **2006**, *18*, 2949.

83. Rechberger, W.; Hohenau, A.; Leitner, A.; Krenn, J. R.; Lamprecht, B.; Aussenegg, F. R. *Opt. Commun.* **2003**, *220*, 137.

84. Grand, J.; Adam, P. M.; Grimault, A. S.; Vial, A.; de la Chapelle, M. L.; Bijeon, J. L.; Kostcheev, S.; Royer, P. *Plasmonics* **2006**, *1*, 135.

85. Ohno, T.; Bain, J. A.; Schlesinger, T. E. *J. Appl. Phys.* **2007**, *101*, 083107.

86. (a) Niidome, Y.; Hori, A.; Sato, T.; Yamada, S. *Chem. Lett.* **2000**, *29*, 310. (b) Mallik, K.; Mandal, M.; Pradhan, N.; Pal, T. *Nano lett*. **2001**, *1*, 319. (c) Giuffrida, S.; Condorelli, G. G.; Costanzo, L. L.; Fragala, I. L.; Ventimiglia, G.; Vecchio, G. *Chem. Mater*. **2004**, *16*, 1260.

87. (a) Park, S. J.; Kim, S.; Lee, S.; Khim, Z. G.; Char, K.; Hyeon, T. *J. Am. Chem. Soc.* **2000**, *122*, 8581. (b) Teranishi, T.; Hasegaqa, S.; Shimuzu, T.; Miyake, M. *Adv. Mater.* **2001**, *13*, 1699. (c) Puntes, V. F.; Krishnan, K. M.; Alivisatos, A. P. *Science* **2001**, *291*, 2115. (d) Smith, T. W.; Wychick, D. *J. Phys. Chem.* **1980**, *84*, 1621.

88. (a) Henglein, A.; Meisel, D. *Langmuir* **1998**, *14*, 7392. (b) Henglein, A. *J. Phys. Chem. B* **2000**, *104*, 1206. (c) Doudna, C. M.; Bertino, M. F.; Blum, F. D.; Tokuhiro, A.; Lahiridey, T. D.; Chattopadhyay, S.; Terry, J. *J. Phys. Chem. B* **2003**, *107*, 2966.

89. Hayashi, Y.; Takizawa, H.; Inoue, M.; Niihara, K.; Suganuma, K. *IEEE Trans. Electron Packag. Manuf.* **2005**, *28*, 338.

90. (a) Boutonnet, M.; Kizling, J.; Stenius, P.; Maire, G. *Colloids Surf.* **1982**, *5*, 209. (b) Nickel, U.; Castell, A.; Pöppl, K.; Schneider, S. *Langmuir* **2000**, *16*, 9087. (c) Zhao, M. Q.; Crooks, R. M. *Chem. Mater.* **1999**, *11*, 3379. (d) Pillai, Z. S.; Kamat, P. V. *J. Phys. Chem. B* **2004**, *108*, 945. (e) Gutiérrez-Wing, C.; Velázquez-Salazar, J. J.; José-Yacamán, M. *Methods Mol. Biol.* **2012**, *906*, 3. (f) Raveendran, P.; Fu, J.; Wallen, S. L. *J. Am. Chem. Soc.* **2003**, *125*, 13940. (g) Filice, M.; Marciello, M.; Morales, M. P.; Palomo, J. M. *Chem. Commun.* **2013**, *49*, 6876. (h) Mittal, A. K.; Chisti, Y.; Banerjee, U. C. *Biotechnol. Adv.* **2013,** *31*, 346.

91. (a) Teranishi, T.; Miyake, M. *Chem. Mater.* **1998**, *10*, 594. (b) Díaz-Álvarez, A. E.; Cadierno, V. *Appl. Sci.* **2013**, *3*, 55.

92. Stepanov, A. L. *Tech. Phys.* **2004**, *49*, 143.

93. (a) Mbhele, Z. H.; Salemane, M. G.; van Sittert, C. G. C. E.; Nedeljković, J. M.; Djoković, V.; Luyt, A. S. *Chem. Mater.* **2003**, *15*, 5019. (b) Mendoza, C.; Pietsch, T.; Gutmann, J. S.; Jehnichen, D.; Gindy, N.; Fahmi, A. *Macromolecules* **2009**, *42*, 1203.

94. Arceo, A.; Meli, L.; Green, P. F. *Nano Lett.* **2008**, *8*, 2271.

95. Heilmann, A. *Polymer Films with Embedded Metal Nanoparticles*, Springer, **2003**.

96. (a) Faupel, F.; Zaporojtchenko, V.; Strunskus, T.; Elbahri, M. *Adv. Eng. Mater.* **2010**, *12*, 1177. (b) Faupel, F.; Zaporojtchenko, V.; Greve, H.; Schürmann, U.; Chakravadhanula, V. S. K.; Hanisch, Ch.; Kulkarni, A.; Gerber, A.; Quandt, E.; Podschun, R. *Contr. Plasma Phys.* **2007**, *47*, 537.

97. (a) Sih, B. C.; Wolf, M. O. *Chem. Commun.* **2005**, 3375. (b) Sangermano, M.; Yagci, Y.; Rizza, G. *Macromolecules* **2007**, *40*, 8827. (c) Feng, J.-J.; Zhang, P.-P.; Wang, A.-J.; Liao, Q.-C.; Xi, J.-L.; Chen, J.-R. *New J. Chem.* **2012**, *36*, 148.

98. Won, J.; Ihn, K. J.; Kang, Y. S. *Langmuir* **2002**, *18*, 8246.

99. Korchev, A. S.; Bozack, M. J.; Slaten, B. L.; Mills, G. *J. Am. Chem. Soc.* **2004**, *126*, 10.

100. Li, J.; Kamata, K.; Watanabe, S.; Iyoda, T. *Adv. Mater.* **2007**, *19*, 1267.

101. Sohn, B.; Seo, B.; Yoo, S. *J. Mater. Chem.* **2002**, *12*, 1730.

102. Horiuchi, S.; Nakao, Y. *Curr. Nanosci.*, **2007**, *3*, 206.

103. Shang, L.; Wang, Y.; Huang, L.; Dong, S. *Langmuir* **2007**, *23*, 7738.

104. Fritzsche, W.; Porwol, H.; Wiegand, A.; Bornmann, S.; Köhler, J. M. *Nanostr. Mater.* **1998**, *10*, 89.

105. Porel, S.; Singh, S.; Harsha, S. S.; Rao, D. N.; Radhakrishnan, T. P. *Chem. Mater.* **2005**, *17*, 9.

106. Porel, S.; Singh, S.; Radhakrishnan, T. P. *Chem. Commun.* **2005**, 2387.

107. Porel, S.; Hebalkar, N.; Sreedhar, B.; Radhakrishnan, T. P. *Adv. Funct. Mater.* **2007**, *17*, 2550.

108. Deshmukh, R. D.; Composto, R. J. *Chem. Mater.* **2007**, *19*, 745.

109. Ramesh, G. V.; Sreedhar, B.; Radhakrishnan, T. P. *Phys. Chem. Chem. Phys.* **2009**, *11*, 10059.

110. Pucci, A.; Bernabò, M.; Elvati, P.; Meza, L. I.; Galembeck, F.; de Paula Leite, C. A.; Tirelli, N.; Ruggeriab, G. *J. Mater. Chem.* **2006**, *16*, 1058.

111. Hasell, T.; Lagonigro, L.; Peacock, A. C.; Yoda, S.; Brown, P. D.; Sazio, P. J. A.; Howdle, S. M. *Adv. Funct. Mater.* **2008**, *18*, 1265.

112. Hariprasad, E.; Radhakrishnan, T. P. *ACS Catal*. **2012**, *2*, 1179.

113. Won, J.; Ihn, K. J.; Kang, Y. S. *Langmuir* **2002**, *18*, 8246.

114. Silva, A. M. B.; de Araujo, C. B.; Santos-Silva, S.; Galembeck, A. *J. Phys. Chem. Solids* **2007**, *68*, 729.

115. Sakamoto, M.; Tachikawa, T.; Fujitsuka, M.; Majima, T. *Adv. Funct. Mater.* **2007**, *17*, 857

116. Clémenson, S.; David, L.; Espuche, E. *J. Polym. Sci. A* **2007**, *45*, 2657.

117. Oates, T. W. H.; Christalle, E. *J. Phys. Chem. C* **2007**, *111*, 182.

118. Porel, S.; Venkatram, N.; Rao, D. N.; Radhakrishnan, T. P. *J. Appl. Phys.* **2007**, *102*, 033107.

119. Karthikeyan, B. *Physica B* **2005**, *364*, 328.

120. Karthikeyan, B.; Anija, M.; Philip, R. *Appl. Phys. Lett.* **2006**, *88*, 053104.

121. Karthikeyan, B.; Anija, M.; Venkatesan, P.; Sandeep, C. S. S.; Philip, R. *Optics Commun.* **2007**, *280*, 482.

122. Ramesh, G. V.; Sudheendran, K.; Raju, K. C. J.; Sreedhar, B.; Radhakrishnan, T. P. *J. Nanosci. Nanotech.* **2009**, *9*, 261.

123. Meng, X.; Fujita, K.; Zong, Y.; Murai, S.; Tanaka, K. *Appl. Phys. Lett.* **2008**, *92*, 20112.

124. Yu, D.-G.; Lin, W.-C.; Lin, C.-H.; Chang, L.-M.; Yang, M.-C. *Mat. Chem. Phys.* **2007**, *101*, 93.

125. Hasell, T.; Lagonigro, L.; Peacock, A. C.; Yoda, S.; Brown, P. D.; Sazio, P. J. A.; Howdle, S. M. *Adv. Funct. Mater.* **2008**, *18*, 1265.

126. Abargues, R.; Marqués-Hueso, J.; Canet-Ferrer, J.; Pedrueza, E.; Valdés, J. L.; Jiménez, E.; Martínez-Pastor, J. P. *Nanotechnology* **2008**, *19*, 355308.

127. Marqués-Hueso, J.; Abargues, R.; Canet-Ferrer, J.; Agouram, S.; Valdés, J. L.; Martínez-Pastor, J. P. *Langmuir* **2010**, *26*, 2825.

128. Ramesh, G. V.; Radhakrishnan, T. P. *ACS Appl. Mater. Interfaces* **2011**, *3*, 988.

129. Nowack, B.; Krug, H. F.; Height, M. *Environ. Sci. Technol.* **2011**, *45*, 1177.

130. Porel, S.; Ramakrishna, D.; Hariprasad, E.; Gupta, A. D.; Radhakrishnan, T. P. *Curr. Sci.* **2011**, *101*, 927.

131. Hariprasad, E.; Radhakrishnan, T. P. *Chem. Eur. J.* **2010** *16*, 14378.

132. Bernabò, M.; Pucci, A.; Galembeck, F.; de Paula Leite, C. A.; Ruggeri, G. *Macromol. Mater. Eng.* **2009**, *294*, 256.

133. Clémenson, S.; Espuche, E.; David, L.; Léonard, D. *J. Membrane Sci. A* **2010**, *361*, 167.

134. Bönnemann, H.; Nagabhushana, K. S. *J. New. Mat. Electrochem. Systems* **2004,** *7*, 93.

135. (a) Bönnemann, H.; Richards, R. *Synth. Met. Organomet. Inorg. Chem.* **2002**, *10*, 209. (b) Thomas, J. M.; Johnson, B. F. G.; Raja, R.; Sankar, G.; Midgley, P. A. *Acc. Chem. Res.* **2003**, *36*, 20. (c) El-Sayed, M. A. *Acc. Chem. Res.* **2001**, *34*, 257. (d) Kralik, M.; Biffis, A. *J. Mol. Catal. A* **2001,** *177*, 113. (e) Kreibig, U.; Bönnemann, H.; Hormes, J. in *"Handbook of Surfaces and Interfaces of Materials";* Eds., Nalwa, H. S. Academic Press, San Diego, **2001.**

136. Beller, M.; Fischer, H.; Kuhlein, K.; Reisinger, C.-P.; Herrmann, W. A. *J. Organomet. Chem.* **1996**, *520*, 257.

137. (a) Ding, J. H.; Gin, D. L. *Polym. Prepr.* **1999**, *40*, 738. (b) Ding, J. H.; Gin, D. L. *Chem. Mater.* **2000**, *12*, 22.

138. (a) Mikami, Y.; Dhakshinamoorthy, A.; Alvaro, M.; García, H. *Catal. Sci. Technol.* **2013**, *3*, 58. (b) Tsunoyama, H.; Sakurai, H.; Negishi, Y.; Tsukuda, T. *J. Am. Chem. Soc.* **2005**, *127*, 9374. (c) Hayakawa, K.; Yoshimura, T.; Esumi, K. *Langmuir* **2003**, *19*, 5517. (d) Tsunoyama, H.; Sakurai, H.; Ichikuni, N.; Negishi, Y.; Tsukuda, T. *Langmuir* **2004**, *20*, 11293. (e) Zhu, Y.; Qian, H.; Drake, B. A.;

Jin, R. *Angew. Chem. Int. Ed.* **2010**, *49*, 1295. (f) Sau, T. K.; Pal, A.; Pal, T. *J. Phys. Chem. B* **2001**, *105*, 9266.

139. Bartholomew, C. H. *Appl. Catal. A* **2001**, *212*, 17.

140. Cao, Y.; Jin, R.; Mirkin, C. A. *J. Am. Chem. Soc.* **2001**, *123*, 7961.

141. Dai, Y.; Lim, B.; Yang, Y.; Cobley, C. M.; Li, W.; Cho, E. C.; Grayson, B.; Fanson, P. T.; Campbell, C. T.; Sun, Y.; Xia, Y. *Angew. Chem. Int. Ed.* **2010**, *49*, 8165.

142. Chen, C.; Nan, C.; Wang, D.; Su, Q.; Duan, H.; Liu, X.; Zhang, L.; Chu, D.; Song, W.; Peng, Q.; Li, Y. *Angew. Chem. Int. Ed.* **2011**, *50*, 3725.

143. Wang, S.; Zhang, M.; Zhang, W. *ACS Catal.* **2011**, *1*, 207.

144. (a) Lee, J.; Park, J. C.; Bang, J. U.; Song, H. *Chem. Mater.* **2008**, *20*, 5839. (b) Ma, Z.; Dai, S. *ACS Catal.* **2011**, *1*, 805.

145. Sun, Y.; Xia, Y. *Nano Lett.* **2003**, *3*, 1569.

146. (a) Liang, H. P.; Zhang, H. M.; Hu, J. S.; Guo, Y. G.; Wan, L. J.; Bai, C. L. *Angew. Chem. Int. Ed.* **2004**, *43*, 1540. (b) Chen, Z. W.; Waje, M.; Li, W. Z.; Yan, Y. S. *Angew. Chem. Int. Ed.* **2007**, *46*, 4060. (c) Chen, H. M.; Liu, R. S.; Lo, M. Y.; Chang, S. C.; Tsai, L. D.; Peng, Y. M.; Lee, J. F. *J. Phys. Chem. C* **2008**, *112*, 7522. (d) Guo, S. J.; Dong, S. J.; Wang, E. *Chem. Eur. J.* **2008**, *14*, 4689.

147. Chen, G.; Desinan, S.; Rosei, R.; Rosei, F.; Ma, D. *Chem. Commun.* **2012**, *48*, 8009.

148. (a) Scholten, J. D.; Leal, B. C.; Dupont, J. *ACS Catal.* **2012**, *2*, 184. (b) Xiao, C.-X.; Cai, Z.-P.; Wang, T.; Kou, Y.; Yan, N. *Angew. Chem. Int. Ed.* **2008**, *47*, 746.

149. Jutz, F.; Andanson, J. M.; Baiker, A. *J. Catal.* **2009**, *268*, 356.

150. (a) Calo, V.; Nacci, A.; Monopoli, A.; Cotugno, P. *Angew. Chem. Int. Ed.* **2009**, *48*, 6101. (b) Calo, V.; Nacci, A.; Monopoli, A.; Montingelli, F. *J. Org. Chem.* **2005**, *70*, 6040. (c) Gao, S. Y.; Zhang, H. J.; Wang, X. M.; Mai, W. P.; Peng, C. Y.; Ge, L. H. *Nanotechnology* **2005**, *16*, 1234. (d) Zhao, D. B.; Fei, Z. F.; Geldbach, T. J.; Scopelliti, R.; Dyson, P. J. *J. Am. Chem. Soc.* **2004**, *126*, 15876. (e) Calo, V.; Nacci, A.; Monopoli, A.; Cotugno, P. *Chem. Eur. J.* **2009**, *15*, 1272.

151. Wojtkow, W.; Trzeciak, A. M.; Choukroun, R.; Pellegatta, J. L. *J. Mol. Catal. A Chem.* **2004**, *224*, 81.

152. Zhu, Y. H.; Chenyan, K.; Peng, A. T.; Emi, A.; Monalisa, W.; Louis, L. K. J.; Hosmane, N. S.; Maguire, J. A. *Inorg. Chem*. **2008**, *47*, 5756.

153. Geldbach, T. J.; Zhao, D. B.; Castillo, N. C.; Laurenczy, G.; Weyershausen, B.; Dyson, P. J. *J. Am. Chem. Soc*. **2006**, *128*, 9773.

154. Calo, V.; Nacci, A.; Monopoli, A.; Damascelli, A.; Ieva, E.; Cioffi, N. *J. Organomet. Chem.* **2007**, *692*, 4397.

155. (a) Campbell, C. T. *Faraday Transactions* **1996**, *92*, 1435. (b) Iglesia, E., *Appl. Catal. A* **1997**, *161*, 59. (c) Shen, W. J.; Ichihashi, Y.; Matsumura, Y. *Catal. Lett.* **2002**, *79*, 125. (d) Matsumura, Y. S.; Ichihashi, Y.; Okumura, M. *J. Catal.* **2001**, *197*, 267. (e) de Oliveira, A. L.; Wolf, A.; Schuth, F. *Catal. Lett.* **2001**, *73*, 157. (f) Rodriguez, J. A.; Liu, G.; Jirsak, T.; Hrbek, J.; Chang, Z. P.; Dvorak, J.; Maiti, A. *J. Am. Chem. Soc.* **2002**, *124*, 5242.

156. Bond, G. C. *Heterogeneous Catalysis: Principles and Applications*, Clarendon Press, **1974**.

157. Cunningham, D. A. H.; Vogel, W.; Kageyama, H.; Tsubota, S.; Haruta, M. *J. Catal.* **1998**, *177*, 1.

158. Chen, Y.; Qiu, J.; Wang, X.; Xiu, J. *J. Catal.* **2006**, *242*, 227.

159. Bradley, J. S.; Hill, E.; Leonowicz, M. E.; Witzke, H. *J. Mol. Catal.* **1987**, *41*, 59.

160. (a) Xiao, W.; Guo, Q.; Wang, E.G. *Chem. Phys. Lett.* **2003**, *368*, 527. (b) Pfau, A.; Schierbaum, K. D. *Surf. Sci.* **1994**, *321*, 71. (c) Berner, U.; Schierbaum, K. D.; Jones, G.; Wincott, P.; Haq, S.; Thornton, G. *Surf. Sci.* **2000**, *467*, 201.

161. Haller, G. L.; Resasco, D. E. *Adv. Catal.* **1989**, *36*, 173.

162. Yamada, Y.; Tsung, C.-K.; Huang, W.; Huo, Z.; Habas, S. E.; Soejima, T.; Aliaga, C. E.; Somorjai, G. A.; Yang, P. *Nature Chem.* **2011**, *3*, 372.

163. (a) Wang, H.; Dong, Z.; Na, C. *ACS Sustainable Chem. Eng.* **2013**, *1*, 746. (b) Tan, X.; Deng, W.; Liu, M.; Zhang, Q.; Wang, Y. *Chem. Commun.* **2009**, 7179. (c) Ye, F.; Cao, X.; Yu, L.; Chen, S.; Lin, W. *Int. J. Electrochem. Sci.* **2012**, *7*, 1251.

164. (a) Králik, M.; Corain, B.; Zecca, M. *Chem. Papers* **2000**, *54*, 254. (b) Buchmeiser, M. R. *Chem. Rev.* **2009**, *109*, 303. (c) Bergbreiter, D. E.; Tian, J.; Hongfa, C. *Chem. Rev.* **2009**, *109*, 530.

165. Sobjerg, L. S.; Gauthier, D.; Lindhardt, A. T.; Bunge, M.; Finster, K.; Meyer, R. L.; Skrydstrup, T. *Green Chem.* **2009**, *11*, 2041.

166. Laska, U.; Frost, C. G.; Price, G. J.; Plucinski, P. K. *J. Catal.* **2009**, *268*, 318.

167. Sullivan, J. A.; Flanagan, K. A.; Hain, H. *Catal. Today* **2009**, *145*, 108.

168. Ameloot, R.; Roeffaers, M. B. J.; Cremer, G. D.; Vermoortele, F.; Hofkens, J.; Sels, B. F.; Vos, D. E. D. *Adv. Mater*. **2011,** *23*, 1788.

169. Falcaro, P.; Hill, A. J.; Nairn, K. M.; Jasieniak, J.; Mardel, J. I.; Bastow, T. J.; Mayo, S. C. et al. *Nature Commun.* **2011,** *2*, 237.

170. Pan, H.; Li, X.; Zhang, D.; Guan, Y.; Wu, P. *J. Mol. Catal. A* **2013**, *377*, 108.

171. Huang, Y.; Ma, T.; Huang, P.; Wu, D.; Lin, Z.; Cao, R. *ChemCatChem* **2013**, *5*, 1877.

172. Wu, F.; Qiu, L.-G.; Ke, F.; Jiang, X. *Inorg. Chem. Commun.* **2013**, *32*, 5.

173. (a) Corma, A. *Chem. Rev.* **1995**, *95*, 559. (b) Kozhevnikov, I. V. *Chem. Rev.* **1998**, *98*, 171. (c) Streb, C. *Dalton Trans.* **2012**, *41*, 1651. (d) Weinstock, I. A. *Chem. Rev.* **1998**, *98*, 113.

174. Maayan, G.; Neumann, R. *Chem. Commun.* **2005**, 4595.

175. Corma, A.; Iborra, S.; Llabres, F. X.; Xamena, I.; Monton, R.; Calvino, J. J.; Prestipino, C. *J. Phys. Chem. C* **2010**, *114*, 8828.

176. Guibal, E. *Prog. Polym. Sci.* **2005**, *30*, 71. (b) Guibal, E.; Vincent, T.; Spinelli, S. *Sep. Sci. Technol.* **2005**, *40*, 633.

177. Kobayashi, S.; Miyamura, H. *Chem. Rec.* **2010,** *10*, 271.

178. Yashtulov, N. A.; Revina, A. A.; Lebedeva, M. V.; Flid, V. R. *Kinet. Catal.* **2013**, *54*, 322.

179. Domènech, B.; Ziegler, K. K.; Carrillo, F.; Muñoz, M.; Muraviev, D. N.; Macanás, J. *Nanoscale Res. Lett.* **2013**, *8*, 238. (b) Wang, M.-L.; Jiang, T.-T.; Lu, Y.; Liu, H.-J.; Chen, Y. *J. Mater. Chem. A* **2013**, *1*, 5923.

180. Chen, C.-W.; Chen, M.-Q.; Serizawa, T.; Akashi, M. *Chem. Commun.* **1998**, 831.

181. Sabadie, J.; Germain, J.-E. *Bull. Chim. France* **1974,** *5/6*, 1133.

182. Lu, Y.; Proch, S.; Schrinner, M.; Drechsler, M.; Kempe, R.; Ballauff, M. *J. Mater. Chem.* **2009**, *19*, 3955.

183. Chauhan, B. P. S. *Hybrid Nanomaterials: Synthesis, Characterization, and Applications*, John Wiley & Sons, **2011**.

184. Wang, D.; Ma, H.; Chu, C.; Hao, J.; Liu. H.-G. *J. Coll. Interf. Sci.* **2013**, *402*, 75.

185. Ma, H.; Geng, Y.; Lee, Y.-I.; Hao, J.; Liu, H.-G. *Coll. Surf. A: Phys. Eng. Asp.* **2013**, *419*, 201.

186. **(a)** Aroca, R. F. *Surface-enhanced vibrational spectroscopy*, Wiley, Berlin **2006. (b)** Cotton, T. M. *Adv. Spectrosc.* **1988**, *16*, 91. **(c)** Garrell, R. L. *Anal. Chem.* **1989**, *61*, 401A. **(d)** Pemberton, J. E. In: Abruna, H. D. (eds) *Electrochemical interfaces: modern technique for in-situ interface characterization.* VCH, Berlin, **1991. (e)** Birke, R. L.; Lu, T.; Lombardi, J. R. In: Varma R, Selman JR (eds) *Techniques for characterization of electrodes and electrochemical processes.* Wiley, New York, **1991**. **(f)** Pettinger, B. In: Lipkowski, J.; Ross, P. N. (eds) *Adsorption at electrode surface.* VCH, New York, **1992. (g)** Campion, A.; Kambhampati, P. *Chem. Soc. Rev.* **1998**, *27*, 241. **(h)** Kneipp, K.; Kneipp, H.; Itzkan, I.; Dasari, R. R.; Feld, M. S. *Chem. Rev.* **1999**, *99*, 2957. **(i)** Tian, Z. Q.; Ren, B.; Wu, D. Y. *J. Phys. Chem. B* **2002**, *106*, 9463. **(j)** Tian, Z. Q.; Ren, B. *Annu. Rev. Phys. Chem.* **2004**, *55*, 197. **(k)** Baker, G. A.; Moore, D. S. *Anal. Bioanal. Chem.* **2005**, *382*, 1751.

187. Hermann, P.; Hermeling, A.; Lausch, V.; Holland, G.; Möller, L.; Bannert, N.; Naumann, D. *Analyst* **2011**, *136*, 1148.

188. Barrios, C.; Malkovskiy, A.; Hartschuh, R. *Proc. SPIE* **2008**, *6954*, 69540C.

189. Yeo, B.-S.; Schmid, T.; Zhang, W.; Zenobi, R. *Appl. Spectrosc.* **2008**, *62*, 708.

190. Yeo, B.-S.; Stadler, J.; Schmid, T.; Zenobi, R.; Zhang, W. *Chem. Phys. Lett.* **2009**, *472*, 1.

191. Fleischmann, M.; Hendra, P. J.; McQuillan, A. J. *Chem. Phys. Lett.* **1974**, *26*, 163.

192. Jeanmaire, D. L.; van Duyne, R. P. *J. Electroanal. Chem.* **1977**, *84*, 1.

193. Albrecht, M. G.; Creighton, J. A. *J. Am. Chem. Soc.* **1977**, *99*, 5215.

194. Micic, M.; Klymyshyn, N.; Suh, Y. D.; Lu, H. P. *J. Phys. Chem. B* **2003**, *107*, 1574.

195. Zhao, J.; Pinchuk, A. O.; McMahon, J. M.; Li, S.; Ausman, L. K.; Atkinson, A. L.; Schatz, G. C. *Acc. Chem. Res.* **2008**, *41*, 1710.

196. (a) Moskovits, M. *J. Raman Spectros.* **2005**, *36*, 485. (b) Campion, A.; Kambhampati, P. *Chem. Soc. Rev.* **1998**, *27*, 241.

197. Nie, S.; Emory, S. R. *Science* **1997**, *275*, 1102.

198. Lassiter, J. B.; Aizpurua, J.; Hernandez, L. I.; Brandl, D. W.; Romero, I.; Lal S.; Hafner, J. H. et al. *Nano Lett.* **2008**, *8*, 1212.

199. (a) Kneipp, K.; Wang, Y.; Kneipp, H.; Perelman, L. T.; Itzkan, I.; Dasari, R. R.; Feld, M. S. *Phys. Rev. Lett.* **1997**, *78*, 1667. (b) Svedberg, F.; Li, Z.; Xu, H.; Käll, M. *Nano Lett.* **2006**, *6*, 2639. (c) Talley, C. E.; Jackson, J. B.; Oubre, C.; Grady, N. K.; Hollars, C. W.; Lane, S. M.; Huser, T. R. et al. *Nano Lett.* **2005**, *5*, 1569.

200. Li, W.; Camargo, P. H. C.; Lu, X.; Xia, Y. *Nano Lett.* **2009**, *9*, 485.

201. (a) Chaudhuri, R. G.; Paria, S. *Chem. Rev.* **2012**, *112*, 2373. (b) Lal, S.; Grady, N. K.; Kundu, J.; Levin, C. S.; Lassiter, J. B.; Halas, N. J. *Chem. Soc. Rev.* **2008**, *37*, 898.

202. (a) McLellan, J. M.; Li, Z.-Y.; Siekkinen, A. R.; Xia, Y. *Nano Lett.* **2007**, *7*, 1013. (b) McLellan, J. M.; Siekkinen, A.; Chen, J.; Xia, Y. *Chem. Phys. Lett.* **2006**, *427*, 122.

203. Camargo, P. H.; Rycenga, M.; Au, L.; Xia, Y. *Angew. Chem. Int. Ed.* **2009,** *48*, 2180.

204. Murray, W. A.; Suckling, J. R.; Barnes, W. L. *Nano Lett.* **2006**, *6*, 1772.

205. Stoerzinger, K. A.; Hasan, W.; Lin, J. Y.; Robles, A.; Odom, T. W.; *J. Phys. Chem. Lett.* **2010**, *1*, 1046.

206. Kumar, J.; Thomas, K. G. *J. Phys. Chem. Lett.* **2011**, *2*, 610.

207. Fang, Y.; Wei, H.; Hao, F.; Nordlander, P.; Xu, H. *Nano Lett.* **2009**, *9*, 2049.

208. (a) Du, C. L.; You, Y. M.; Chen, T.; Hu, H. L.; Zhu, Y.; Shi, D. N.; Chen, H. Y.; Shen, Z. X. *Plasmonics* **2011**, *6*, 761. (b) Chikkaraddy, R.; Singh, D.; Kumar, G. V. P. *Appl. Phys. Lett.* **2012**, *100*, 043108.

209. (a) Baik, J. M.; Lee, S. J.; Moskovits, M. *Nano Lett.* **2009**, *9*, 672. (b) Seung, J. L.; Jeong, M. B.; Moskovits, M. *Nano Lett.* **2008**, *8*, 3244.

210. (a) Van Duyne R. P.; Haushalter, J. P. *J. Phys. Chem.* **1983**, *87*, 2999. (b) Oblonsky, L. J.; Devine, T. M.; Ager, J. W.; Perry, S. S.; Mao, X. L.; Russo, R. E. *J. Electrochem. Soc.* **1994**, *141*, 3312.

211. (a) Aramaki, K.; Ohi, M.; Uehara, J. *J. Electrochem. Soc.* **1992**, *139*, 1525. (b) Leung, L. W. H.; Weaver, M. J. *J. Am. Chem. Soc.* **1987**, *109*, 5113.

212. Ren, B.; Liu, G.-K.; Lian, X.-B.; Yang, Z.-L.; Tian, Z.-Q. *Anal. Bioanal. Chem.* **2007**, *388*, 29.

213. Guo, L.; Huang, Q. J.; Li, X. Y.; Yang, S. H. *Phys. Chem. Chem. Phys.* **2001**, *3*, 1661.

214. Tian, Z. Q.; Ren, B.; Wu, D. Y. *J. Phys. Chem. B* **2002**, *106*, 9463.

215. Zuo, C.; Jagodzinski, P. W. *J. Phys. Chem. B* **2005**, *109*, 1788.

216. (a) Freeman, R. G.; Grabar, K. C.; Allison, K. J.; Bright, R. M.; Davis, J. A.; Guthrie, A. P.; Hommer, M. B. et al. *Science* **1995**, *267*, 1629. (b) Guo, H.; Jiang, D.; Li, H.; Xu, S.; Xu, W. *J. Phys. Chem. C* **2013**, *117*, 564.

217. (a) Cheng, M.; Tsai, B.; Yang, J. *Anal. Chim. Acta* **2011**, *708*, 89. (b) Yu, W.; White, I. M. *Anal. Chem.* **2010**, *82*, 9626.

218. Ru, E. C. L.; Blackie, E.; Meyer, M.; Etchegoin, P. G. *J. Phys. Chem. C* **2007**, *111*, 13794.

219. Brown, R. J. C.; Milton, M. J. T. *J. Raman Spectrosc.* **2008**, *39*, 1313.

220. Natan, M. J. *Faraday Discuss.* **2006**, *132*, 321.

CHAPTER 2

Silver Nanoparticle-Embedded Polymer Thin Film: A Highly Efficient and Extensively Reusable "Dip Catalyst"

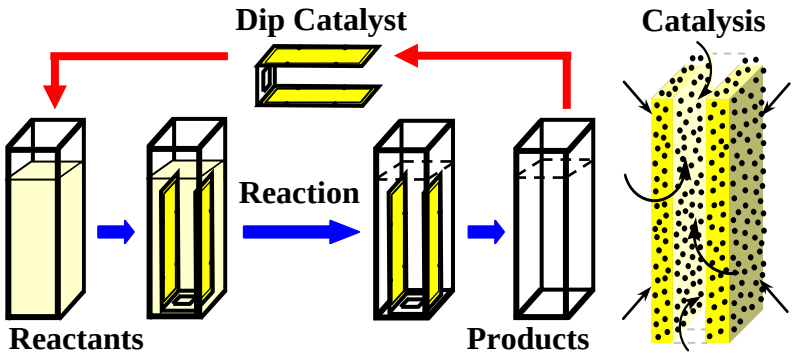

The high efficiency and extensive reusability of a Ag-PVA nanocomposite thin film catalyst in the reduction of 4-nitrophenol by sodium borohydride, demonstrates effective harnessing of the benefits of homogeneous and heterogeneous catalysis.

Paper published

Hariprasad, E.; Radhakrishnan, T. P. *Chem. Eur. J.* **2010**, *16*, 14378.

Scope

Achieving a harmonious combination of the efficiency of homogeneous catalysts with the reusability of heterogeneous catalysts is a fundamental and challenging problem. Metal nanoparticles in a suitable matrix offer a potential solution. However an ideal design is yet to be realized, because the critical requirements of facile access to the catalyst, its durability, and ease of retrieval and reuse are difficult to reconcile. We present in this chapter, a multilayer free-standing thin film catalyst based on silver nanoparticles, generated in situ inside poly(vinyl alcohol) by using a facile protocol, which shows excellent efficiency and extensive reusability in the prototypical reaction, the reduction of 4-nitrophenol by sodium borohydride. We call this a 'dip catalyst' as it can start/stop the reaction instantaneously by mere insertion/removal. It is used 30 times leading to a total turn-over-number (TON) of ~3390, which is very high for this reaction. The efficiency of the catalyst is reduced only marginally at the end of these runs, promising further extended usage. The unique advantage of convenient catalyst monitoring is illustrated by the periodic spectroscopic and microscopic examinations of the thin film, which revealed the basis of its durability.

2.1 Introduction

According to the definition of a catalyst, it undergoes no transformation itself while promoting a chemical reaction therefore, in principle, the reusability of a catalyst and hence its efficiency is limitless. However, due to several constraints, including chemical instability and physical loss, such potentials are rarely realized. Metal nanoparticles are efficient catalysts for a number of reactions including cross coupling reactions, electron transfer reactions, hydrogenations and oxidations, their large surface area to volume ratio and specific surface structure being key factors.[1] They are potential candidates for addressing the fundamental issue of unifying and harnessing the benefits of homogeneous and heterogeneous catalysis.[2,3] In addition to their efficiency and selectivity in enhancing reaction rates,[4] an aspect that makes a catalyst genuinely

superior is the feasibility and ease of multiple reuse. Monitoring a nanocatalyst through reuse cycles to assess problems like leaching or shape/size alteration is extremely valuable in the optimization of catalyst design. Even though metal nanoparticle catalysts encapsulated in, or supported on, a wide range of host structures have been explored,[3,5] efficient reuse and catalyst monitoring remain major challenges. We envisaged that polymer thin films with *in situ* generated metal nanoparticles would be a class of easily fabricated, efficient, and reusable catalysts; the catalyst separation would be trivial and the thin film would be amenable to convenient examination between uses. Even though metal nanoparticles in polymer membranes have been used in sorption-diffusion-based separations and catalysis,[6] major issues, such as extensive reuse and efficient catalyst monitoring have not been addressed.

Polymer thin films with embedded metal nanoparticles combine the versatility of the former with the unique properties of the latter. These nanocomposites find applications in several areas, including electronics, photonics, sensors, and medicine.[7-13] Various soft chemical routes have been developed for their fabrication;[12,14-17] *in situ* growth of metal nanoparticles within a polymer film is especially efficient among them.[12,15-17] A general protocol that we have optimized involves spin-coating a solution of the polymer such as poly(vinyl alcohol) (PVA) and the metal precursor onto a substrate followed by thermal *in situ* reduction of the metal ions to atoms by the polymer itself, which leads to the formation of nanoparticles inside the film.[12,18-20] This methodology is environmentally benign, since the medium used is mostly aqueous, and the potentially toxic[21] nanoparticles are never exposed. Other advantages of this approach include the convenience of monitoring the *in situ* formation of the metal nanoparticles,[20] even in real time,[22] and the feasibility of fabricating both free-standing films amenable to direct imaging and multilayer films for specific applications.[23]

The efficacy of a metal nanoparticle-embedded thin film catalyst is best demonstrated by using a well-studied nanoparticle-catalyzed reaction as a benchmark; we chose to investigate the reduction of 4-nitrophenol (4NP) by sodium borohydride ($NaBH_4$). Several metal nanoparticles, including those of palladium, gold, and silver,

have been used as catalysts for this reaction.[24-27] The use of silver nanoparticles and host matrices to facilitate catalyst retrieval[28,29] is advantageous in terms of the cost factor; catalysts in the form of powders are, however, prone to losses during filtration or magnetic separation and washing. Efficient retrieval and recycling of the catalyst, as well as assessment of the catalyst between uses, have rarely been realized in the reported studies. It is also notable that characteristics like turn-over-number (TON) and turn-over-frequency (TOF) have been reported only in a few cases.

A critical problem with a catalyst based on metal nanoparticles in a polymer thin film (or any other matrix) is the effective reconciliation of conflicting issues such as the durability of the nanocatalyst in the film matrix and facile access of the reactants to the catalyst. We have investigated the efficacy of an Ag-PVA thin film, fabricated by using our methodology, in catalyzing the reduction of 4NP by $NaBH_4$. A multilayer structure, Ag-PVA/PVA/Ag-PVA is shown to provide robust free-standing films with excellent catalytic efficiency. Choice of a polymer with optimal characteristics and the multilayer design facilitate reversible swelling in the aqueous reaction medium, ensuring easy passage of reactants to the catalyst embedded in the polymer matrix without leaching or degradation of the catalyst. *In situ* monitoring of the reaction kinetics is facile with no interference from the catalyst; high rate constants are observed. Experiments carried out on larger scales establish the high TON and TOF that can be achieved. The catalyst can be reused extensively; there is only a marginal reduction in the efficiency of the catalyst after 30 runs, which is promising for further extended usage. Periodic monitoring of the catalyst film unambiguously establishes its stability and durability. Because the catalyst film is removed cleanly at the end of the reaction, workup of the products is convenient. Comparison of the Ag-PVA catalyst with the silver nanoparticle systems reported earlier for the same reaction, coupled with its ease of fabrication, demonstrates the significant benefits of using metal nanoparticle-embedded polymer thin films in chemical catalysis. We call them 'dip catalysts'[30] to highlight their mode of deployment and ease of reuse. The relevance of this term is accentuated by the fact that insertion/removal of the film can be used to turn the reaction on/off almost instantaneously.

2.2 Fabrication of the Catalyst Film

Ag-PVA film was prepared according to our previously reported methodology, [12-18] with relevant modifications; a schematic representation of the film fabrication is shown in Fig. 2.1. Special attention was paid to factors such as the specific polymer used, optimization of the concentration of silver, and accessibility of the reactant molecules to the catalyst. A relatively high molecular weight PVA with nearly complete hydrolysis was employed (PVA with lower molecular weight and lower degree of hydrolysis had been used in the earlier studies[18-20]), so that the heat-treated film was insoluble in the aqueous medium under the ambient temperature conditions used in the catalytic studies. However, the hydrophilic nature of PVA ensures sufficient swelling in the reaction medium which in turn facilitates the approach of the reactant molecules to the silver nanoparticles. The film must be sufficiently thick and robust for repeated use in the reaction involving stirring, with washing in between uses. At the same time, efficient utilization of the silver nanoparticles demands that the film is sufficiently thin and that the particles are available close to the film surface. These requirements are reconciled effectively in the design of the multilayer structure with thin active layers (Fig. 2.1).

We have explored a range of Ag/PVA weight ratios (x), temperatures (T), and times (t) of heat treatment of the $AgNO_3$-PVA film to achieve appreciable concentration of relatively small silver nanoparticles; the optimal values determined are x = 0.2, T = 130 ^oC, and t = 4 h; films with different values of x were fabricated for the kinetics experiments. Required weights (16, 32, and 64 mg) of silver nitrate ($AgNO_3$) dissolved in 2.0 mL of water was mixed with 200 mg of PVA dissolved in 4 mL of water to prepare three different compositions which are designated using the Ag/PVA weight ratio, x = 0.05, 0.10, 0.20 respectively. The solution mixture was stirred for 5 min at 27-30 ^oC. Glass plates used as substrates were cleaned using soap solution and water followed by sonication in isopropyl alcohol for 10 min and dried. A few drops of a solution of polystyrene (PS) in toluene (1 g in 8 mL) was spin-coated using a standard photo-resist spinner operated at 1000 rpm for 10 s and dried in a hot air oven at 90 ^oC for 15 min.

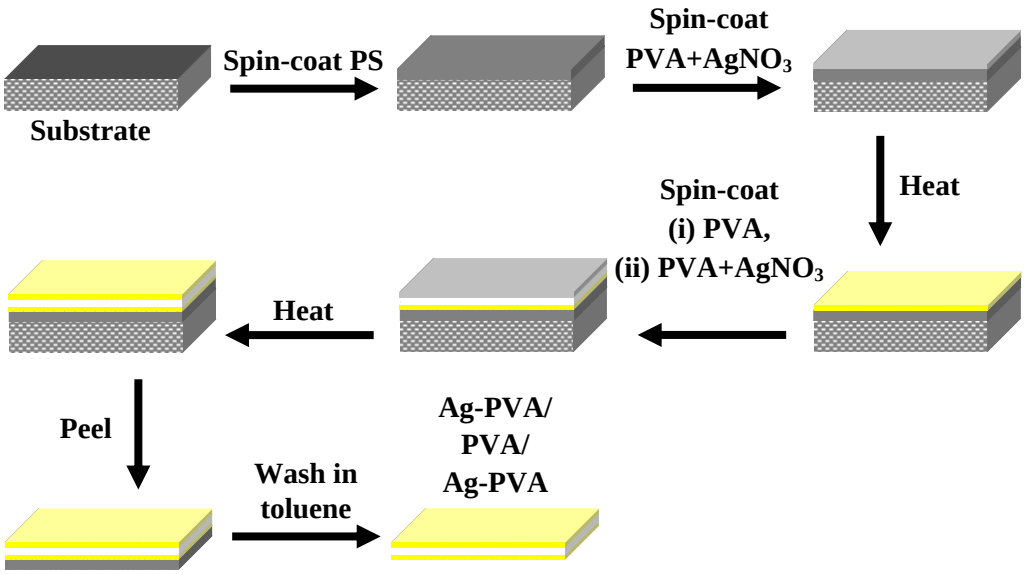

Figure 2.1. *Schematic representation of the fabrication of Ag-PVA/PVA/Ag-PVA free-standing polymer film. (Dimensions are not to scale). PS = polystyrene, PVA = poly(vinyl alcohol).*

The solution ($AgNO_3$-PVA) was spin-coated at 500 rpm for 10 s followed by 6000 rpm for 10 s on top of the PS layer. After heating at 90 ^oC for 30 min, an aqueous solution of PVA (200 mg in 4 mL of water) was spin-coated at 500 rpm for 10 s followed by 2000 rpm for 10 s and dried in hot air oven at 90 ^oC for 30 min. The final layer was formed by spin-coating the $AgNO_3$-PVA solution as before; the multilayer film was heated at 130 ^oC for 4 h. The extended heating ensures complete reduction of the Ag^+ ions as well as stability of the film in aqueous medium. The film was peeled off the glass substrate and the PS layer removed by washing in toluene to obtain the free-standing Ag-PVA/PVA/Ag-PVA film.

2.3 Characterization of the Catalyst Film

Film thickness was measured using a surface profilometer. The thickness of the individual layers was regulated by varying the solution viscosity and spin-coating conditions. Typical values of the thickness of the PS, Ag-PVA (I), PVA, and Ag-PVA (II) layers in the films used in our study are ~3.20, 0.19, 1.00 and 0.13 μm

Table 2.1. *Typical thickness values obtained for the multilayer films, from which the thickness of each individual layer was estimated. The spin-coating conditions are also indicated.*

Film	Spin-coating speed (rpm) [time (s)]	Total thickness (nm)	Thickness of each new layer (nm)
PS	1000 [10]	3180	3180
PS + Ag-PVA	500 [10] & 6000 [10]	3367	187
PS + Ag-PVA + PVA	500 [10] & 2000 [10]	4372	1005
PS + Ag-PVA + PVA + Ag-PVA	500 [10] & 6000 [10]	4498	126

respectively; the specific measurements and spin-coating conditions of the films used were tabulated in Table 2.1. The thickness of the 3-layer Ag-PVA/PVA/Ag-PVA is effectively ~1.3 μm.

The characteristic localized surface plasmon resonance (LSPR) extinction of the silver nanoparticles in the multilayer film is shown in Fig. 2.2a. Fig. 2.2b shows the AFM image of the smooth film surface; average roughness = 0.77 nm. Samples for TEM were prepared using the technique we have developed earlier.[18] A layer of

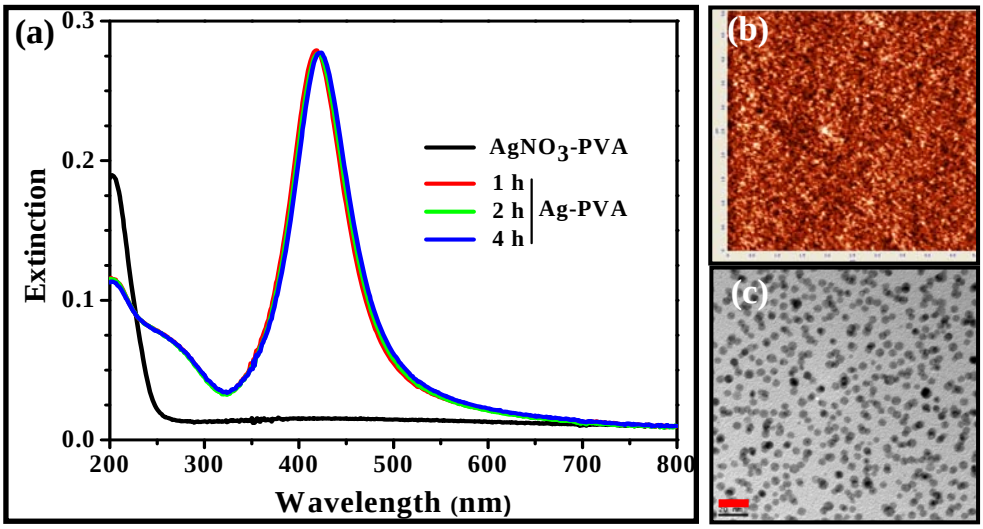

Figure 2.2. ***(a)*** *Electronic spectrum of the $AgNO_3$-PVA film (before heating) and the LSPR extinction spectra of the Ag-PVA multilayer film prepared by heating at 130 ^oC for different times.* ***(b)*** *AFM topography image (5 μm x 5 μm) and* ***(c)*** *TEM image (scale bar = 20 nm) of the Ag-PVA film (x = 0.2).* ***(a)*** *and* ***(b)*** *are of the multilayer film and* ***(c)*** *of a single layer film with the same composition(see text for details).*

$AgNO_3$-PVA with the required composition was coated on a PS-coated glass and annealed at 130 ^oC for 4 h. The film was peeled and placed on a 200 mesh copper grid and the PS dissolved by dipping in toluene. The Ag-PVA film sticking to the grid was imaged directly. Fig. 2.2c shows the TEM image of a single-layered film, which reveals a homogeneous distribution of spherical nanoparticles with an average diameter of ~5.0 nm.

The film was weighed accurately after coating each layer, and the final content of silver estimated based on the Ag/PVA ratio used in the initial solution mixture and assuming complete reduction of the Ag^+ ions; this assumption is justified by the observation of saturation of the LSPR extinction under the fabrication conditions (Fig. 2.2a).

2.4 Catalytic Studies

Since the efficiency of the 'dip catalyst' is best demonstrated using a reaction which is well-studied and convenient to monitor, we have chosen to investigate the reduction of 4NP by $NaBH_4$. The pale yellow aqueous solution of 4NP was mixed with $NaBH_4$ aqueous solution, whereupon the coloration deepened due to the formation of 4-nitrophenolate. Fig. 2.3 shows the electronic absorption spectra of 4NP and its anion

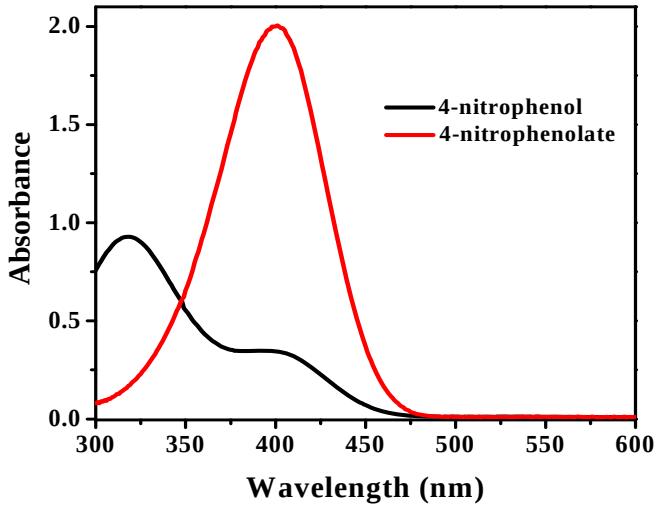

Figure 2.3. *Electronic absorption spectra of aqueous solutions of 4NP and 4-nitrophenolate.*

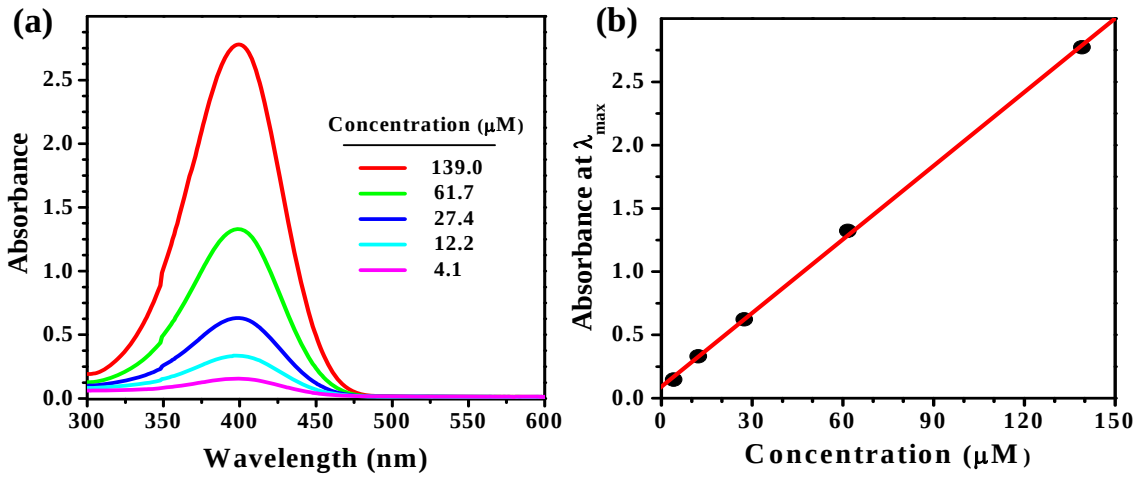

Figure 2.4. ***(a)*** *Electronic absorption spectra of aqueous solutions of 4-nitrophenolate at different concentrations.* ***(b)*** *Plot of the absorbance at* λ_{max} *versus concentration based on the spectra in* ***(a)***.

with a clear shift in the λ_{max} from 318 nm to 400 nm. The reaction can be monitored by measuring the absorbance of the reaction mixture at 400 nm.

We have recorded the electronic absorption spectra of 4-nitrophenolate solutions of different concentrations covering the range of concentrations used in the catalytic studies (Fig. 2.4a) and verified the adherence to the Beer-Lambert law (Fig. 2.4b); it is clear that the exact concentrations can be reliably estimated from the absorbance values. If no catalyst is introduced, the peak at 400 nm remains unaltered with time as the

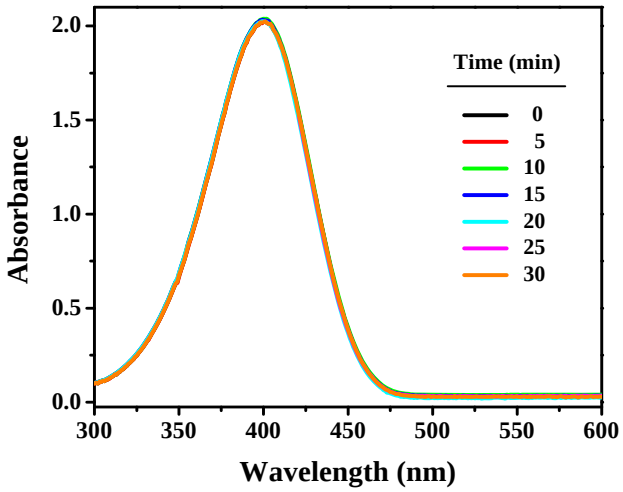

Figure 2.5. *Electronic absorption spectra of 4-nitrophenolate in presence of 100-fold excess of* $NaBH_4$ *in water, but with no catalyst introduced, as a function of time.*

reduction of the 4-nitrophenolate is a sluggish process (Fig. 2.5). However, within a few seconds of introducing the catalyst film the peak begins to decay as reduction of the nitro group starts (as discussed below); a concomitant rise of the peak due to the 4-aminophenolate is observed.

2.4.1 *Kinetic Studies*

We have investigated the kinetics of reduction of 4NP, catalyzed by the Ag-PVA film, using the setup depicted in Fig. 2.6. A standard PS cuvette (4.5 mL, 1 cm path length) was used. In the cuvette 3.0 mL of a 0.12 mM 4NP aqueous solution was taken and to this 0.2 mL of 0.18 M $NaBH_4$ aqueous solution was added (final concentrations: [4NP] = 0.11 mM, [$NaBH_4$] = 11 mM). The solution was stirred for 6 min. The Ag-PVA multilayer (Ag-PVA/PVA/Ag-PVA) catalyst film (thickness ~1.3 μm, total surface area = 35 cm^2, total weight = 0.42 mg) wrapped on a Teflon frame was introduced in such a way that the light beam is transmitted freely through the solution.

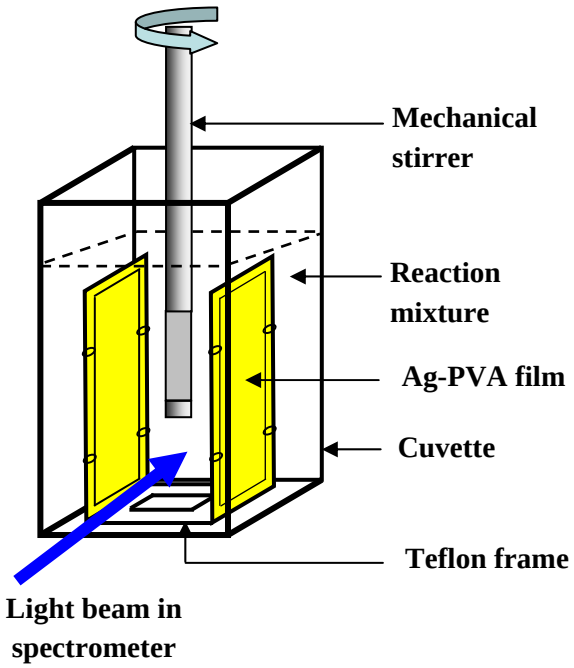

Figure 2.6. *Setup used in the catalysis studies: The schematic representation shows the placement of the catalyst film wrapped on a Teflon frame, mechanical stirrer, reaction mixture in the cuvette and the light beam path.*

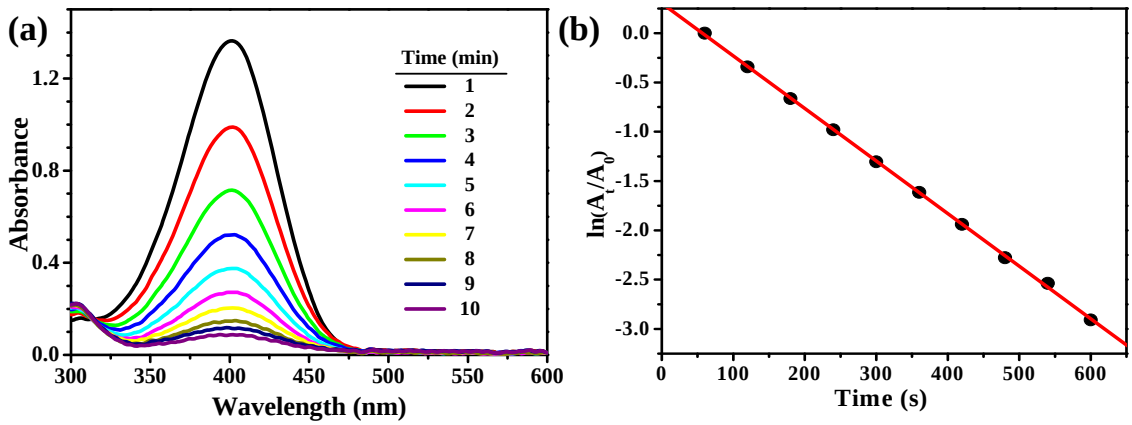

Figure 2.7. ***(a)*** *Electronic absorption spectra of the reaction mixture ([4NP] = 0.11 mM, [$NaBH_4$] = 11 mM) at 25 ^oC, as a function of time, following the insertion of the Ag-PVA multilayer catalyst film.* ***(b)*** *Plot of ln(A_t/A_0) versus time; A_0 and A_t are the absorbances at 400 nm at time 0 and t, respectively. The red line in figure is the least square fit straight line.*

The reaction mixture was stirred with a glass/Teflon mechanical stirrer introduced from the top, ending just above the light beam path.

The absorption spectrum was recorded at regular intervals to monitor the decay of the peak due to the reduction of 4-nitrophenolate. Fig. 2.7a shows the profile of a typical run; the peak decays steadily with time. As a large excess of $NaBH_4$ is used, the reaction is expected to be pseudo first-order; this is confirmed by the plot in Fig. 2.7b. Note that this procedure, whereby the catalyst film is introduced after the reagents are mixed in solution and stirred for a few minutes, gives rise to a clean first-order reaction profile from time zero, with no evidence of the induction period that was observed in some of the earlier studies.[24]

We have investigated the dependence of the rate constant of the reaction on two relevant parameters, the value of x of the catalyst film and the ratio [$NaBH_4$]/[4NP] in the reaction mixture. The kinetics plots are shown in Fig. 2.8a, b and the estimated rate constants in Table 2.2. Based on these observations, we conclude that x = 0.2 and [$NaBH_4$]/[4NP] = 100 are optimal for this catalytic reaction. The pseudo first-order rate constant is found to scale linearly with the amount of catalyst as well as [$NaBH_4$] as expected (Fig. 2.9).

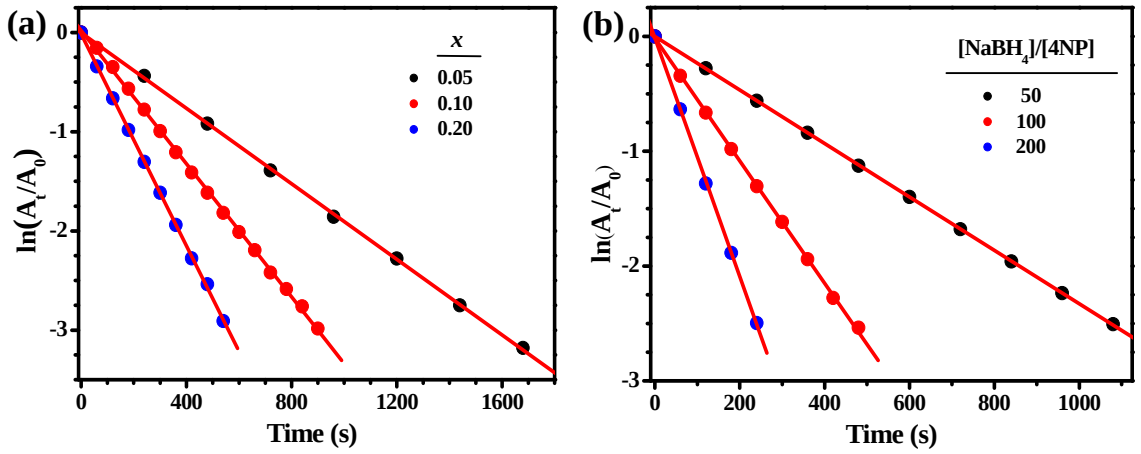

Figure 2.8. *Kinetics plots for* ***(a)*** *different weight ratios Ag/PVA (x) of the catalyst film (with [4NP] = 0.11 mM, [NaBH₄] = 11 mM),* ***(b)*** *different ratios, [NaBH₄]/[4NP] (with [4NP] = 0.11 mM, x = 0.2). The red line in each figure is the least square fit straight line.*

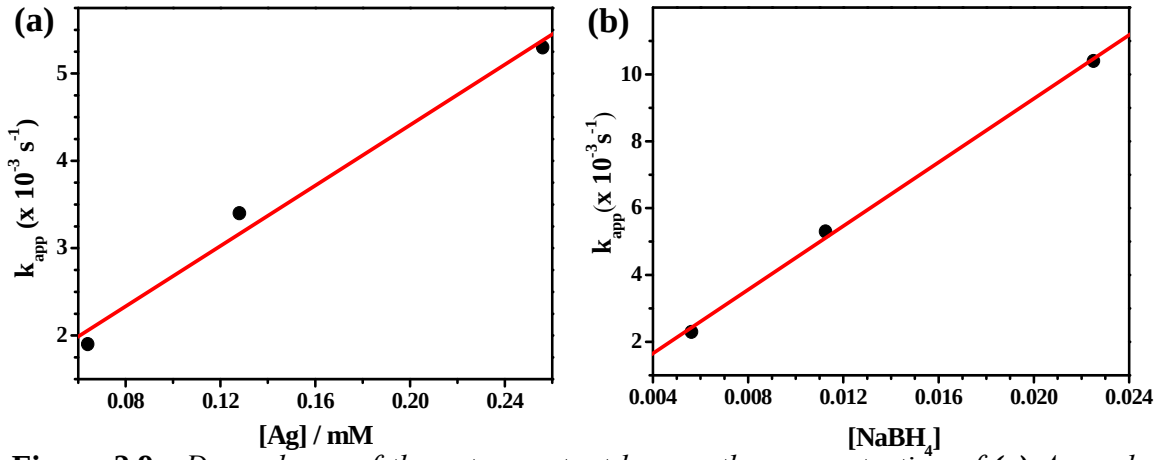

Figure 2.9. *Dependence of the rate constant k_{app} on the concentration of* ***(a)*** *Ag and* ***(b)*** *[NaBH₄] in the reaction mixture.*

Table 2.2. *Apparent rate constants determined for the reduction of 4NP by NaBH₄ at 25 °C catalyzed by the Ag-PVA multilayer film, for different weight ratios Ag/PVA (x) (with [NaBH₄]/[4NP] = 100) and different reactant ratios [NaBH₄]/[4NP] (with x = 0.2); relevant plots are shown in Fig. 2.8a, b.*

Catalyst / Reaction parameter	***x***			**[NaBH₄]/[4NP]**		
	0.05	0.10	0.20	50	100	200
k_{app} (10^{-3} s^{-1})	1.9	3.4	5.3	2.3	5.3	10.4

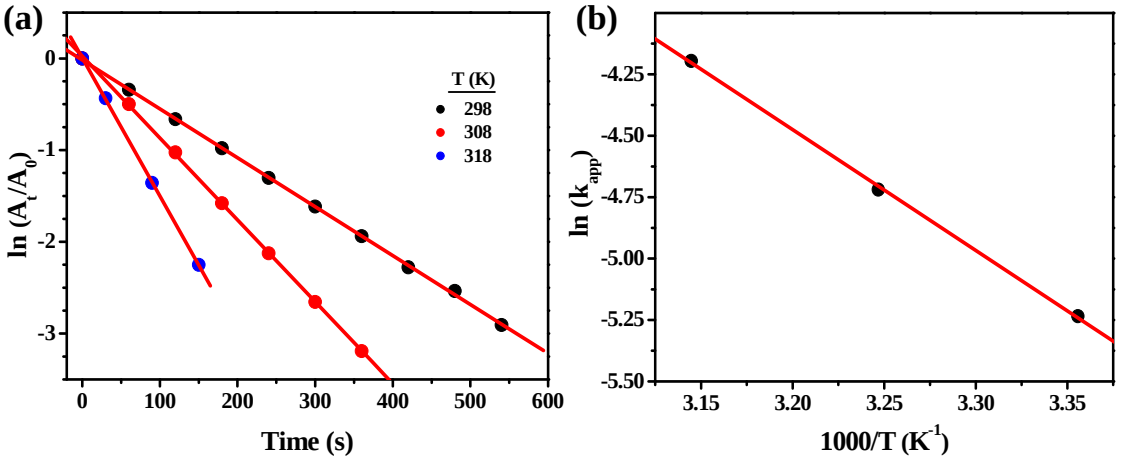

Figure 2.10. ***(a)*** *Kinetics plots for the reduction of 4-nitrophenol (4NP) by $NaBH_4$, catalyzed by the Ag-PVA multilayer film, at different temperatures (with [4NP] = 0.11 mM, [$NaBH_4$] = 11 mM),* ***(b)*** *the corresponding ln(k_{app}) versus 1/T plots. Least square fit lines are shown in all cases.*

We have explored also the temperature dependence of the catalytic process (Fig. 2.10). Based on the rate constants determined in the range 298-318 K, the activation energy of the reaction is estimated to be 40.9 kJ/mol, in good agreement with reported values.[29,31]

We have demonstrated the switching on or off of the reaction by the catalyst film using an experiment in which the catalyst film is removed during the reaction and reinserted after a brief interval. The prompt response of the reaction is vividly captured

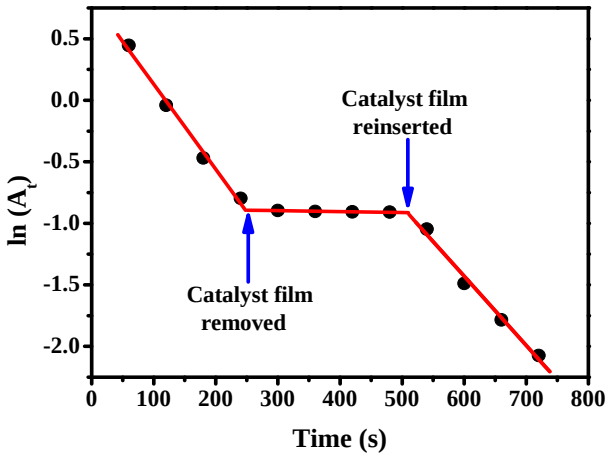

Figure 2.11. *Plot of ln(A_t) as a function of time, in an experiment in which the catalyst film was removed and reinserted. The red line is the least square fit straight line shown for each segment of the data.*

in the reaction profile shown in Fig. 2.11. This observation proves that there is practically no leaching of silver nanoparticles into the reaction medium. This not only ensures efficient retrieval of the catalyst after the reaction, but also easy workup of the reaction products after withdrawal of the catalyst film.

2.4.2 *Evaluation of Turn-Over-Number and Turn-Over-Frequency*

We have estimated the amount of silver present in the catalyst film based on the total weight of the Ag-PVA layers in the film used in the catalysis reaction and the Ag/PVA weight ratio used in the original solutions (Sec. 2.3). The silver content is found to be 0.65 μmol. Reliability of this estimate was confirmed using the TEM image of the single layer film (Fig. 2.2c) as shown in Box 2.1.

The efficacy of our 'dip catalyst' was investigated by increasing the scale of the reaction while keeping the catalyst film unchanged (x = 0.2, silver content = 0.65 μmol) and attempting multiple uses of a single film; the [$NaBH_4$]/ [4NP] ratio of 100 was used in all reactions carried out at the ambient temperature of 25 ^oC. With a stiff limit of 15 min kept for completion of the reaction (>99.9% in the first run), it was found that the film could catalyze the reduction of up to 75 μmol of 4NP in a single run. This implies a high TON of ~114 in one cycle of catalytic use. The TOF for the reaction catalyzed

Box 2.1. Estimation of the Content of Silver in the Fresh Catalyst Film, Using the TEM Image

The catalyst consists of two free-standing films wrapped one on each arm of the Teflon frame, as shown in Fig. 2.6. Each film is 2.5 cm wide and 3.5 cm long with two Ag-PVA layers and hence with a total area of ~ 35 cm^2 (2 × 2 × 2.5 × 3.5 cm^2) used in catalytic reaction. Weight of silver per unit area of the film is estimated from average number of nanoparticles per unit area (2.45×10^{12} cm^{-2} from TEM image) and average mass of Ag nanoparticle (diameter = 5 nm, density = 10.5 gcm^{-3}); and the value is ~ 1.68×10^{-6} g cm^{-2}. Hence, weight of silver in the catalyst film = 58.8 μg (0.54 μmol).

by the Ag-PVA film is 0.127 s^{-1}, which is, once again a high value. These values will be compared with those from earlier reports in the next section.

It is important to note that the catalytic process is still heterogeneous and hence only the surface atoms will play an effective role. Therefore a more realistic estimate of TON and TOF should take into account only the surface atoms of the nanoparticles (for example, some of entries in Table 2.3). We have estimated the fraction of surface atoms of the silver nanoparticles in the catalyst film using TEM image of the single layer film (Fig. 2.2c) (Box 2.2). Therefore the TON based on the atoms present on the surface of

Box 2.2. Calculation of the Fraction of Surface Atoms in the Ag Nanoparticles

The TEM image shows that the particles are mostly spherical with an average diameter of 5.0 nm.

$\therefore$ The average volume of nanoparticle, $V = (4/3)\pi r^3 = 6.54 \times 10^{-20}$ cm^3

Electron diffraction shows that the silver nanoparticles formed in the PVA film have the fcc structure of silver. Assuming the density, ρ to be the same as that- of bulk silver (10.5 g cm^{-3}),

The average mass of nanoparticle = $V \times \rho = 6.87 \times 10^{-19}$ g

$\therefore$ The number of Ag atoms in a nanoparticle = 3835

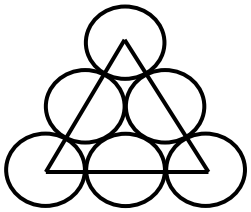

Area occupied by two atoms in a close packed plane is the area of the equilateral triangle shown in the figure. This corresponds to the (111) plane of the fcc lattice. Using the unit cell length of the fcc lattice of silver, a = 4.07 Å,

Side of this triangle, $x = \sqrt{2}\, a = 5.76 \times 10^{-8}$ cm

$\therefore$ The area of the triangle = $(\sqrt{3}/4)x^2 = 1.44 \times 10^{-15}$ cm^2

$\therefore$ The area occupied by one Ag atom in a close packed plane = 7.18×10^{-16} cm^2

The average surface area of nanoparticle, $S = 4\pi r^2 = 7.85 \times 10^{-13}$ cm^2

$\therefore$ The number of Ag atoms on the surface of a nanoparticle = 1093

Fraction of Ag atoms on the surface of the nanoparticle $\approx$ 0.28

the nanoparticles alone will be ~3.57 times that of the TON calculated based on the total silver in the nanoparticles. Hence the effective TON per cycle would be much higher, ~407.

2.4.3 *Catalyst Recycling and Monitoring*

Following the above observations, we have explored repeated use of the same catalyst film in multiple reaction runs, each one at the scale of 75 μmol of 4NP ([4NP] = 0.03 M, [$NaBH_4$] = 3 M; total volume = 2.5 mL, absolute amount of 4NP = 75 μmol at 25 ^oC). After each run, the film was removed, washed with water followed by isopropyl alcohol, and dried under vacuum for 20 min before being inserted into a new reaction setup (Fig. 2.12a). The Ag-PVA film was found to be catalytically active even after 30 runs. When the reaction nears completion, the absorbance of the mixture at 400 nm becomes low enough to be measured, and follows the Beer-Lambert law (Sec. 2.4). It is also found that the reaction continues to follow a first-order rate law (Fig. 2.13).

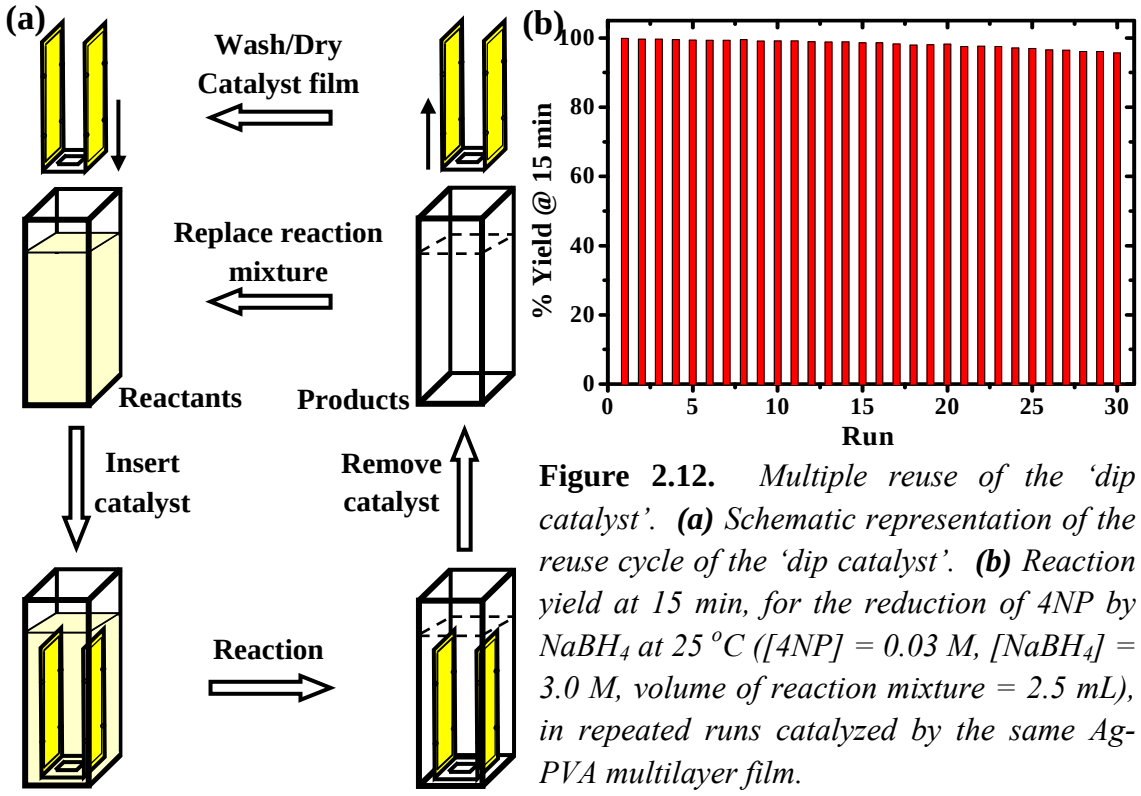

Figure 2.12. *Multiple reuse of the 'dip catalyst'.* ***(a)*** *Schematic representation of the reuse cycle of the 'dip catalyst'.* ***(b)*** *Reaction yield at 15 min, for the reduction of 4NP by $NaBH_4$ at 25 ^oC ([4NP] = 0.03 M, [$NaBH_4$] = 3.0 M, volume of reaction mixture = 2.5 mL), in repeated runs catalyzed by the same Ag-PVA multilayer film.*

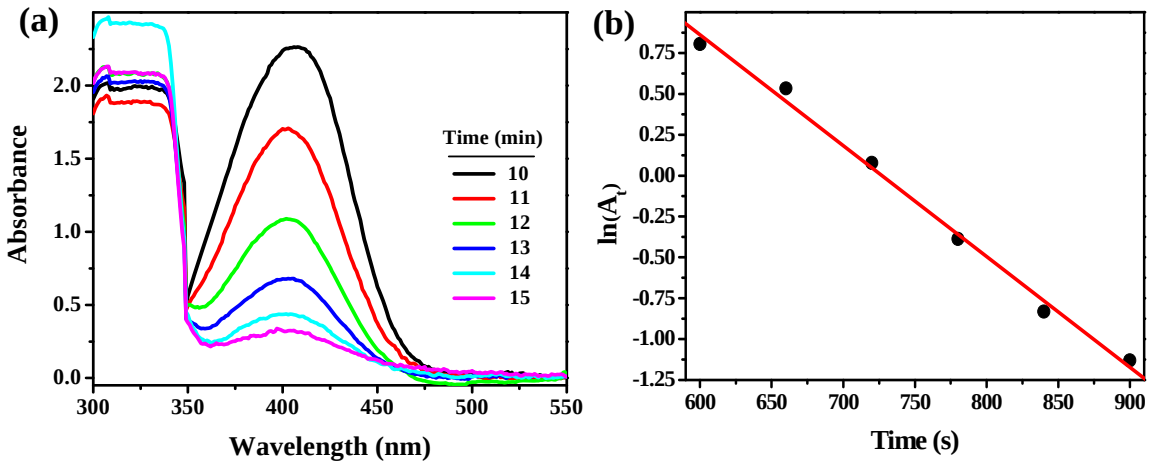

Figure 2.13. ***(a)*** *Electronic absorption spectra of the reaction mixture as a function of time, after the absorbance has reached measurable values.* ***(b)*** *The corresponding plot of ln(A_t) versus time; A_t is the absorbance at 400 nm at time t.*

Based on these observations we have estimated the yield of the reaction at 15 min in each run; Fig. 2.12b shows that it decreases only nominally from 99.9 to 95.3% over 30 cycles of use of the same film. This implies that the reaction rate is only slightly reduced after multiple reuses. The highest number of repeated uses reported earlier for this catalytic reaction is 21, which was achieved with an Ag/Fe_2O_3 catalyst.[29] In that case, catalyst removal was carried out by using a magnet, and the catalytic activity showed an abrupt decline at the end of 21 runs. Our catalyst film, on the contrary, is easy to remove and reinstall in a new reaction setup, and continues to be quite active after 30 runs. As we have used the same catalyst through all of the runs, the total TON at the end of 30 runs amounts to the very high value of ~3395 (based on the yield at 15 min in each case). The highest TON's for the silver nanoparticle catalyzed reduction of 4NP with $NaBH_4$ estimated from literature data are 515[24] and 660.[29] A detailed comparison of the performance of the Ag-PVA multilayer film relative to silver nanoparticle based catalyst systems reported earlier for the reduction of 4NP by $NaBH_4$ is provided in Table 2.3; the superior efficiency and reusability of our new dip catalyst is clearly evident.

Compared to the various forms in which metal nanoparticles have been used as catalysts, the nanocomposite polymer thin film offers critical advantages not only in terms

Table 2.3. *Comparison of reports on silver nanoparticle-catalyzed reduction of 4NP by $NaBH_4$. Only those which have reported details such as the rate constants / TON's are included.* [@] *N = number of uses, E_a = activation energy, T = temperature of the reaction.*

Catalyst system	Rate constant[#]	TON	TOF (s^{-1})	N	E_a (kJ mol^{-1})	T (K)	Ref.
Ag on PS beads	5.3×10^{-3} s^{-1}	-	-	4	24.1	303	32
Ag-PS-NIPA	5.2×10^{-2} s^{-1} m^{-2} l	-	-	-	-	303	33
Ag + Chitosan	1.5×10^{-1} s^{-1} m^{-2} l	4	0.0015	-	-	297	34
Ag-PS-PEGMA	7.3×10^{-2} s^{-1} m^{-2} l	-	-	-	62	293	35
Ag-PPI	1.2×10^{-3} s^{-1}	10	-	-	-	-	36
Ag colloid	9.5×10^{-3} s^{-1}	12	0.04	-	-	-	37
Ag@ polymer nanocapsules	1.2×10^{-4} s^{-1}	515	0.034	-	-	288	38
Ag@Fe_2O_3 powder	1.5×10^{-2} s^{-1}	660[†]	0.227	21	45	308	39
Ag-PVA	**5.3×10^{-3}** **8.9×10^{-3} s^{-1}** **1.5×10^{-2}**	**3395**	**0.127** - -	**30** - -	**40.9**	**298** **308** **318**	**40**

[@] *Entries shown in red are estimated based on the data available in the reports and assuming 100% yield of reaction. The hyphens indicate that adequate data are not available.*

[#] *Rate constants in a few cases are per unit catalyst surface area per volume.*

[†] *TON estimated for the total number of reuses.*

of convenient reuse as shown above, but also in terms of easy monitoring of the catalyst between the reuses. We have examined the Ag-PVA multilayer film at regular intervals through the reuse cycles by using microscopy and spectroscopy. AFM images of a film recorded between repeated uses are shown in Fig. 2.14; the morphology is largely preserved and the surface roughness nearly constant throughout, which reflects the stability and durability of the film.

The intensity of the LSPR extinction of the film also remains nearly constant through the 30 reaction runs (Fig. 2.15), which indicates, once again, negligible leaching of the silver nanoparticles. There is a small (ca. 10 nm) blue shift of the absorption peak after the first use of the film. Subsequently, the spectral position and

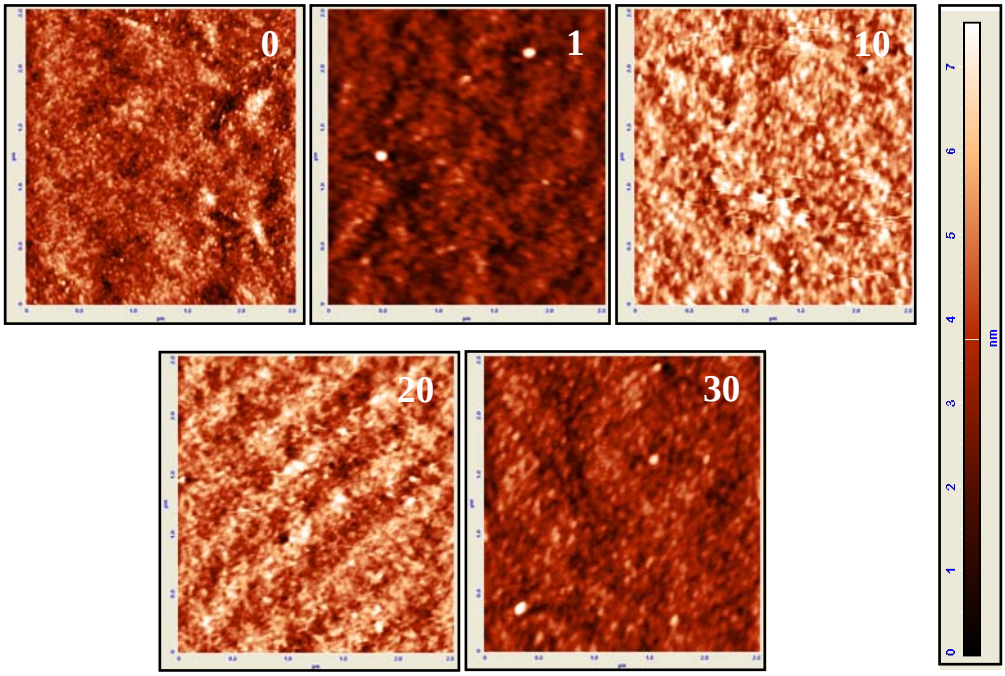

Figure 2.14. *AFM topography images (2.5 μm × 2.5 μm, height scale is shown on the right side) of an Ag-PVA multilayer film catalyst through repeated runs of the reduction of 4NP by $NaBH_4$; the run number is indicated on the images, the zeroth run corresponds to the fresh film.*

shape remain consistent throughout, except for a very small increase of the baseline near 550 nm. The TEM images of the film through the multiple reuses (Fig. 2.16) provide useful insight into these observations and the status of the catalyst nanoparticles. The film

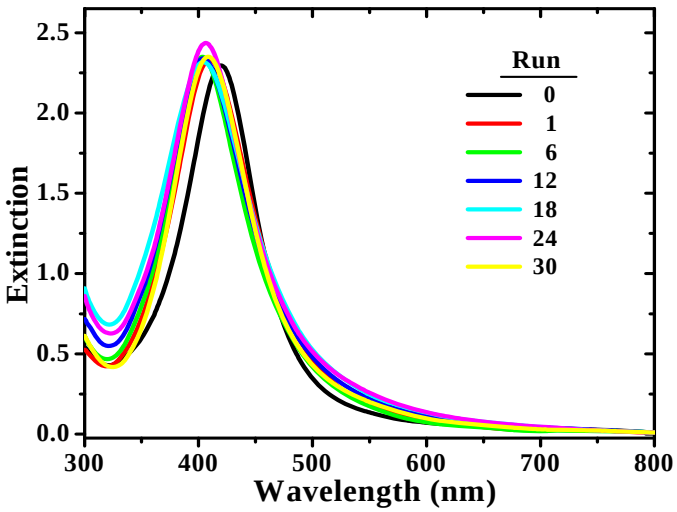

Figure 2.15. *LSPR extinction of one Ag-PVA multilayer film catalyst through repeated runs of the reaction.*

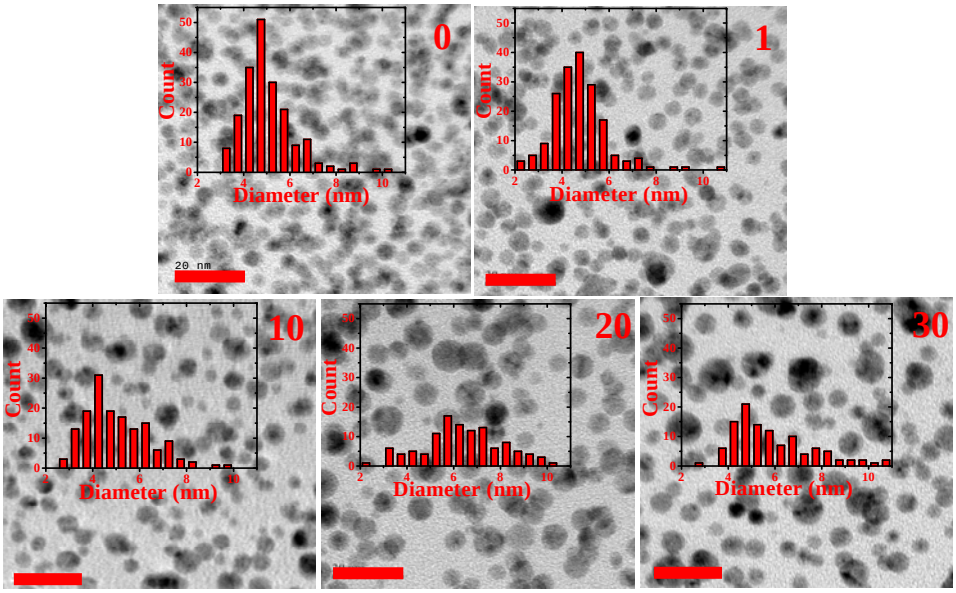

Figure 2.16. *TEM images of single layer Ag-PVA film during multiple use in the 4NP+$NaBH_4$ reaction (scale bars = 20 nm); the run number is indicated on the image and the zeroth run corresponds to the fresh film. Histograms show the particle size distribution in each case. The images shown are representative ones based on several images recorded and analyzed.*

used in the reaction medium is found to have a slightly broader distribution of nanoparticle sizes, including some smaller ones, than the fresh film. While the average sizes of the nanoparticles show very little variation, the number of nanoparticles observed in a unit area of the film, as well as their total surface area, decrease slightly over repeated uses (Table 2.4). The formation of smaller particles (which results in the

Table 2.4. *Statistics regarding the silver nanoparticles observed in the TEM images (area = 7975 nm^2) shown in Fig. 2.16.*

Run No.	Diameter of nanoparticles (nm)		Total count of nanoparticles	Total surface area of nanoparticles (10^4 nm^2)
	Range	Mean [standard deviation]		
0	3.0 – 10.4	5.1 [1.2]	195	1.65
1	2.2 – 10.8	4.8 [1.2]	180	1.35
10	2.8 – 9.8	5.2 [1.4]	152	1.40
20	2.0 – 10.2	6.4 [1.7]	114	1.55
30	2.8 – 13.4	6.0 [1.9]	112	1.38

blue shift of the LSPR peak) and minor aggregation effects (reflected in the baseline shift) are possibly induced by the slight dissolution/reformation of the nanoparticles effected by the reaction medium with high concentration of $NaBH_4$. As the changes in the nanoparticles are quite small, the impact on catalyst efficiency is marginal.

We also explored the possibility of using the catalyst film for a single run on a mmol scale: 1 mmol of 4NP and 100 mmol of $NaBH_4$ were used in the reaction, in which the concentration of 4NP was maintained as in earlier runs. As the volume of solution was now larger, the film was suspended in the reaction mixture, which was stirred using a magnetic bar. After the strong yellow color had mostly disappeared, completion of the reaction was detected by recording the electronic absorption spectrum of aliquots of the reaction mixture. It was found that 95% of the reaction was completed in around 3.5 h, which implied a TON of 1461 and TOF of 0.116 s^{-1} achieved in a single run. The various experiments described above attest to the robustness and efficiency of the Ag-PVA thin film catalyst. The fact that the film effects efficient catalysis over several rounds of reaction and on a relatively large scale suggests that the nanoparticles are accessible to the reactant molecules throughout, but retain their integrity through repeated uses. The crucial role of the polymer matrix in channeling the reactants to the catalyst and the products away is clearly significant.

2.5 Ag-PVA/PVA/Ag-PVA Catalyst Film in Action

The hydrogel character of PVA is expected to assist in facilitating the access of reagents to the silver nanoparticle catalyst within the polymer matrix. In order to gain some insight into the action of the nanocomposite polymer thin film catalyst, we have carried out some imaging studies. The optical micrographs of the film in its original state, upon wetting with water and the subsequent dried state (Fig. 2.17a-c) clearly show the swelling in the wet state. This is further confirmed by the atomic force microscopy images shown in Fig. 2.17d-f. Based on the thickness and area increase on wetting the swelling can be estimated in terms of a volume increase of ~40%.

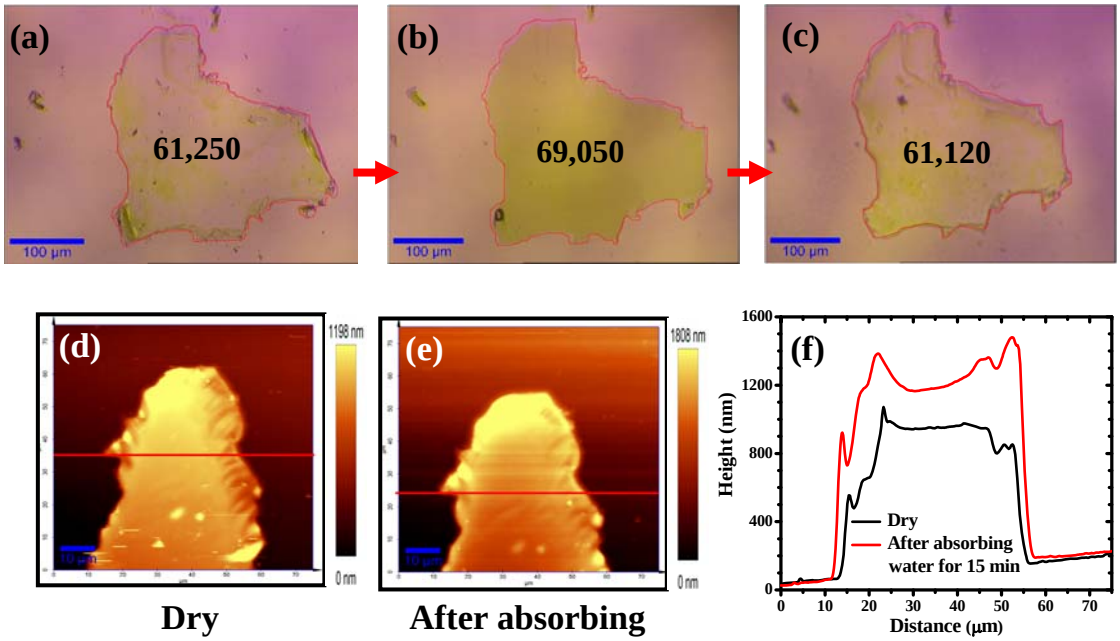

Figure 2.17. *Optical micrographs of an Ag-PVA/PVA/Ag-PVA film,* ***(a)*** *in the dry state,* ***(b)*** *after absorbing water for 15 min and* ***(c)*** *subsequent drying; area of the films (in µm^2) indicated were estimated using the outline shown on the micrograph. AFM images of an edge of Ag-PVA/PVA/Ag-PVA film* ***(d)*** *before and* ***(e)*** *after absorbing water for 15 min; line profiles are indicated in* ***(f)****.*

Based on these studies we can envisage a plausible mechanism of action of the multilayered polymer film catalyst (Fig. 2.18). In aqueous medium, the PVA matrix swells to allow admission of the solution into the film. The reactant molecules have

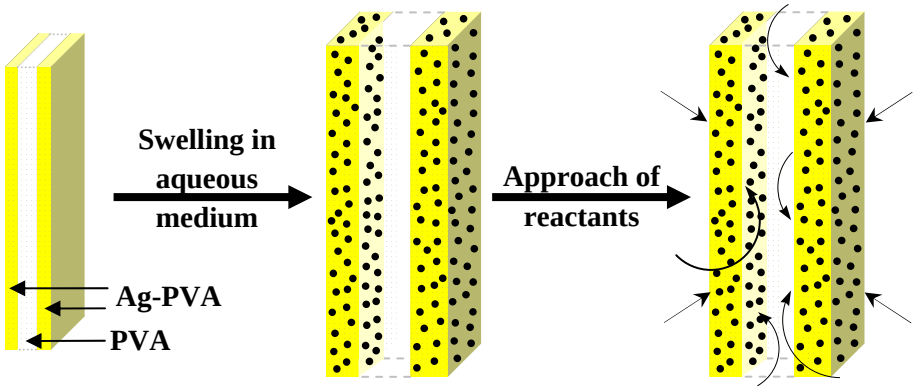

Figure 2.18. *Ag-PVA/PVA/Ag-PVA catalyst film in action; schematic representation of the swelling in the aqueous reaction medium and the facile approach of the reactants to the silver nanoparticles (shown as black dots) embedded inside the Ag-PVA layers.*

unhindered access to the metal nanoparticles from the outer surfaces of the multilayer film as well as through the middle layer of pure PVA, which enhances the catalytic activity. The minor decline observed in the rate of the reaction with increasing reuses may be due to the nanoparticles migrating deeper into the polymer matrix as a result of repeated swelling and drying cycles, or small changes occurring in the size distribution. The nature of the polymer and the multilayer structure are indeed critical to the efficient functioning of the catalyst system.

2.6 Conclusions

The present study demonstrates the unique advantages of metal nanoparticle-embedded polymer thin film as a superior catalyst system that mediates reactions effectively while retaining its integrity. A simple multilayer film design is developed, and a convenient protocol for its fabrication through *in situ* formation of silver nanoparticles inside PVA film was optimized. The kinetics of the catalytic reaction was investigated, and optimal catalyst composition and reactant ratio determined. The thin film catalyst is shown to produce a TON of ~114 in a single reaction run that lasted around 15 min. Retrieval and reintroduction of the thin film 'dip catalyst' are easy to implement, providing a simple mechanical control of the reaction. The same catalyst film can be reused more than 30 times, which leads to a total TON of ~3390. The cheap materials and simple methods used in catalyst fabrication, in combination with the large TON achieved, establish the cost effectiveness of the present approach. Spectroscopy and microscopy are used to monitor the catalyst film during the repeated usage, and demonstrate the basis of its durability and stability. Embedding the metal nanoparticles inside the polymer film effectively precludes aggregation, and enables long-term storage of these nanocomposite films, an aspect of considerable practical relevance. The present study illustrates the promise of metal nanoparticle-embedded polymer thin films as versatile and effective catalysts. The wide range of polymer-metal combinations that can be exploited, and the plethora of reactions that can be addressed, point to the enormous potential of the general approach presented in this chapter.

References

1. (a) Moreno-MaÇas, M.; Pleixats, R. *Acc. Chem. Res.* **2003**, *36*, 638. (b) Narayanan, R.; El-Sayed, M. A. *J. Am. Chem. Soc.* **2004**, *126*, 7194. (c) Burda, C.; Chen, X.; Narayanan, R.; El-Sayed, M. A. *Chem. Rev.* **2005**, *105*, 1025. (d) Heiz, U.; Landman, U. *Nanocatalysis*, Springer, Berlin, **2007**. (e) Somorjai, G. A.; Park, J. Y. *Top. Catal.* **2008**, *49*, 126.

2. Witham, C. A.; Huang, W.; Tsung, C.; Kuhn, J. N.; Somorjai, G. A.; Toste, F. D. *Nat. Chem.* **2010**, *2*, 36.

3. (a) Schmid, G. *Chem. Rev.* **1992**, *92*, 1709. (b) Roucoux, A.; Schulz, J.; Patin, H. *Chem. Rev.* **2002**, *102*, 3757. (c) Shylesh, S.; Schünemann, V.; Thiel, W. R. *Angew. Chem. Int. Ed.* **2010**, *49*, 3428.

4. Zaera, F. *J. Phys. Chem. Lett.* **2010**, *1*, 621.

5. (a) Crooks, R. M.; Zhao, M.; Sun, L.; Chechik, V.; Yeung, L. K. *Acc. Chem. Res.* **2001**, *34*, 181. (b) Kim, J.; Gewirth, A. A. *J. Phys. Chem. B* **2005**, *109*, 9684. (c) Song, H.; Rioux, R. M.; Hoefelmeyer, J. D.; Komor, R.; Niesz, K.; Grass, M.; Yang, P. D.; Somorjai, G. A. *J. Am. Chem. Soc.* **2006**, *128*, 3027. (d) Wang, S.; He, X.; Song, L.; Wang, Z. *Synlett* **2009**, 447. (e) Jiang, H.; Liu, B.; Akita, T.; Haruta, M.; Sakurai, H.; Xu, Q. *J. Am. Chem. Soc.* **2009**, *131*, 11302.

6. (a) Ozdemir, S. S.; Buonomenna, M. G.; Drioli, E. *Appl. Catal. A* **2006**, *307*, 167. (b) McKeown, N. B.; Budd, P. M. *Chem. Soc. Rev.* **2006**, *35*, 675.

7. (a) Heilmann, A. *Polymer Films with Embedded Metal Nanoparticles*, Springer, Berlin, **2003**. (b) Faupel, F.; Zaporojtchenko, V.; Greve, H.; Schürmann, U.; Chakravadhanula, V. S. K.; Hanisch, Ch.; Kulkarni, A.; Gerber, A.; Quandt, E.; Podschun, R. *Contrib. Plasma Phys.* **2007**, *47*, 537.

8. (a) Caseri, W. *Macromol. Rapid Commun.* **2000**, *21*, 705. (b) Stepanov, A. L. *Tech. Phys.* **2004**, *49*, 143.

9. Abargues, R.; Marqués-Hueso, J.; Canet-Ferrer, J.; Pedrueza, E.; Valdés, J. L.; Jiménez, E.; Martínez-Pastor, J. P. *Nanotechnology* **2008**, *19*, 355308.

10. Meng, X.; Fujita, K.; Zong, Y.; Murai, S.; Tanaka, K. *Appl. Phys. Lett.* **2008**, *92*, 201112.

11. Leong, W. L.; Lee, P. S.; Lohani, A.; Lam, Y. M.; Chen, T.; Zhang, S.; Dodabalapur, A.; Mhaisalkar, S. G. *Adv. Mater*. **2008**, *20*, 2325.

12. Ramesh, G. V.; Porel, S.; Radhakrishnan, T. P. *Chem. Soc. Rev*. **2009**, *38*, 2646.

13. Zijlstra, P.; Chon, J. W. M.; Gu, M. *Nature* **2009**, *459*, 410.

14. Mbhele, Z. H.; Salemane, M. G.; van Sittert, C. G. C. E.; Nedeljkovic´, J. M.; Djokovic´, V.; Luyt, A. S. *Chem. Mater.* **2003**, *15*, 5019.

15. (a) Sih, B. C.; Wolf, M. O. *Chem. Commun*. **2005**, 3375. (b) Sangermano, M.; Yagci, Y.; Rizza, G. *Macromolecules* **2007**, *40*, 8827.

16. (a) Won, J.; Ihn, K. J.; Kang, Y. S. *Langmuir* **2002**, *18*, 8246. (b) Korchev, A. S.; Bozack, M. J.; Slaten, B. L.; Mills, G. *J. Am. Chem. Soc.* **2004**, *126*, 10. (c) Li, J.; Kamata, K.; Watanabe, S.; Iyoda, T. *Adv. Mater.* **2007**, *19*, 1267. (d) Horiuchi, S.; Nakao, Y. *Curr. Nanosci.* **2007**, *3*, 206. (e) Hasell, T.; Lagonigro, L.; Peacock, A. C.; Yoda, S.; Brown, P. D.; Sazio, P. J. A.; Howdle, S. M. *Adv. Funct. Mater.* **2008**, *18*, 1265.

17. (a) Fritzsche, W.; Porwol, H.; Wiegand, A.; Bornmann, S.; Kçhler, J. M. *Nanostruct. Mater.* **1998**, *10*, 89. (b) Rifai, S.; Breen, C. A.; Solis, D. J.; Swager, T. M. *Chem. Mater.* **2006**, *18*, 21. (c) Shang, L.; Wang, Y.; Huang, L.; Dong, S. *Langmuir* **2007**, *23*, 7738. (d) Zhang, J.; Gao, Y.; Alvarez-Puebla, R. A.; Buriak, J. M.; Fenniri, H. *Adv. Mater.* **2006**, *18*, 3233. (e) Deshmukh, R. D.; Composto, R. J. *Chem. Mater.* **2007**, *19*, 745.

18. Porel, S.; Singh, S.; Harsha, S. S.; Rao, D. N.; Radhakrishnan, T. P. *Chem. Mater.* **2005**, *17*, 9.

19. Porel, S.; Singh, S.; Radhakrishnan, T. P. *Chem. Commun*. **2005**, 2387.

20. Porel, S.; Hebalkar, N.; Sreedhar, B.; Radhakrishnan, T. P. *Adv. Funct. Mater*. **2007**, *17*, 2550.

21. Asharani, P. V.; Mun, G. L. K.; Hande, M. P.; Valiyaveettil, S. *ACS Nano* **2009**, *3*, 279.

22. Ramesh, G. V.; Sreedhar, B.; Radhakrishnan, T. P. *Phys. Chem. Chem. Phys*. **2009**, *11*, 10059.

23. Porel, S.; Venkatram, N.; Rao, D. N.; Radhakrishnan, T. P. *J. Appl. Phys*. **2007**, *102*, 033107.

24. Gao, Y.; Ding, X.; Zheng, Z.; Cheng, X.; Peng, Y. *Chem. Commun*. **2007**, 3720.

25. (a) Lu, Y.; Mei, Y.; Schrinner, M.; Ballauff, M.; Mçller, M. W.; Breu, J. *J. Phys. Chem. C* **2007**, *111*, 7676. (b) Rashid, M. H.; Mandal, T. K. *J. Phys. Chem. C* **2007**, *111*, 16750. (c) Murugadoss, A.; Chattopadhyay, A. *Nanotechnology* **2008**, *19*, 015603. (d) Wang, A.; Yin, H.; Lu, H.; Xue, J.; Ren, M.; Jiang, T. *Langmuir* **2009**, *25*, 12736. (e) Khalavka, Y.; Becker, J.; Sçnnichsen, C. *J. Am. Chem. Soc*. **2009**, *131*, 1871. (f) Zeng, J.; Zhang, Q.; Chen, J.; Xia, Y. *Nano Lett*. **2010**, *10*, 30.

26. (a) Oh, S.; Kim, M.; Choi, S.; Chun, J.; Lee, K.; Gopalan, A.; Hwang, C.; Sang-Ho, K.; Hoon, O. J. *J. Ind. Eng. Chem*. **2008**, *14*, 687. (b) Huang, J.; Vongehr, S.; Tang, S.; Lu, H.; Shen, J.; Meng, X. *Langmuir* **2009**, *25*, 11890.

27. (a) Esumi, K.; Isono, R.; Yoshimura, T. *Langmuir* **2004**, *20*, 237. (b) Liu, Z.; Wang, X.; Wu, H.; Li, C. *J. Colloid Interface Sci.* **2005**, *287*, 604. (c) Dotzauer, D. M.; Bhattacharjee, S.; Wen, Y.; Bruening, M. L. *Langmuir* **2009**, *25*, 1865. (d) Wunder, S.; Polzer, F.; Lu, Y.; Mei, Y.; Ballauff, M. *J. Phys. Chem. C*. **2010**, *114*, 8814.

28. (a) Jana, S.; Pal, T. *J. Nanosci. Nanotechnol*. **2007**, *7*, 2151. (b) Jia, X.; Ma, X.; Wei, D.; Dong, J.; Qian, W. *Colloids Surf. A* **2008**, *330*, 234.

29. Shin, K. S.; Choi, J.; Park, C. S.; Jang, H. J.; Kim, K. *Catal. Lett*. **2009**, *133*, 1.

30. Reminiscent of the familiar "dip tea" that comes in porous sachets.

31. Pradhan, N.; Pal, A.; Pal, T. *Colloids Surf. A* **2002**, *196*, 247.

32. Jana, S.; Ghosh, S. K.; Nath, S.; Pande, S.; Praharaj, S.; Panigrahi, S.; Basu, S.; Endo, T.; Pal, T. *Appl. Catal. A* **2006,** *313*, 41.

33. Lu, Y.; Mei, Y.; Walker, R.; Ballauff, M.; Drechsler, M. *J. Phys. Chem. B* **2006,** *110*, 3930.

34. Murugadoss, A.; Chattopadhyay, A. *Nanotechnology* **2008,** *19*, 015603.

35. Lu, Y.; Mei, Y.; Walker, R.; Ballauff, M.; Drechsler, M. *Polymer* **2006,** *47*, 4985.

36. Esumi, K.; Isono, R.; Yoshimura, T. *Langmuir* **2004,** *20*, 237.

37. Pradhan, N.; Pal, A.; Pal, T. *Langmuir* **2001**, *17*, 1800.

38. Gao, Y.; Ding, X .; Zheng, Z.; Cheng, X.; Peng, Y. *Chem. Commun*. **2007,** 3720.

39. Shin, K. S.; Choi, J.; Park, C. S.; Jang, H. J.; Kim, K. *Catal. Lett.* **2009**, *133*, 1.

40. Hariprasad, E.; Radhakrishnan, T. P. *Chem. Eur. J.* **2010,** *16,* 14378.

CHAPTER 3

Palladium Nanoparticle-Embedded Polymer Thin Film: "Dip Catalyst" for C-C Coupling Reactions

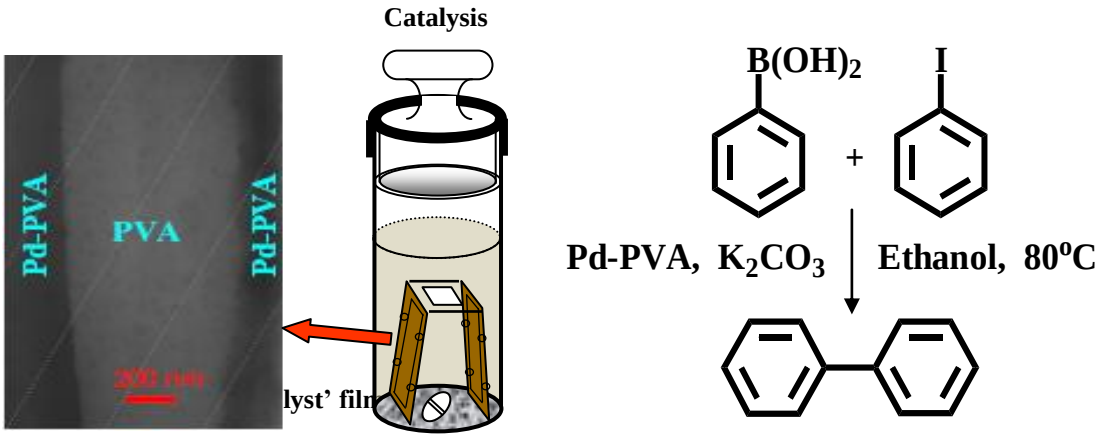

A 3-layer 'dip catalyst' based on palladium nanoparticles used in the Suzuki-Miyaura coupling reaction.

Paper published

Hariprasad, E.; Radhakrishnan, T. P. *ACS Catal.* **2012,** *2,* 1179.

Scope

Simplicity of design, low cost of fabrication, high efficiency, facile recovery and extensive reusability, amenability to monitoring between reuses, and ease of scale up are some of the characteristics of a successful catalyst. Even though the number of palladium nanoparticle based catalysts reported for the Suzuki-Miyaura reaction has grown exponentially in recent years, the above mentioned criteria are not often met in a single system. In this chapter we present a highly efficient and reusable palladium nanoparticle based 'dip catalyst', for the Suzuki-Miyaura reaction. The methodology for fabrication of multilayer free-standing nanocomposite thin film has been discussed in Chapter 2 (Sec. 2.2). Fabrication parameters of the Pd-PVA film are optimized for enhanced catalyst efficiency. The catalyst is shown to produce very high yield, turn-over-number and turn-over-frequency in the prototypical reaction of iodobenzene with phenylboronic acid. The 'dip catalyst' film is easily retrieved from the reaction system and reintroduced in successive batches; the high efficiency is retained beyond 30 cycles. The thin film structure enabled convenient catalyst monitoring by spectroscopy and microscopy between reuses. Efficient use of the catalyst up to 5 mmol scale reaction is demonstrated. A simple figure-of-merit is formulated to quantify the catalyst performance, and the present catalyst is evaluated in the context of those reported earlier. Preliminary exploration of the utility of the thin film catalyst in the Suzuki-Miyaura reaction with several substrates as well as in the Heck and Sonogashira coupling reactions are carried out.

3.1 Introduction

Efficiency of a catalyst is generally enhanced under homogeneous conditions as it is molecularly dispersed. However the same factor hampers its recovery and reuse. Heterogeneous formulation facilitates recycling, however at the cost of efficiency as the reaction is confined to the interface region. Metal nanoparticles tend toward molecular level efficiency, and deployment in a suitable framework can improve the reusability, paving the way to harness the advantages of homogeneous and heterogeneous catalysis.

This general concept has motivated extensive explorations. As an example of enormous contemporary interest, we take the case of palladium catalyzed cross coupling reactions, focusing on nanoparticle catalysts and the issue of catalyst recycling. Even though catalyst recovery through, nanofiltration[1] and magnetic separation[2] have been used; the procedures are often laborious or the catalyst fabrication elaborate, making the process expensive. Some of the supports that have been used to load the palladium nanoparticle catalyst are mesoporous organosilica and grafted silica foam,[3,4] layered double hydroxide and clays,[5,6] zeolites and molecular sieves,[7-9] various metal oxides,[9,10] activated or nitrogen doped carbon,[9,11,12] and polymeric networks, capsules, and resins.[9,13-15] However, most of these approaches are prone to catalyst leaching or degradation through the repeat cycles, impairing the reaction yields and limiting the reuse. An optimal solution that combines a simple and cheap fabrication of a highly efficient catalyst with effective recovery and reuse remains elusive.

The concept of a 'dip catalyst' that we have developed (Chapter 2)[16] is relevant in this context. The high efficiency and extensive reusability of a catalyst based on silver nanoparticle embedded poly(vinyl alcohol) (Ag-PVA) thin film fabricated through a simple *in situ* protocol,[17] in the reduction of 4-nitrophenol by sodium borohydride was demonstrated in that study (chapter 2). Easy fabrication, convenient recycling, and facile monitoring of the 'dip catalyst' thin film between uses, are the highlights of this approach. Its generality and versatility stem from the wide variations possible in the catalyst-polymer combinations. Moving beyond the 'proof-of-principle' exploration in the earlier chapter, we now demonstrate the utility of the approach in a reaction of wide applicability in organic synthesis, the palladium catalyzed Suzuki-Miyaura coupling. Choice of this reaction also allows an appraisal of our concept against the background of a large collection of nanoparticle catalysts reported earlier.

A survey of the extensive literature on palladium catalyzed Suzuki-Miyaura reaction in particular and the subject of catalysis in general, reveals the critical need to evaluate a catalyst on the basis of multiple parameters. It is desirable to have an integrated view of the various relevant factors including the TON or TOF, the number

of reuse cycles, scale of the reaction, the temperature at which it is carried out (hence the energy input), the solvent/special atmosphere required, and the cost of catalyst fabrication. While quantification of some of these is straightforward, others are complicated. An attempt to evolve a figure-of-merit (FOM) that takes into account as many of the clearly quantifiable factors as possible appears to be worthwhile. Even though FOM's have been invoked for the specific purpose of designing some catalysts,[18] rarely they have been employed for the direct comparison of catalysts available for a chosen reaction. We have made a preliminary effort toward this goal which allowed us to make a meaningful comparison of our 'dip catalyst' with those reported earlier for the same reaction.

Extending the *in situ* method for the synthesis of dendritic palladium nanostructures in a PVA film developed in our laboratory earlier,[19] we have fabricated a multilayer Pd-PVA thin film catalyst. The multilayer structure makes the free-standing film robust while facilitating easy access of the reagents to the ligand-free catalyst nanoparticles embedded and stabilized within the polymer matrix. Experiments were carried out to optimize the Pd/PVA ratio and the reaction conditions for the Suzuki-Miyaura coupling of iodobenzene and phenylboronic acid to yield biphenyl. Under optimal conditions, nearly 100% yield is obtained, and the yield and reaction time show negligible change over 30 reuses. Very large TON's and TOF's can be realized by using tiny pieces of the catalyst film, and the reaction is found to be facile at scales up to 5 mmol. An FOM of the catalyst is defined incorporating the values of average TOF, number of reuses, scale of the reaction, and the temperature condition required. Using this FOM, we compare the Pd nanoparticle based catalysts reported for this reaction including our 'dip catalyst'. The utility of our catalyst in the Suzuki-Miyaura reaction with a range of substrates, as well as in the Heck and Sonogashira reactions are demonstrated.

3.2 Fabrication of the Catalyst Film

The general procedure for the fabrication follows the method described in Chapter 2 (Sec. 2.2). Here we describe the specific details related to palladium and PVA.

Aqueous solutions of K_2PdCl_4 and PVA were mixed in the required proportions; for example, 80 mg of K_2PdCl_4 dissolved in 2 mL of water was mixed with 200 mg of PVA dissolved in 4 mL of water to prepare a film with a Pd/PVA weight ratio, x = 0.13. Spin-coating of the K_2PdCl_4-PVA solution on glass (pre-coated with PS layer) at 500 rpm for 10 s followed by 6000 rpm for 10 s and heating the film at 90 °C for 30 min produced ~180 nm thick film. On top of this layer, an aqueous solution of PVA was spin-coated at 500 rpm for 10 s followed by 3000 rpm for 10 s and heated at 90 °C for 30 min; a second coating of PVA was added to increase the thickness. The final layer was formed by spin-coating the K_2PdCl_4-PVA solution as before, and the film was heated at 130 °C for 4 h.

The film was peeled off the glass substrate and wrapped around a Teflon frame. It was then dipped in toluene to dissolve the PS layer and yield the free-standing 3-layer Pd-PVA/PVA/Pd-PVA film fixed on the frame. The film was finally washed in water to remove the unreduced K_2PdCl_4 and the byproduct KCl formed during the *in situ* reduction of K_2PdCl_4 by PVA; the observation of KCl and its removal are discussed in reference 19.

3.3 Characterization of the Catalyst Film

We have prepared the 3-layer films with various Pd/PVA weight ratios, x, in the Pd-PVA layer. The following characterization refer to the film with x = 0.13. Thickness of the films prepared on polystyrene coated glass plates was measured using a surface profilometer. For the purpose of estimating the thickness, the 3-layer film was prepared in steps, covering each layer partially with a Teflon tape before spin-coating the next one. Thickness of each layer was measured. Average values of the thickness of each layer estimated by measurements at several different points on 3 samples are listed in Table 3.1; the spin-coating condition for each layer is also indicated.

Electronic absorption spectra of the film, recorded through the different stages of fabrication are shown in Fig. 3.1a. The first layer (K_2PdCl_4-PVA) shows the peaks due

Table 3.1. *Average thickness of each layer in a Pd-PVA/PVA/Pd-PVA film; the spin-coating condition for each layer is indicated.*

Layer	Film	Spin-coating speed (rpm), [time (s)]	Thickness of layer (nm)
1	Pd-PVA	500 [10], 6000 [10]	184 ± 25
2	PVA	500 [10], 3000 [10]	532 ± 52
3	Pd-PVA	500 [10], 6000 [10]	167 ± 61

to the precursor salt; after the short heating step there is little change in the spectrum. The visible change upon coating the second layer (PVA) is due to increased light scattering and the localized surface plasmon resonance (LSPR) absorption of the Pd nanostructures formed in the film; the latter may result from the higher net ratio of PVA to Pd that enhances the chemical reduction of the Pd^{2+} ions.[19] The LSPR peak becomes prominent on heating the 2-layer film for 30 min. As expected, the precursor peaks appear clearly again on coating the third layer (K_2PdCl_4-PVA). The subsequent heating leads to the emergence of the strong LSPR absorption of palladium nanoparticles extending into the visible region; changes become negligible after 4 h of heating. It was found that longer heating did not enhance the extent of reduction of the Pd^{2+} ions or the stability of the film. The spectrum of the final film dipped briefly in water (Fig. 3.1b) indicates the removal of the soluble precursor left unreacted in the film.

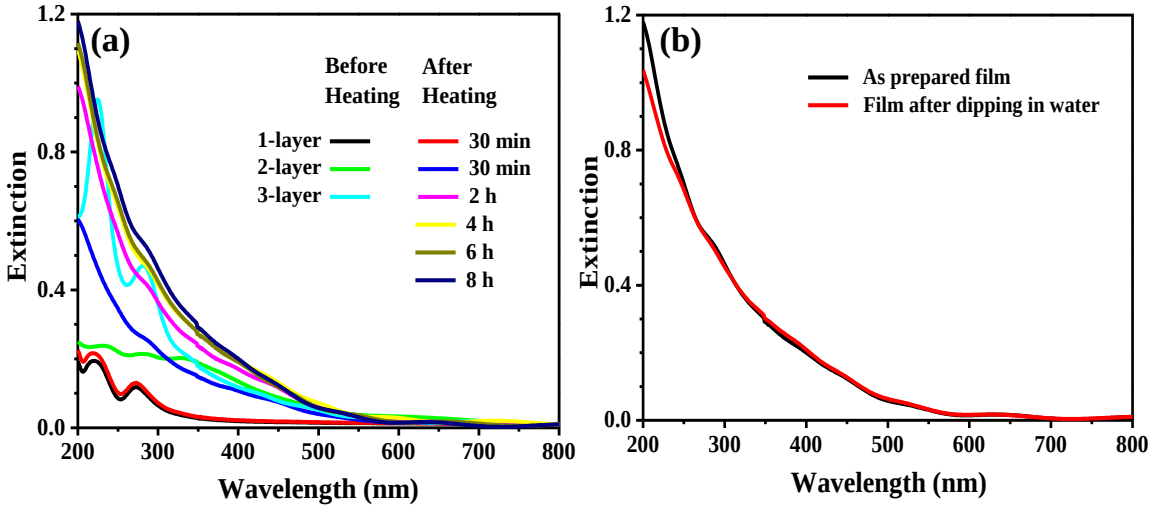

Figure 3.1. *Electronic absorption spectra of the catalyst film* ***(a)*** *recorded through the different stages of spin-coating and heating,* ***(b)*** *as prepared and after dipping briefly in water and drying.*

TEM images of the first layer shows dendritic structures due to the precursor and some Pd formed on heating (Fig. 3.2a). The electron diffraction spots can be indexed to the precursor K_2PdCl_4 (blue) and product Pd (red) crystals (Fig. 3.2b); this is consistent with the partial reduction of the precursor in 30 min heating, which is similar to the observation in the precursor-to-palladium nanocrystal transformation investigated in detail earlier.[19] The film washed briefly in water shows the diffraction rings corresponding to the product Pd, but the spots due to K_2PdCl_4 disappear. Upon coating the second layer (PVA), the film is too thick to get a clear TEM image; however, one can visualize some morphological changes; spherical particles ~100-300 nm in diameter is observed (Fig. 3.3a). The increased net PVA/Pd ratio and the extended heating contribute to the morphology change.[19] Cross section samples were prepared by fixing the free-standing film in Araldite resin and cutting into 50 nm thin sections using an ultramicrotome. The TEM image of the cross section of the final 3-layer film reveals the layer structure (Fig. 3.3b); thicknesses of the layers are consistent with those noted above. Because of the high density of particles in the outer two layers, individual ones are not resolved, but the low density in the middle layer reveals spherical particles ~15-30 nm in size.

The FESEM image of the cross-section sample (Fig. 3.4) shows similar layer structure and the thickness of individual layers are consistent with those above. EDXS

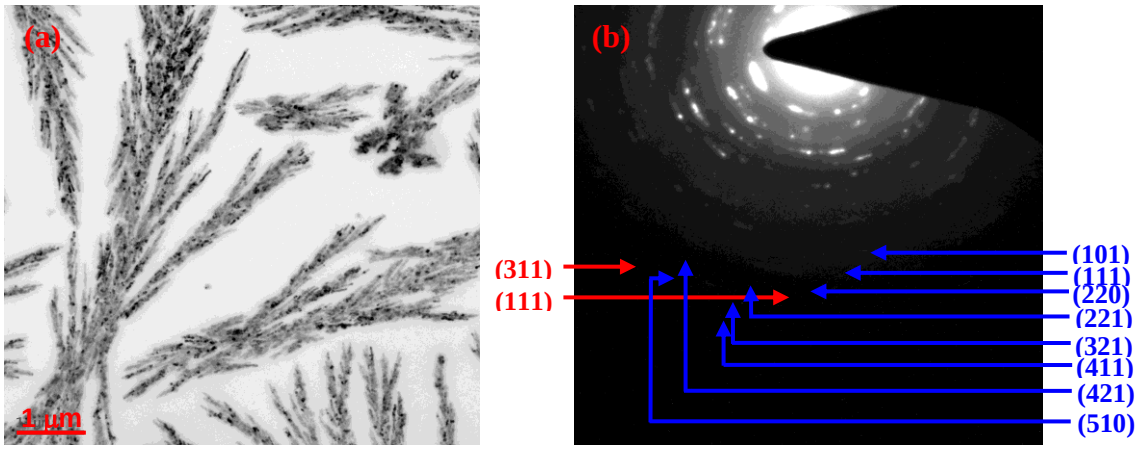

Figure 3.2. ***(a)*** *TEM image of the 30 min heated single layer film,* ***(b)*** *Electron diffraction recorded on the 1-layer Pd-PVA film. The diffraction spots can be indexed to the precursor K_2PdCl_4 (blue) and product Pd (red) crystals.*

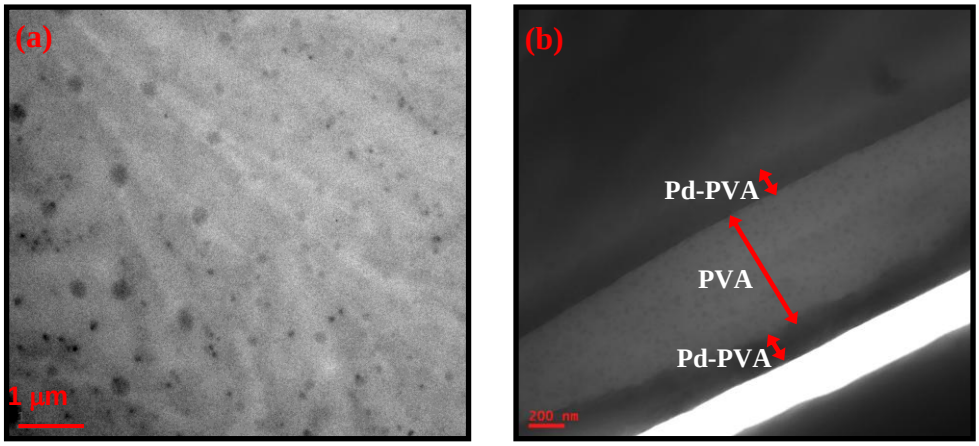

Figure 3.3. *TEM images of the heated **(a)** 2-layer film and **(b)** final 3-layer film cross section. The corresponding layers are indicated.*

analysis across the layer thickness shows a lower concentration of Pd in the middle layer of the film (Fig. 3.4). The microscopy images are thus consistent with the Pd-PVA/PVA/Pd-PVA coating sequence.

The content of palladium was estimated by weighing films at different steps of fabrication; coating polystyrene on glass and heating (G + PS), after coating the first layer and heating (G + PS + Pd-PVA), after coating the second layer and heating (G + PS + Pd-PVA + PVA), and after coating the third layer and heating (G + PS + Pd-PVA + PVA + Pd-PVA). An electronic balance with a sensitivity of 10^{-5} g was used and

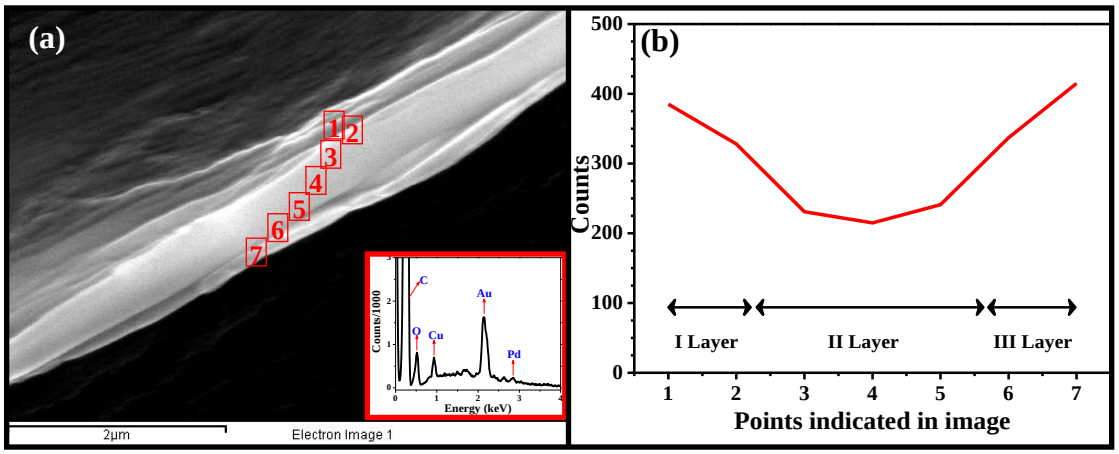

Figure 3.4. ***(a)** FESEM image of the cross section of Pd-PVA/PVA/Pd-PVA thin film; EDXS spectrum (inset) at point 3 is shown. **(b)** Counts collected at different points (**1-7** in **(a)**) across the film at 2.84 keV (corresponding to Pd).*

Table 3.2. *Average weight of the individual layers in a multilayer film; the standard deviations are also indicated.*

Layer	Average weight (mg)
I layer (Pd-PVA)	0.12 ± 0.03
II layer (PVA)	2.00 ± 0.54
III layer (Pd-PVA)	0.11 ± 0.01

3 measurements on 10 samples were made for each stage. The average weights of individual layers are tabulated in Table 3.2. Pd content in the catalyst film is estimated based on the weights of the Pd-PVA layers and found to be ~0.58 μmol. Inductively coupled plasma-optical emission spectrometer (ICP-OES) analysis of samples prepared by dissolving a known weight of the free-standing film in 100 mL of 60% nitric acid revealed the amount of Pd in the film to be ~0.6 μmol, in close agreement with the above estimate.

3.4 Catalytic Studies

Carbon-carbon bond forming reactions have wide applicability in organic synthesis. The Suzuki-Miyaura coupling is one of the most popular, and is generally catalyzed by Pd complexes or Pd nanoparticles; it is frequently used in the synthesis of complex compounds.[20] We have chosen to deploy our 'dip catalyst' for the Suzuki-Miyaura reaction, in order to compare its efficacy with the large number of other nanoparticle based catalytic systems reported for this reaction.

The procedure followed in a typical reaction is as follows. 2 mmol of the base was introduced into a reaction tube in which a magnetic stirring bar was placed. This was followed by the addition of 15 mL of the solvent and 1 mmol of the aryl halide. The catalyst film wrapped on a Teflon frame was introduced. After adding 1.1 mmol of phenylboronic acid, the reaction tube was closed with a stopper and keck clip, and introduced into an oil bath preheated to the required temperature. The reaction mixture was stirred with the magnetic bar. The setup of the reaction tube and scheme of the reaction are shown in Fig. 3.5. Formation of the product was monitored through gas

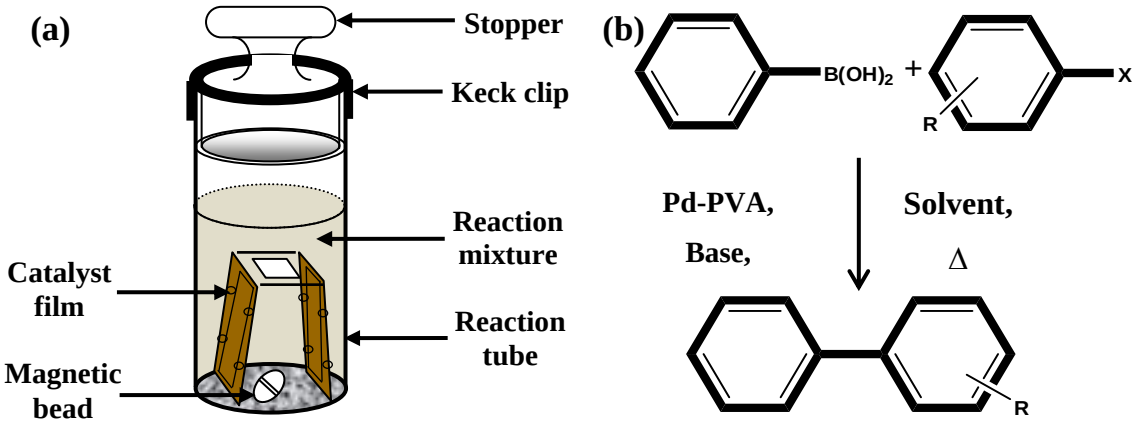

Figure 3.5. ***(a)*** *Schematic diagram of the reaction tube used to study the Suzuki-Miyaura reaction using the Pd-PVA 'dip catalyst';* ***(b)*** *Scheme of the reaction.*

chromatograph-mass spectrometer (GC-MS) analysis of 0.2 mL samples of the reaction mixture retrieved periodically from the reaction tube. All reactions were carried out under normal atmosphere; inert conditions were not required.

3.4.1 *Optimization of Solvent and Base*

A wide range of solvents and bases have been employed in the Suzuki−Miyaura reaction (iodobenzene with phenylboronic acid). The catalyst film is robust enough to be used in any of these solvents. However, as the swelling of the polymer film in the solvent enhances the catalyst activity by improving access of the reactants to the catalyst, we have focused in particular on aqueous and alcoholic solvents. We have chosen a film with x = 0.13 and a reaction temperature of 80 °C (basis of these choices are discussed in following sections) to investigate the effect of different solvents and bases. All the reactions were carried out using 1 mmol of iodobenzene and 1.1 mmol of phenylboronic acid. Observations with the different solvents (using 2 mmol of K_2CO_3 as the base) are collected in Table 3.3. The rates and yields are poor with pure water and water-ethanol mixtures, but enhanced considerably by the addition of tetrabutylammonium bromide. However, as the base dissolves in the solvent, the product has to be isolated by extraction. Ethanol is an optimal choice of solvent, as there is no need of a phase-transfer agent, the reaction is fast, work up of the reaction mixture is simple, and the yields are quantitative.

Table 3.3. *Time and yield of the reaction of phenylboronic acid with iodobenzene in different solvents using K_2CO_3 as the base and the thin film catalyst (Pd-PVA layer, x =0.13). Details about reaction conditions are discussed in the text.*

Solvent	Time (h)	Yield (%)
Water	5	8
	2[a]	100[a]
Water-ethanol (10:1)	5	22
	2[a]	100[a]
Water-ethanol (1:1)	5	58
	1.5[a]	100[a]
Toluene	3	45
N,N-dimethylacetamide	2	100
Ethanol	1.5	100

[a]*With 0.01 mmol of tetrabutylammonium bromide as phase transfer catalyst.*

We have also explored the utility of different bases; Table 3.4 lists the yields obtained for the reaction run in ethanol for 1.5 h by using 2 mmol of base and the reactants as mentioned for the solvent optimization. Even though K_2CO_3, K_3PO_4, and NaOH provided similar quantitative yields, K_2CO_3 is preferred as it is non hygroscopic and easy to handle.

Table 3.4. *Yield of the reaction of phenylboronic acid with iodobenzene in ethanol using different bases and the thin film catalyst (Pd-PVA layer, x = 0.13).*

Base	Yield (%)	Remarks
Triethylamine	60	convenient to use
Sodium acetate	85	convenient to use
Potassium phosphate	100	hygroscopic
Sodium hydroxide	100	hygroscopic
Potassium carbonate	100	convenient to use

3.4.2 *Optimization of the Catalyst and Reaction Temperature*

Using ethanol as the solvent and K_2CO_3 as the base, we have carried out several batches of exploratory reactions to determine the optimal value of *x* of the catalyst film and the reaction temperature. It may be noted that only a single product is observed in all the reactions and test runs excluding iodobenzene or phenylboronic acid showed negligible homocoupling reaction. Fig. 3.6a shows the yield as a function of time, when catalyst films with different *x* values are employed; considerable improvement is observed when *x* is increased from 0.07 to 0.13, but there is little enhancement beyond this. It is seen that with *x* = 0.13, 100% conversion is achieved in 1.5 h.

The TON's for the different catalyst films are not influenced by the reaction temperature. However, the TOF's increase substantially at 80 °C for the films with *x* = 0.13 and 0.15 (Fig. 3.6b). The slightly higher TOF obtained using the film with *x* = 0.13 can be attributed to the lower catalyst content and the only marginal increase in the time for 100% conversion.

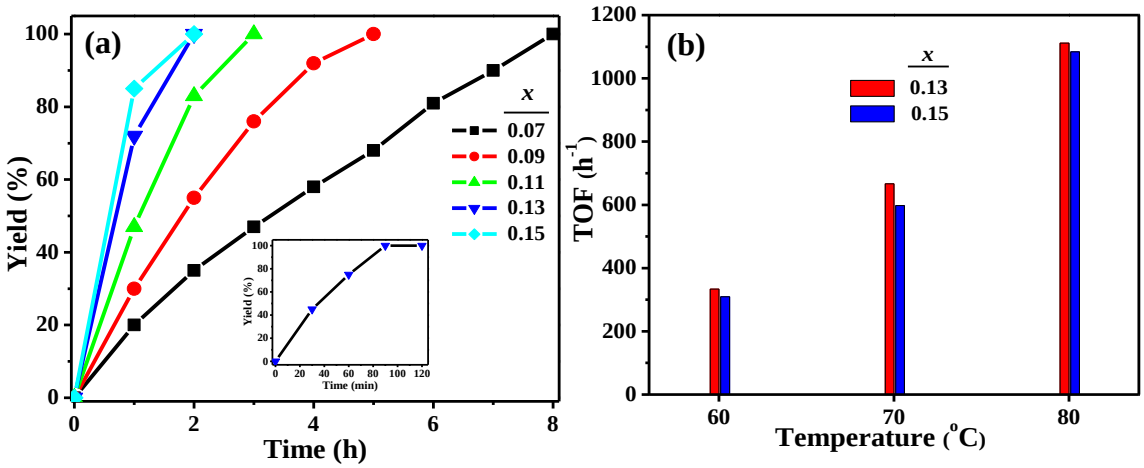

Figure 3.6. ***(a)*** *Progress of the Suzuki–Miyaura reaction catalyzed by the thin film catalyst with different Pd/PVA weight ratios (x) in the Pd-PVA layer; Inset: Progress of the reaction using the catalyst with x = 0.13 monitored at shorter time intervals. Reaction conditions: 1 mmol of PhI, 1.1 mmol of PhB(OH)₂, 2 mmol of K₂CO₃, temperature = 80 °C. Inset: Progress of the reaction using the catalyst with x = 0.13 monitored at shorter time intervals.* ***(b)*** *Turn-over-frequency (TOF) of the Suzuki–Miyaura reaction at different temperatures, using the thin film catalysts with different Pd/PVA weight ratios (x) in the Pd-PVA layer.*

3.4.3 *Catalyst Recycling and Monitoring*

On the basis of the experiments above, we have chosen the catalyst with $x = 0.13$ (in the Pd-PVA layers), ethanol as the solvent, K_2CO_3 as the base, and a reaction temperature of 80 °C to demonstrate the recycling capability of our 'dip catalyst'. These reactions were run using 1 mmol of iodobenzene and 1.1 mmol of phenylboronic acid. Nearly 100% yield was obtained in the first run in 1.5 h. The catalyst film taken out of the reaction mixture was dipped briefly in diethyl ether and washed with dichloromethane to remove organic residues, dipped in water and isopropanol to remove the base, and finally dried in vacuum for 30 min. The film was ready for reuse. It is found that the same film can be reused extensively. The yields obtained at 1.5 h in the 30 cycles we have run are shown in Fig. 3.7a; it may be noted that 100% yield can be obtained even in the last few cycles by slight increase in the reaction time. Yield of the isolated product from the combined reaction mixtures of the 30 cycles is 89%. The ease of redeployment of the catalyst and the quantitative conversion observed over such a large number of cycles testifies to the versatility of the 'dip catalyst' concept. The activity at the end of these runs suggests that the recycling can indeed be continued further. As mentioned earlier, ICP-OES analysis of the catalyst film with $x = 0.13$ used in these reactions indicated that the Pd content is 0.6 μmol. This implies a TON of 1667 in the runs with 100% yield; the total TON for the 30 cycles is the high value of 4.96×10^4. The average TOF works out to be 1102 h^{-1}. We have monitored the progress of the reaction at various points during the repeat cycles. As seen in Fig. 3.7b, the kinetics remains nearly unchanged through the large number of repeated uses.

TEM and X-ray photoelectron spectroscopy (XPS) studies carried out earlier[19] have unambiguously proved that the Pd-PVA formed through extended thermal annealing does still contain some amount of unreacted Pd^{2+}. Even though our catalyst film is washed in water following the 4 h heating process, it is possible that it contains trace Pd^{2+}. This may indeed be advantageous for the Suzuki−Miyaura reaction as Pd^{2+} alone being the active catalyst,[21] we have attempted the reaction with unheated films of K_2PdCl_4-PVA (with $x = 0.13$). Under identical reaction conditions as above, we find

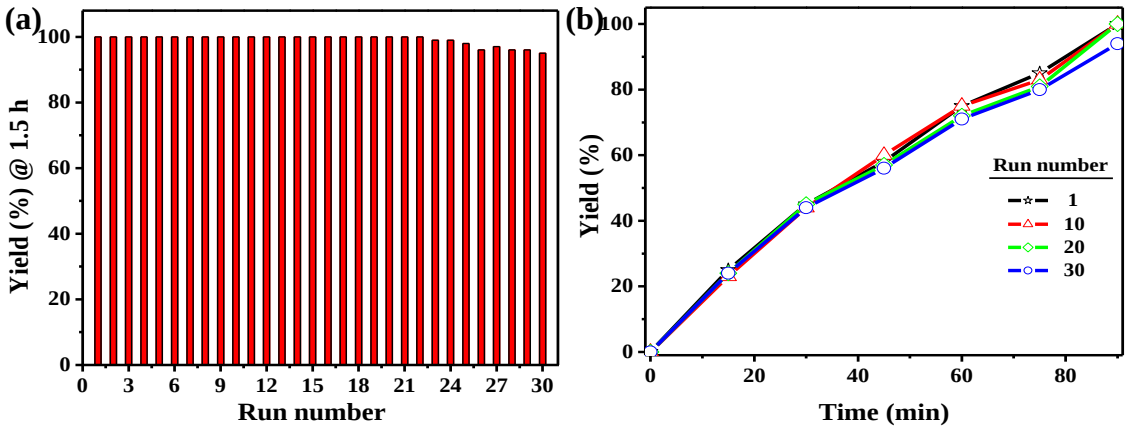

Figure 3.7. ***(a)*** *Yield obtained at 1.5 h reaction time in repeated runs of the Suzuki−Miyaura reaction using the same piece of thin film catalyst (Pd-PVA layer, x = 0.13. Reaction conditions: 1 mmol of PhI, 1.1 mmol of* $PhB(OH)_2$*, 2 mmol of* K_2CO_3*, temperature = 80 °C.* ***(b)*** *Kinetics plot showing the yield as a function of time for selected reaction runs.*

that the reaction hardly proceeds; less than 10% yield is obtained even after 2 h (Fig. 3.8). An experiment in which the Pd-PVA/PVA/Pd-PVA film was removed after 30 min of reaction showed the yield reached in that time (~40%) remaining unchanged for several hours afterward (Fig. 3.8), which clearly ruling out the possibility of Pd leached from the film catalyzing the reaction. Further, extremely low concentration (5 ppb) of Pd was detected by ICP-OES analysis in the reaction mixture, which is insufficient to catalyze the reaction. ICP-OES analysis of a control sample containing all the reagents including the base but no catalyst film showed the Pd content to be <1.0 ppb; this is significant in view of the report[22] of Pd impurity in the base catalyzing the Suzuki−Miyaura reaction.

An important advantage of the 'dip catalyst' is the ease with which the catalyst can be monitored during the reuse cycles; this is difficult with most of the catalyst immobilization schemes reported earlier. Such examinations provide useful insight into the basis of the durability of the catalyst. The electronic absorption spectra and FESEM images of the catalyst film before the first use and after 15 and 30 cycles of usage are shown in Fig. 3.9. The spectrum shows faint signs of Pd^{2+} generation, but negligible impact on the nanoparticle content, ruling out once again any significant leaching. The

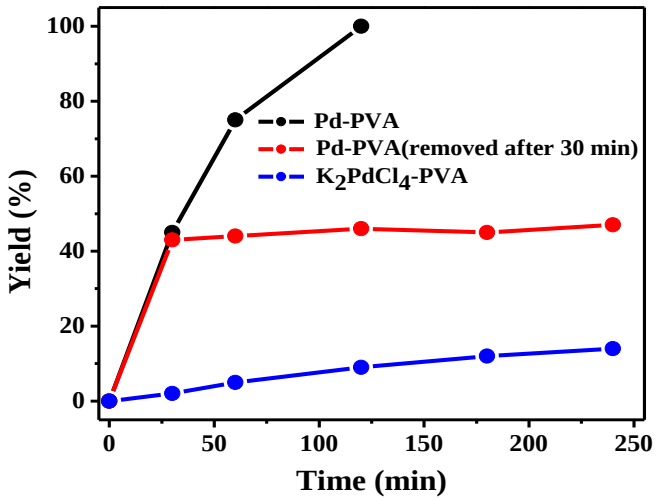

Figure 3.8. *Yield of biphenyl obtained at different times for the reaction carried out using the films with only the precursor (K_2PdCl_4) and the Pd-PVA film. The plot shows also the kinetics data for a run in which the Pd-PVA film is removed after 30 min.*

microscopy images show that the film morphology is affected very little; but small particles emerge near the surface after extensive recycling. The FESEM image of the catalyst film that has been used 30 times reveals well-defined particles (sizes similar to those seen in the TEM image in Fig. 3.3b). This is indicative of partial reorganization of Pd nanoparticles in the film, possibly towards the surface. Retention of the morphology of the nanoparticles is a significant observation, as it is different from the case of spherical particles aggregating into needles in solution based catalysts.[23] EDXS

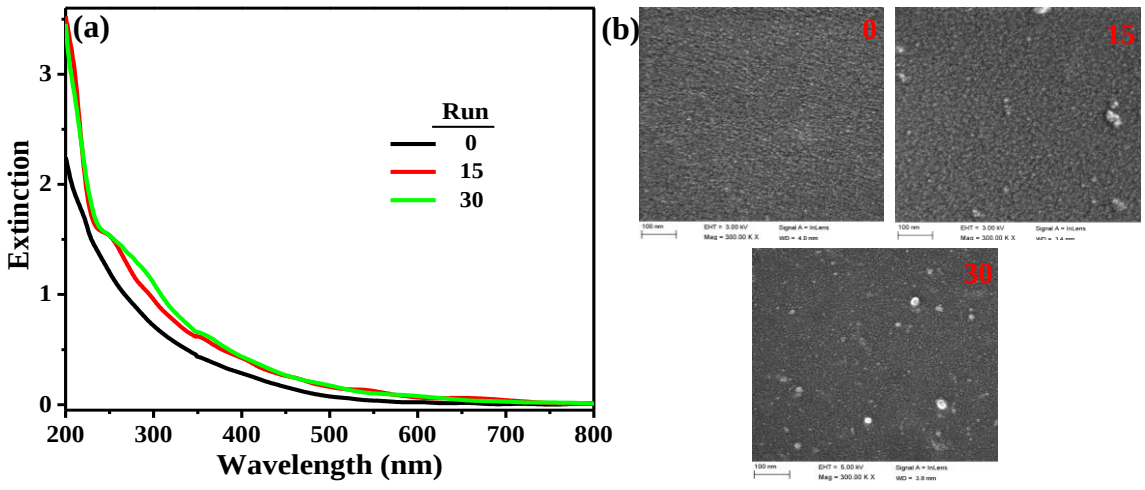

Figure 3.9. ***(a)*** *Electronic absorption spectra and* ***(b)*** *FESEM images (scale bar = 100 nm) of the same thin film catalyst (Pd-PVA layer, x = 0.13) after different number of uses (zero corresponds to the fresh film).*

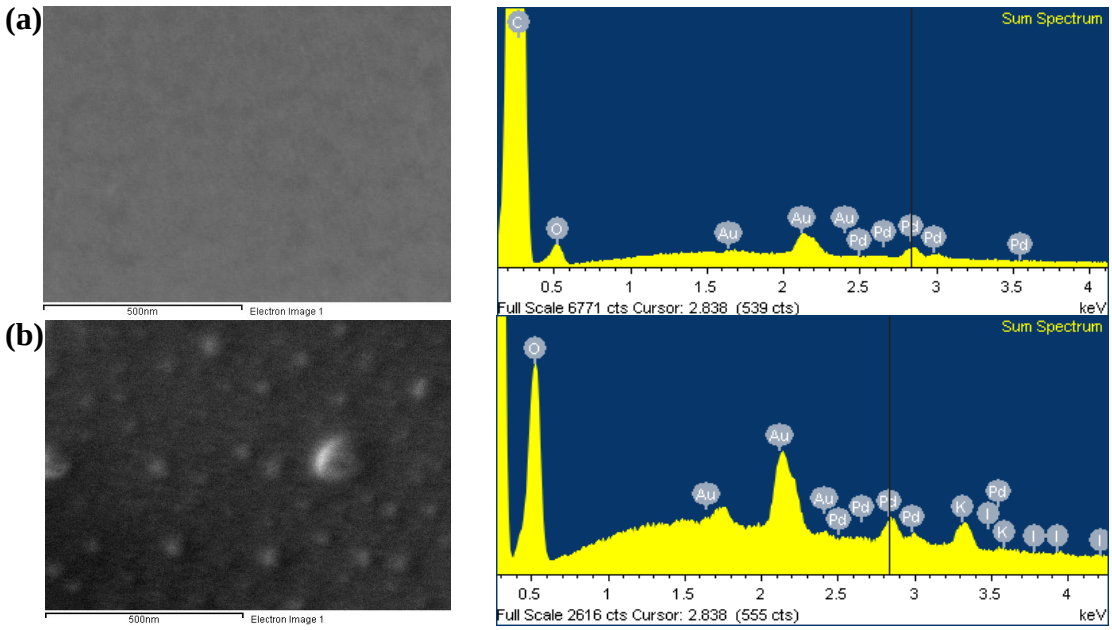

Figure 3.10. *FESEM image and EDX spectrum recorded on the corresponding area of the thin film catalyst* ***(a)*** *before use and* ***(b)*** *after 30 uses.*

of a fresh film and the film used as catalyst in 30 runs reveals a similar count for the Pd peak (Fig. 3.10), it may also be noted that the EDX spectrum of used film shows peaks due to K and I, due to remnants of the reagents in the reaction.

3.4.4 *Scale up and Extension*

Very large TON's of the order of 10^5–10^7 have been reported for the Suzuki-Miyaura reaction.[13,24–31] However, specialized catalyst preparation including high temperature treatments or special reaction conditions,[24-27] catalyst degradation or decline of yield with reuse[13,28] or relatively low reaction yields[29–31] are involved in most cases. To test the high TON's that we can realize, the reaction was carried out with a very small piece of the catalyst film containing 0.014 μmol (14 ppm) of the catalyst; reactants were scaled up to 5 mmol of iodobenzene and 6 mmol of phenylboronic acid. Because of the very small size, the film could not be fixed on a Teflon scaffold and hence could not be used in several cycles. However, in just 2 runs, a total TON of 7.2×10^5 could be realized, and a high TOF of 1.1×10^4 h^{-1}. In addition to the efficient

circulation in the reaction tube, the smaller size of the film is likely to enhance the accessibility of the Pd nanoparticles embedded within the film contributing to the enhanced TON and TOF. An important factor for the development of a catalyst system is the scale of the reaction that it can be employed in. Fig. 3.11 shows the reaction times for obtaining quantitative conversion in the reactions of 1-5 mmol of iodobenzene, using catalyst films (x = 0.13) with different areas and hence palladium content. It is seen that with the catalyst film with an area of 35 cm^2, even a 5 mmol scale reaction is satisfactorily completed in a short time; yield of the isolated product is 91%.

To evaluate the general applicability of our thin film catalyst we have explored the Suzuki-Miyaura reaction with iodo and bromobenzenes bearing various electron donating and withdrawing groups in different positions. Similar conditions as above were employed: catalyst film (x = 0.13), ethanol solvent, K_2CO_3 base, 80 °C, and ambient atmosphere. The observations collected in Table 3.5 show that the catalyst is very effective in all cases except with methoxy substituted bromobenzene. It does not work well with chlorobenzene and its derivatives.

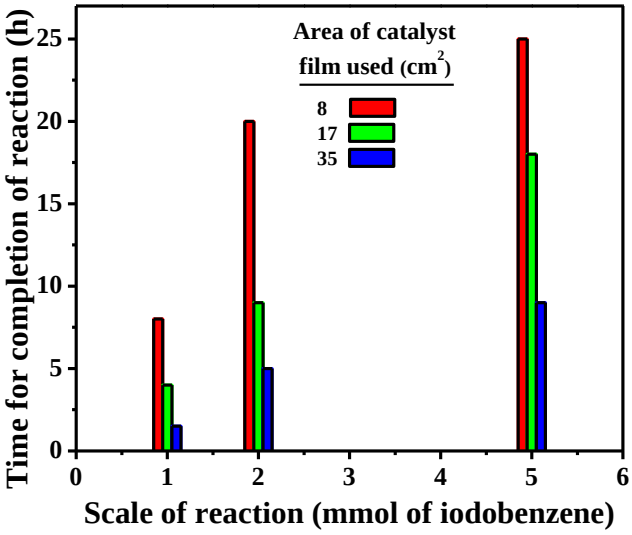

Figure 3.11. *Time for completion (100% yield) of the Suzuki-Miyaura reaction of phenylboronic acid (1.1 equivalent) with different amounts of iodobenzene, using Pd-PVA film with different areas. Reaction conditions: 1.1 equiv of $PhB(OH)_2$, 2 equiv of K_2CO_3, temperature = 80 °C.*

Table 3.5. *Time (h) required for 100% conversion in the Suzuki - Miyaura reaction of phenylboronic acid with different aryl halides (X = halogen; R = substituent on aromatic ring) using Pd-PVA thin film catalyst (Pd-PVA layer, x = 0.13).*

X	H	4-$COCH_3$	4-NO_2	4-NH_2	4-CH_3	4-OCH_3	2-OCH_3
I	1.5	1.5	1.5	1.5	1.5	2.0	3.5
Br	2.5	2.5	2.5	3.0	3.5	10.0	20.0

Preliminary studies suggest that our catalyst film works well in other C−C coupling reactions as well. Progress of the Heck and Sonogashira reactions of styrene and phenylacetylene with iodo and bromobenzenes using ethanol as the solvent, K_2CO_3 as the base, and the thin film catalyst (Pd-PVA layer, x = 0.13) at 80 ^{o}C yielding stilbene and diphenylacetylene respectively, is shown in Fig. 3.12. These observations point to the feasibility of extending the application of the nanocomposite thin film catalyst to a number of organic transformations.

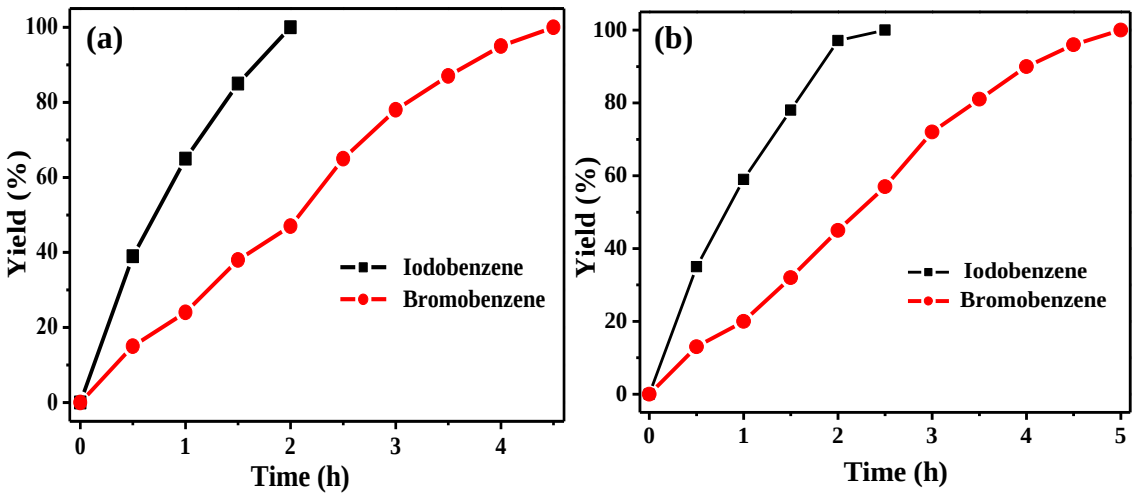

Figure 3.12. *Progress of the **(a)** Heck reaction of styrene and **(b)** Sonogashira reaction of phenylacetylene, with iodo and bromobenzenes. reaction conditions: 1 mmol of halobenzene, 1.1 mmol of styrene or phenylacetylene, 2 mmol of K_2CO_3, temperature = 80 °C.*

3.5 Figure-of-Merit of the Catalyst

As mentioned earlier, a fair appraisal of the performance of a catalyst for a reaction should take into account several parameters. Using the clearly quantifiable ones among them we define the following FOM,

$$\mathrm{FOM} = \frac{(\mathrm{TOF})_{\mathrm{av}} \times \mathrm{N} \times \mathrm{S}}{298 + |\Delta \mathrm{T}|}$$

where $(TOF)_{av}$ is the average TOF, N the number of runs (cycles), S the maximum scale of reaction demonstrated, and ΔT the magnitude of the deviation in the reaction temperature from the ambient (taken as 298 K). We have carried out a search of the reports on the Suzuki-Miyaura reaction from the year 2000, employing Pd nanoparticles for the specific reaction of iodobenzene with phenylboronic acid. Taking into account all the reports which have provided unambiguous information on the parameters listed above, the FOM of the various catalysts have been estimated. The complete list is collected in Table 3.6.

Table 3.6. *Calculated FOM for Pd nanoparticle based catalysts used in the Suzuki-Miyaura reaction of phenylboronic acid with iodobenzene. Reports from the year 2000 are considered and the relevant data from the reports are indicated. (T_{av} = average time per cycle, Yav = Average yield (%) per cycle). Data are arranged according to increasing FOM.*

Ref. No.	S (mmol)	T_{av} (h)	Y_{av} (%)	Amount of catalyst (µmol)	N	ΔT (K)	$(TOF)_{av}$ (h^{-1})	FOM (mmol h^{-1} K^{-1})
63	0.5	12	81	8	1	55	4.2	0.006
64	0.5	24	93	5	1	0	4.2	0.007
65	0.5	6	100	10	1	85	8.3	0.011
66	1.0	10	92	20	1	75	4.6	0.012
67	0.5	6	90	5	1	75	15	0.020
68	2.0	22	100	20	1	75	4.5	0.024
69	1.0	8	95	8	1	65	14.8	0.041
70	1.0	12	28	3	2	75	7.8	0.042
71	2	48	95	20	5	85	2.0	0.052
72	1.0	1	68	36	1	53	18.9	0.054

Table 3.6 continued…

73	1.0	4	84	10	1	55	21	0.059
74	1.0	4	94	10	1	85	23.5	0.061
75	0.5	4	95	2.5	1	75	47.5	0.064
76	1.0	12	95	3	1	55	26.4	0.075
77	0.6	20	93.4	3	5	75	9.3	0.075
78	1.0	18	100	2	1	55	27.8	0.079
79	1.0	4	97	110	11	0	2.2	0.081
80	1.0	8	98	20	5	65	6.1	0.084
81	0.5	14	90	0.5	1	65	64.3	0.089
82	0.5	1.5	100	5	1	75	66.7	0.089
83	1.0	5	70	4	1	45	35	0.102
84	0.5	1	99	7.5	1	0	66	0.111
85	1.0	5	100	5	1	55	40	0.113
86	0.2	2	100	0.55	1	85	200	0.115
87	1.0	4	88.7	16	3	60	13.9	0.116
88	1	5	100	5	1	45	40	0.117
89	1.0	5	95.3	45	9	0	4.2	0.127
90	0.5	5	100	1.11	1	45	90.1	0.131
91	0.5	1	98	5	1	55	98	0.139
92	1.0	4	77.1	3.76	1	70	51.3	0.139
93	1.0	1	53	10	1	75	53	0.142
4	2.0	72	70	4	6	90	4.9	0.152
94	1	2	100	9.9	1	35	50.5	0.152
2	0.1	1	95	1.0976	25	40	48.5	0.201
95	0.1	1	95	1.0976	25	40	48.5	0.201
96	1.0	14	90	1	1	5	64.3	0.212
97	1.0	0.5	94	15	1	55	125.3	0.355
98	1.0	3	99	2.5	1	65	132	0.364
99	0.5	1.5	95	0.94	1	65	316.7	0.410
100	1.0	5	88.2	11	10	75	16.	0.429
101	2.0	6	98	4	1	55	81.7	0.463
102	2.0	5	99	4	1	65	99	0.545
103	2.0	1	100	20	1	38	100	0.595
104	0.5	3	96.3	2.5	7	55	64.2	0.636
105	1.0	1	100	4.2	1	75	238.1	0.638
106	2.0	2	98	10	1	0	98	0.658
107	1.0	0.5	98	10	1	0	196	0.658
108	1.0	0.17	100	25	1	45	235.3	0.686
21	0.2	1	98	0.2001	1	55	1126.4	0.734
109	3.0	18	98	1.66	1	53	98.4	0.841
110	1.0	10	96	0.3	1	55	320	0.907
5	1.0	0.5	93	5	1	55	372	1.054
111	5.0	24	91	2	1	115	94.8	1.148

Table 3.6 continued…

112	1.0	0.5	99	5	1	15	396	1.265
113	1.0	0.33	85	5	1	55	515.2	1.459
114	1.0	0.3	92	5.2	1	65	589.7	1.625
115	1.0	0.5	59	2	1	65	590	1.625
116	1.0	0.167	99	10	1	55	592.8	1.679
15	1.0	1.5	96.7	1	1	25	644. 7	1.996
31	1.0	6	85	0.2	1	45	708.3	2.065
32	1.0	0.17	93.5	34	5	75	161.8	2.169
33	1.3	20	88.8	0.75	9	75	74	2.232
34	1.0	720	54	1E-3	1	0	750	2.517
35	1.0	0.5	95	10.5	5	55	181.0	2.564
36	1.0	1	95	1	1	65	950	2.617
37	1.0	24	47	0.02	1	55	979.2	2.774
38	1.0	0.25	99	3.6	1	55	1100	3.116
39	1.0	1	99	1	1	0	990	3.322
40	1.0	0.67	96	1	1	55	1432.8	4.059
41	0.1	1	100	0.0055	1	35	18182	5.46
42	1.0	0.5	97	1	1	55	1940	5.496
43	1.5	1	100	4.62	5	75	324.7	6.529
44	1.0	0.33	95	1	1	85	2878.8	7.516
45	1.0	2	99	1.6	10	95	309.4	7.873
46	1.0	0.67	97	0.5	1	45	2895.5	8.442
47	1.0	3	99	1.1	10	45	300	8.746
48	1.0	0.33	98.6	5	5	15	597.6	9.546
49	1	0.3	99	5	5	15	660	10.543
50	2.0	5	99	0.2	1	53	1980	11.282
51	1.0	1	97	1	5	75	970	13.003
52	0.8	1	97	0.64	5	55	1212.5	13.739
53	1.0	0.2	100	1	1	55	5000	14.164
54	0.5	0.05	99.5	3.8	4	55	2618.4	14.835
55	5.1	6	71	0.45	1	105	1341.1	16.972
56	0.5	0.05	99	3.76	5	55	2633	18.647
57	1	0.067	92	11	7	75	1255	23.544
58	5	3.5	94.2	2.5	5	60	538.3	37.590
59	1.0	0.33	96.8	1	5	65	2933.3	40.404
60	6.0	3.5	94.2	3	5	60	538.3	45.108
61[#]	1.0	0.2	99	0.25	1	95	19800	50.382
62[#]	1.0	1.5	99.2	0.6	30	55	1102.2	93.671
61[#]	1.0	0.2	83	0.05	1	95	83000	211.196
62[#]	5.0	32.5	100	0.014	2	50	10989.0	315.776

[#] *Values for two different conditions reported are provided; the higher one is represented in Fig. 3.13.*

Those catalysts which exhibit FOM ≥ 2.0 are represented schematically in Fig. 3.13. As a result of the simultaneous realization of the several beneficial features, our 'dip catalyst' scores highest in the list. It is indeed quite possible that the relevant parameters of the various catalysts are not optimized in the reported studies and their FOM's could be enhanced; it is also likely that higher FOM's can be realized for reactions with other substrates or Pd catalysts that are not based on nanoparticles.

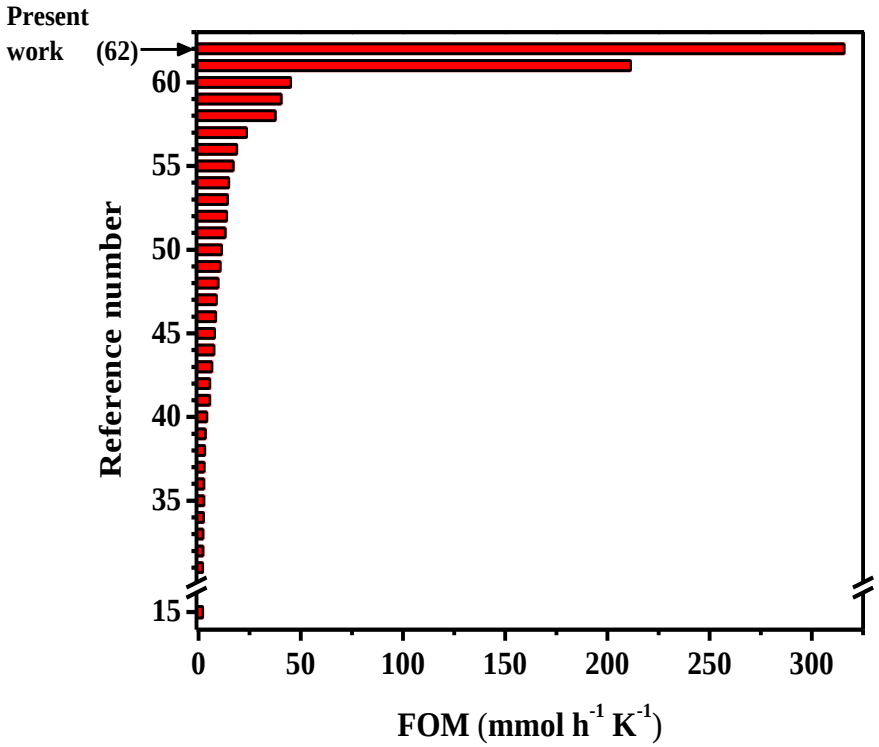

Figure 3.13. *Schematic representation of the figure-of-merit (FOM) of various reported catalysts and the present thin film catalyst (Pd-PVA layer, x = 0.13) used for the Suzuki-Miyaura reaction of iodobenzene with phenylboronic acid.*

3.6 Conclusions

We have developed a simple protocol for the fabrication of a multilayer Pd-PVA thin film using commercially available Pd precursor and aqueous medium for mixing with the polymer, and spin-coating/mild thermal annealing steps for the *in situ* generation of Pd nanoparticles inside the film. The thin film 'dip catalyst' is gainfully

employed in the Suzuki−Miyaura reaction of iodobenzene with phenylboronic acid, providing a very high yield, TON and TOF, and the possibility of scale up. Extensive recycling capability and the unique advantage of convenient catalyst monitoring between reuse cycles are demonstrated. A simple FOM is defined to integrate the various significant and quantifiable parameters related to the catalyst performance. An appraisal of the present catalyst in the context of the others reported in the recent literature is presented on the basis of the FOM. The ‘dip catalyst’ with its ease and low cost of fabrication, convenience of deployment and recycling, and high catalytic efficiency is expected to be extremely useful in organic reactions of great synthetic utility.

References

1. Datta, A.; Ebert, K.; Plenio, H. *Organometallics* **2003**, *22*, 4685.
2. Rosario-Amorin, D.; Wang, X.; Gaboyard, M.; Clérac, R.; Nlate, S.; Heuzé, K. *Chem. Eur. J.* **2009**, *15*, 12636.
3. Yang, H.; Han, X.; Li, G.; Ma, Z.; Hao, Y. *J. Phys. Chem. C* **2010**, *114*, 22221.
4. Ungureanua, S.; Deleuze, H.; Babot, O.; Achard, M. -F.; Sanchez, C.; Popa, M. I.; Backov, R. *Appl. Catal. A* **2010**, *390*, 51.
5. Shiyong, L.; Qizhong, Z.; Zhengneng, J.; Huajiang, J.; Xuanzhen, J. *Chin. J. Cat.* **2010**, *31*, 557.
6. Ramchandani, R. K.; Uphade, B. S.; Vinod, M. P.; Wakharkar, R. D.; Choudhary, V. R.; Sudalai, A. *Chem. Commun.* **1997**, 2071.
7. Djakovitch, L.; Koehler, K. *J. Am. Chem. Soc.* **2001**, *123*, 5990.
8. Durap, F.; Rakap, M.; Aydemir, M.; Özkar, S. *Appl. Catal. A* **2010**, *382*, 339.
9. Biffis, A.; Zecca, M.; Basato, M. *J. Mol. Catal. A* **2001**, *173*, 249.
10. Köhler, K.; Wagner, M.; Djakovitch, L. *Catal. Today* **2001**, *66*, 105.
11. Zhao, F.; Bhanage, B. M.; Shirai, M.; Arai, M. *Chem. Eur. J.* **2000**, *6*, 843.
12. Deshmukh, A. A.; Islam, R. U.; Witcomb, M. J.; van Otterlo, W. A. L.; Coville, N. J. *ChemCatChem* **2010**, *2*, 51.
13. Ogasawara, S.; Kato, S. *J. Am. Chem. Soc.* **2010**, *132*, 4608.
14. Ley, S. V.; Ramarao, C.; Gordon, R. S.; Holmes, A. B.; Morrison, A. J.; McConvey, I. F.; Shirley, I. M.; Smith, S. C.; Smith, M. D. *Chem. Commun.* **2002**, 1134.
15. Zhang, P.; Weng, Z. H.; Guo, J.; Wang, C. C. *Chem. Mater.* **2011**, *23*, 5243.
16. Hariprasad, E.; Radhakrishnan, T. P. *Chem. Eur. J.* **2010**, *16*, 14378.
17. Ramesh, G. V.; Porel, S.; Radhakrishnan, T. P. *Chem. Soc. Rev.* **2009**, *38*, 2646.

18. Breuer, C.; Lucas, M.; Schütze, F.; Claus, P. *Combinator. Chem. High Through. Screen.* **2007**, *10*, 59.

19. Porel, S.; Hebalkar, N.; Sreedhar, B.; Radhakrishnan, T. P. *Adv. Func. Mater.* **2007**, *17*, 2550.

20. Liu, J.; Lotesta, S. D.; Sorensen, E. J. *Chem. Commun.* **2011,** *47*, 1500.

21. Xu, J.; Wilson, A. R.; Rathmell, A. R.; Howe, J.; Chi, M.; Wiley, B. J. *ACS Nano* **2011**, *5*, 6119.

22. Hu, J.; Liu, Y. *Langmuir* **2005**, *21*, 2121.

23. Okumura, K.; Matsui, H.; Tomiyama, T.; Sanada, T.; Honma, T.; Hirayama, S.; Niwa, M. *ChemPhysChem* **2009**, *10*, 3265.

24. Luzyanin, K. V.; Tskhovrebov, A. G.; Carias, M. C.; da Silva, M. F. C. G.; Pombeiro, A. J. L.; Kukushkin, V. Y. *Organometallics* **2009**, *28*, 6559.

25. Okumura, K.; Tomiyama, T.; Okuda, S.; Yoshida, H.; Niwa, M. *J. Catal.* **2010**, *273*, 156.

26. Chen, L.; Yang, Y.; Jiang, D. *J. Am. Chem. Soc.* **2010**, *132*, 9138.

27. Rao, G. K.; Kumar, A.; Ahmedz, J.; Singh, A. K. *Chem. Commun.* **2010**, *46*, 5954.

28. Kopylovich, M. N.; Lasri, J.; da Silva, M. F. C. G.; Pombeiro, A. J. L. *Dalton Trans.* **2009**, 3074.

29. Takemoto, T.; Iwasa, S.; Hamada, H.; Shibatomi, K.; Kameyama, M.; Motoyama, Y.; Nishiyam, H. *Tetrahedron Lett.* **2007**, *48*, 3397.

30. Jiang, N.; Ragauskas, A. J. *Tetrahedron Lett.* **2006**, *47*, 197.

31. Ul Islam, R.; Witcomb, M. J.; van der Lingen, E.; Scurrell, M. S.; Van Otterlo, W.; Mallick, K. *J. Organomet. Chem.* **2011,** *696*, 2206.

32. Polshettiwar, V.; Nadagouda, M. N.; Varma, R. S. *Chem. Commun*. **2008,** 6318.

33. Wu, L.; Li, B. -L.; Huang, Y. -Y.; Zhou, H. -F.; He, Y. -M.; Fan, Q. -H. *Org. Lett*. **2006,** *8*, 3605.

34. Diallo, A. K.; Ornelas, C.; Salmon, L.; Aranzaes, J. R.; Astruc, D. *Angew. Chem. Int. Ed*. **2007,** *46,* 8644.

35. Zhong, L. -S.; Hu, J. -S.; Cui, Z. -M.; Wan, L. -J.; Song, W. -G. *Chem. Mater.* **2007,** *19,* 4557.

36. Zhang, M.; Zhang, W. *J. Phys. Chem. C* **2008,** *112,* 6245.

37. Gopidas, K. R.; Whitesell, J. K.; Fox, M. A. *Nano Lett.* **2003,** *3,* 1757.

38. Qi, S.; LongFeng, Z.; ZhenHua, S.; XiangJu, M.; Feng-Shou, X. *Sci. China Chem.* DOI: 10.1007/s11426-011-4491-8.

39. Wan, L.; Cai, C. *Catal. Lett.* **2011,** *141*, 839.

40. Tamami, B.; Ghasemi, S. *J. Mol. Catal. A* **2010,** *322*, 98.

41. Li, W.; Fu, Y.; Fu, Y.; Wang, X.; Zhang, J. *Catal. Lett.* **2013**, *143*, 578.

42. Shiyong, L.; Qizhong, Z.; Huajiang, J. *Chin. J. Chem.* **2010**, *28*, 589.

43. Zhu, M.; Diao, G. *J. Phys. Chem. C* **2011**, *115*, 24743.

44. Zhang, Z.; Wang, Z. *J. Org. Chem.* **2006**, *71*, 7485.

45. Chandrasekhar, V.; Narayanan, R. S.; Thilagar, P. *Organometallics* **2009,** *28*, 5883.

46. Wang, J.; Song, G.; Peng, Y. *Tetrahedron Lett.* **2011,** *52,* 1477.

47. Zhu, W.; Yang, Y.; Hu, S.; Xiang, G.; Xu, B.; Zhuang, J.; Wang, X. *Inorg. Chem.* **2012**, *51*, 6020.

48. Cao, M.; Lin, J.; Yanga, H.; Cao, R. *Chem. Commun*. **2010**, *46*, 5088.

49. Cao, M.; Wei, Y.; Gao S.; Cao R. *Catal. Sci. Technol.* **2012,** *2,* 156.

50. Das, D. D.; Sayari, A. *J. Catal.* **2007,** *246,* 60.

51. Deshmukh, K. M.; Qureshi, Z. S.; Bhatte, K. D.; Venkatesan, K. A.; Srinivasan, T. G.; Rao, P. R. V.; Bhanage, B.M. *New J. Chem.* **2011**, *35,* 2747.

52. Zhi, J.; Song, D.; Li, Z.; Lei, X.; Hu, A. *Chem. Commun*. **2011**, *47,* 10707.

53. Li, Y.; Boone, E.; El-Sayed, M. A. *Langmuir* **2002,** *18,* 4921.

54. Chen, Z.; Cui, Z. -M.; Niu, F.; Jiang, L.; Song, W.-G. *Chem. Commun.* **2010**, *46*, 6524.

55. Makhubela, B. C. E.; Jardine, A.; Smith, G. S. *Appl. Catal. A* **2011,** *393*, 231.

56. Sun, J.; Dong, Z.; Sun, X.; Li, P.; Zhang, F.; Hu, W.; Yang, H.; Wang, H.; Li, R. *J. Mol. Catal. A, Chem*. **2013**, *367* 46.

57. Qu, K.; Wu, L.; Ren, J.; Qu, X. *ACS Appl. Mater. Interfaces* **2012**, *4*, 5001.

58. Zhou, P.; Wang, H.; Yang, J.; Tang, J.; Sun, D.; Tang, W. *RSC Advances*, **2012**, *2*, 1759.

59. Borhade, S. R.; Waghmode, S. B. *Beil. J. Org. Chem.* **2011,** *7*, 310.

60. Zhou, P.; Wang, H.; Yang, J.; Tang, J.; Sun D.; Tang W. *RSC Advances* **2012,** *2*, 1759.

61. Martins, D. L.; Alvarez, H. M.; Aguiar, L. C. S. *Tetrahedron Lett.* **2010,** *51*, 6814.

62. Hariprasad E.; Radhakrishnan, T. P. *ACS Catal.* **2012,** *2*, 1179.

63. Senapati, K. K.; Roy, S.; Borgohain, C.; Phukan P. *J. Mol. Catal. A* **2012,** *352*, 128.

64. Ganapathy, D.; Sekar, G. *Catal. Commun.* **2013**, *39*, 50.

65. Thathagar, M. B.; Beckers, J.; Rothenberg, G. *J. Am. Chem. Soc.* **2002,** *124*, 11858.

66. Krishnan, G. R.; Sreekumar, K. *Soft Matter* **2010,** *8*, 114.

67. Yang, X.; Fei, Z.; Zhao, D.; Ang, W. H.; Li, Y.; Dyson, P. J. *Inorg. Chem.* **2008**, *47*, 3292.

68. Desforges, A.; Backov, R.; Deleuze, H.; Mondain-Monoval, O. *Adv. Funct. Mater.* **2005,** *15*, 1689.

69. Modak, A.; Mondal, J.; Sasidharan, M.; Bhaumik, A. *Green Chem.* **2011,** *13*, 1317.

70. Narayanan, R.; El-Sayed, M. A. *J. Am. Chem. Soc.* **2003,** *125*, 8340.

71. Kim, S.-H.; Jeong, G. H.; Choi, D.; Yoon, S.; Jeon, H. B.; Lee, S.-M.; Kim, S.-W. *J. Coll. Interf. Sci.* **2013**, *389*, 85.

72. Zhou, B.; Li, Y.-Q. *E. J. Chem.* **2011,** *8*, 1490.

73. Liu, J.; Li, Y.-Q.; Zheng,W.-J. *Monatsh. Chem*. **2009,** *140*, 1425.

74. Dutta, P.; Sarkar, A. *Adv. Synth. Catal.* **2011,** *353*, 2814.

75. Fihri, A.; Cha, D.; Bouhrara, M.; Almana, N.; Polshettiwar V. *ChemSusChem* **2012,** *5*, 85.

76. Li, Y.; Hong, X. M.; Collard, D. M.; El-Sayed, M. A. *Org. Lett.* **2000,** *2*, 2385.

77. Liu, Y.; Khemtong, C.; Hu**,** J. *Chem. Commun.* **2004**, 398.

78. de Souza, A. L. F.; da Silva, L. C.; Oliveira, B. L.; Antunes, O. A. C. *Tetrahedron Lett.* **2008,** *49*, 3895.

79. Kalbasia, R. J.; Mosaddegh, N. *Mater. Chem. Phys.* **2011,** *130*,1287.

80. Cargnello, M.; Wieder, N. L.; Canton, P.; Montini, T.; Giambastiani, G.; Benedetti, A.; Gorte, R. J.; Fornasiero, P. *Chem. Mater.* **2011,** *23*, 3961.

81. Monopoli, A.; Nacci, A.; Calò, V.; Ciminale, F.; Cotugno, P.; Mangone, A.; Giannossa, L. C.; Azzone, P.; Cioffi, N. *Molecules* **2010**, *15*, 4511.

82. Shokouhimehr, M.; Lee, J. E.; Han, S. I.; Hyeon, T. *Chem. Commun.*, **2013**, *49*, 4779.

83. Primo, A.; Liebel, M.; Quignard, F. *Chem. Mater.* **2009,** *21*, 621.

84. Khalily, M. A.; Ustahuseyin, O.; Garifullin, R.; Genca, R.; Guler, M. O. *Chem. Commun.* **2012**,*48*, 11358.

85. Li, S.; Wang, J.; Kou, Y.; Zhang, S. *Chem. Eur. J.* **2010,** *16*, 1812.

86. Karousis, N.; Tsotsou, G.-E.; Evangelista, F.; Rudolf, P.; Ragoussis, N.; Tagmatarchis N. *J. Phys. Chem. C* **2008,** *112*, 13463.

87. Chen, Y.-H.; Hung, H.-H.; Huang, M. H. *J. Am. Chem. Soc.* **2009**, *131*, 9114.

88. Kong, G.-Q.; Ou, S.; Zou, C.; Wu, C.-D. *J. Am. Chem. Soc.* **2012**, *134*, 19851.

89. JavadKalbasi, R.; Mosaddegh, N. *J. Solid State Chem.* **2011**, *184*, 3095.

90. Coccia, F.; Tonucci, L.; d'Alessandro, N.; D'Ambrosio, P.; Bressan, M. *Inorg. Chim. Acta* **2013,** *399*, 12.

91. Rongzhao, Z.; Jianming, L.; Fuwei, L.; Shoufeng, W.; Chungu, X.; Wei, S. *Chin. J. Chem.* **2011**, *29*, 525.

92. Chang, W.; Shin, J.; Oh, Y.; Ahn, B. J. *J. Ind. Eng. Chem.* **2008,** *14*, 423.

93. Durapa, F.; Metin, O.; Aydemir, M.; Ozkar, S. *Appl. Organometal. Chem.* **2009,** *23*, 498.

94. Li, R.; Zhang, P.; Huang, Y.; Zhang, P.; Zhong, H.; Chen, Q. *J. Mater. Chem.* **2012**, *22*, 22750.

95. Rosario-Amorin, D.; Gaboyard, M.; Clerac, R.; Vellutini, L.; Nlate, S.; Heuze, K. *Chem. Eur. J.* **2012,** *18*, 3305.

96. Samanta, S.; Layek, R. K.; Nandi, A. K. *React. Funct. Polym.* **2011,** *71*, 1045.

97. Gurbuz, N.; Ozdemir, I.; Cetinkaya, B.; Seckin, T. *Appl. Organometal. Chem.* **2003,** *17*, 776.

98. Wen, F.; Zhang, W.; Wei, G.; Wang, Y.; Zhang, J.; Zhang, M.; Shi, L. *Chem. Mater.* **2008,** *20*, 2144.

99. Putta, C. B.; Ghosh, S. *Adv. Synth. Catal.* **2011,** *353*, 1889.

100. Li, Y.; Fan, X.; Qi, J.; Ji, J.; Wang, S.; Zhang, G.; Zhang, F. *Nano Res.* **2010**, *3*, 429.

101. Zheng, P.; Zhang, W. *J. Catal.* **2007,** *250*, 324.

102. Wei, G.; Zhang, W.; Wen, F.; Wang, Y.; Zhang, M. *J. Phys. Chem. C* **2008,** *112*, 10827.

103. Lu, F.; Ruiz, J.; Astruc, D. *Tetrahedron Lett.* **2004,** *45*, 9443.

104. Wang, J.; Xu, B.; Sun, H.; Song, G. *Tetrahedron Lett.* **2013**, *54*, 238.

105. Lemo, J.; Heuze, K.; Astruc, D. *Inorg. Chim. Acta* **2006,** *359*, 4909.

106. Zhou, S.; Johnson, M.; Veinot, J. G. C. *Chem. Commun.* **2010,** *46*, 2411.

107. Sawoo, S.; Srimani, D.; Dutta, P.; Lahiri, R.; Sarkar A. *Tetrahedron* **2009,** *65*, 4367.

108. Xiang, G.; He, J.; Li, T.; Zhuang, J.; Wang, X. *Nanoscale* **2011**, *3*, 3737.

109. Pittelkow, M.; Moth-Poulsen, K.; Boas, U.; Christensen, J. B. *Langmuir* **2003,** *19*, 7682.

110. Singha, S.; Sahoo, M.; Parida, K. M. *Dalton Trans.* **2011**, *40*, 7130.

111. Burguete, M. I.; García-Verdugo, E.; Garcia-Villar, I.; Gelat, F.; Licence, P.; Luis, S. V.; Sans, V. *J. Catal.* **2010,** *269*, 150.

112. Huang, Y.; Zheng, Z.; Liu, T.; Lü, J.; Lin, Z.; Li, H.; Cao, R. *Catal. Commun.* **2011,** *14*, 27.

113. Du, Q.; Li, Y. *Beil. J. Org. Chem.* **2011,** *7*, 378.

114. Firouzabadi, H.; Iranpoor, N.; Gholinejad, M.; Kazemi, F. *RSC Advances* **2011,** *1*, 1013.

115. Ren, L. Z.; Meng, L. J. *eXPRESS Polym. Lett.* **2008,** *2*, 251.

116. Erathodiyil, N.; Ooi, S.; Seayad, A. M.; Han, Y.; Lee, S. S.; Ying, J. Y. *Chem. Eur. J.* **2008,** *14*, 3118.

CHAPTER 4

Polymer-Silver Nanocomposite Thin Film: An Inexpensive and Efficient Substrate for Surface Enhanced Raman Scattering

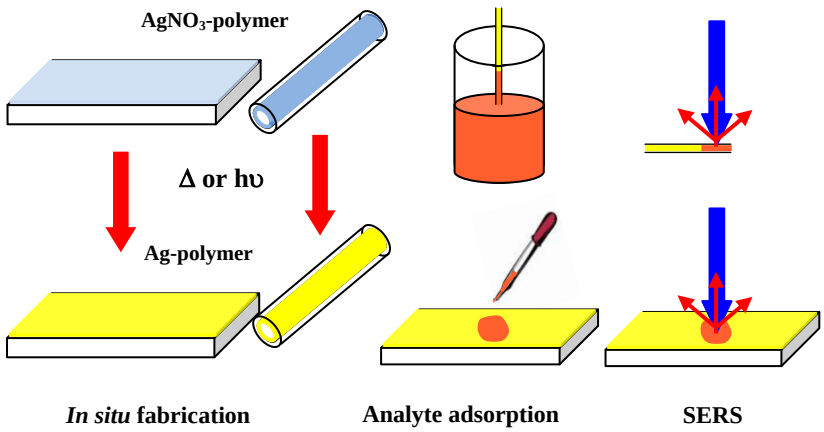

SERS substrates based on silver nanoparticle embedded polymer thin films.

Paper published

Hariprasad, E.; Radhakrishnan, T. P. *Langmuir*, (DOI: 10.1021/la402594j)

Scope

The utility of polymer-metal nanocomposite thin films with in situ generated silver nanoparticles, as substrates for surface enhanced Raman scattering (SERS) is demonstrated in this chapter. Thin films of poly(vinyl alcohol) and poly(vinyl butyral-co-vinyl alcohol-co-vinyl acetate) containing silver nanoparticles generated in situ through thermal annealing and photoirradiation respectively (Ag-PVA and Ag-PVVV), are investigated as potential SERS substrates using 4-aminothiophenol and rhodamine 6G as probe molecules. The Ag-PVA substrate is found to produce Raman spectral enhancement factors of ~10^6, whereas Ag-PVVV, a novel nanocomposite thin film developed during this study provides enhancement factors of ~10^7. A unique advantage of these nanocomposite films is demonstrated by fabricating them by the in situ process, as a thin coating inside glass capillaries and using these disposable SERS substrates for the sensitive detection of the probe molecules. The thin film substrates prepared on glass plates and capillaries facilitate convenient sample preparation for recording the Raman spectra and provide strongly enhanced spectra with high reproducibility, allowing picomols of the analytes to be detected. These aspects combined with the ease of fabrication and low cost of these in situ fabricated nanocomposite thin films make them highly attractive SERS substrates.

4.1 Introduction

The enhanced Raman scattering of molecules adsorbed on rough metal surfaces and especially metal nanoparticles and nanostructures (surface enhanced Raman scattering, SERS) serves as a highly sensitive detection tool.[1-3] Nanostructures of noble metals such as silver and gold are preferred, as visible light can be used to excite their localized surface plasmon resonance (LSPR) and exploit the resulting local electromagnetic field. A wide range of substrates have been developed based on these nanoparticles and nanostructures for adsorbing molecules and observing their SERS.[4] The simplest structure would be a monolayer of the nanoparticles on substrates like a

silicon wafer[5] or a polymer thin film.[6,7] Interesting variations on this approach include the use of temperature-sensitive polymer membranes[8] and conducting polymer fibers.[9] Other substrates used for assembling metal nanoparticles and nanostructures include graphene[10] and graphene oxide,[11] glass capillary,[12] silicon nanopillar,[13] core-shell microsphere,[14] porous alumina membrane[15] and unconventional choices like filter paper,[16] ink-jet printed cellulose paper[17] and aluminum foil.[18] Nanogap[19,20] and nanodome[21] arrays, nanodroplets on nanowall networks,[22] plasmonic lenses[23] and metastable nanoparticle film[24] have also been developed as efficient SERS substrates.

Important considerations for the development of a SERS substrate are the cost of materials, ease of fabrication, durability, facility of use, and of course sensitivity and reproducibility of the Raman spectral measurements. Polymer-metal nanocomposite thin films offer one of the simplest designs that address the wide range of requirements. PVA is a particularly convenient choice for the polymer. A SERS substrate has been developed using a nanocomposite prepared from silver nanoparticles formed in solution using PVA and poly(γ-glutamic acid) as reductant and stabilizer.[25] PVA film containing silver generated using ferrous sulfate as the reducing agent, has been shown to produce SERS response;[26] however, this study did not provide any details of the silver nanoparticles or the spectral enhancement factor. Another substrate design involved electrospun PVA nanofibers with aligned silver nanoparticles.[27] The protocols discussed in the earlier chapters provide a simple and facile route for the *in situ* generation of silver nanoparticles inside PVA thin films.[28,29] The method is environmentally benign, allows convenient monitoring of the nanoparticle formation[30,31] and produces free-standing thin films that can be directly imaged in a transmission electron microscope. Application of these nanocomposite thin films as optical limiter,[28,32] bactericide,[33] and chemical sensor[34] have been demonstrated earlier in our laboratory. The previous chapters have described their use as 'dip catalysts' for organic reactions.[35,36]

In this study, we have explored the utility of the *in situ* synthesized polymer-metal nanocomposite thin films as easily fabricated and inexpensive SERS substrates.

Ag-PVA thin film prepared using our protocol is found to be a durable SERS substrate showing enhancement factors (EF) of ~10^6 with good reproducibility. In order to explore the possibility of achieving higher EF in similar substrates, we have investigated several variants of PVA, as these can influence considerably the surface morphology of the thin films as well as the size and shape of the silver nanoparticles generated within. Thin film of PVVV with the silver nanoparticles generated *in situ* by photoirradiation is identified as an efficient SERS substrates with EF of ~10^7. We present below, the details of the fabrication and characterization of these substrates followed by their deployment as SERS substrates. We also describe studies on the fabrication of a glass capillary with the Ag-polymer thin film coated on the inner walls that serves as a cheap and disposable SERS substrate.

4.2 Fabrication of Polymer-Ag Substrate

Ag-PVA

Ag-PVA film was prepared following the general methodology developed in our laboratory as described in Sec. 1.3.1. The amount of silver nitrate required to obtain a specific Ag/PVA weight ratio (x), dissolved in 0.3 mL of water was mixed with 0.6 mL of a solution of PVA in water (1.0 g PVA in 20 mL water); for example 18.9 mg of $AgNO_3$ is used to prepare the Ag-PVA substrate with x = 0.4. Ag-PVA substrates with other weight ratios were also prepared by altering the amount of $AgNO_3$ in the solutions. Silicon wafers were cleaned in soap solution and water followed by sonication with isopropyl alcohol for 10 min and dried under nitrogen flow. The $AgNO_3$-PVA solution was spin-coated on the wafer (typically 2.5 × 1.2 cm^2) using a two step program; 500 rpm for 10 s followed by 10,000 rpm for 10 s. The film was heated in a hot air oven at 130 ^oC for 3 h to generate *in situ* the silver nanoparticles within the film.

Ag-PVVV

Based on the trial experiments with different polymers containing the hydroxy functionality that is essential to reduce the silver ions to silver atoms in the formation of the nanoparticles, PVVV was found to be the best choice. The fabrication followed similar procedure as that used for Ag-PVA, but with some significant changes. 40.0 mg of PVVV and the required amount of $AgNO_3$ (for example 24.0 mg gives an Ag/PVVV weight ratio, x = 0.4) were added to 1.2 mL of ethanol and stirred for 10 min at 25 °C. The $AgNO_3$-PVVV solution was spin-coated on Si wafer in a single step, at 8000 rpm for 10 s. The film was either heated in a hot air oven at 130 ^oC or UV-irradiated (λ = 254 nm) in a photo-reactor for 3 h. The latter procedure was found to be a more efficient method to produce *in situ* silver nanoparticles inside the PVVV film.

4.3 Characterization of Polymer-Ag Thin Film

Initial characterization of Ag-PVA and Ag-PVVV thin films were carried out by recording their LSPR extinction spectra. A series of substrates were fabricated by varying the Ag/polymer weight ratio (x), solution viscosity and spin-coating conditions to determine the optimal concentration of silver nanoparticles and the thin film thickness that will lead to the maximum sensitivity for SERS. The LSPR extinction spectra of the films fabricated with different Ag/polymer weight ratios, used for the SERS studies are shown in Fig. 4.1. In the case of Ag-PVA, increasing x leads to increase in the extinction as well as broadening of the spectra. This suggests increase in the nanoparticle density, as well as increase in the size dispersion. With Ag-PVVV, when x increases from 0.2 to 0.4, the prominent change is the enhancement of the extinction suggesting an increase in the population of nanoparticles; a small broadening of the spectrum is also observed. When x increases further the extinction increases very little, but the broadening becomes more conspicuous, indicating nanoparticle aggregation. Based on these observations, we have chosen films with the optimal value of x = 0.4 for the detailed studies. Dependence of the SERS efficiency on the value of x will be discussed later in Sec. 4.4.2.

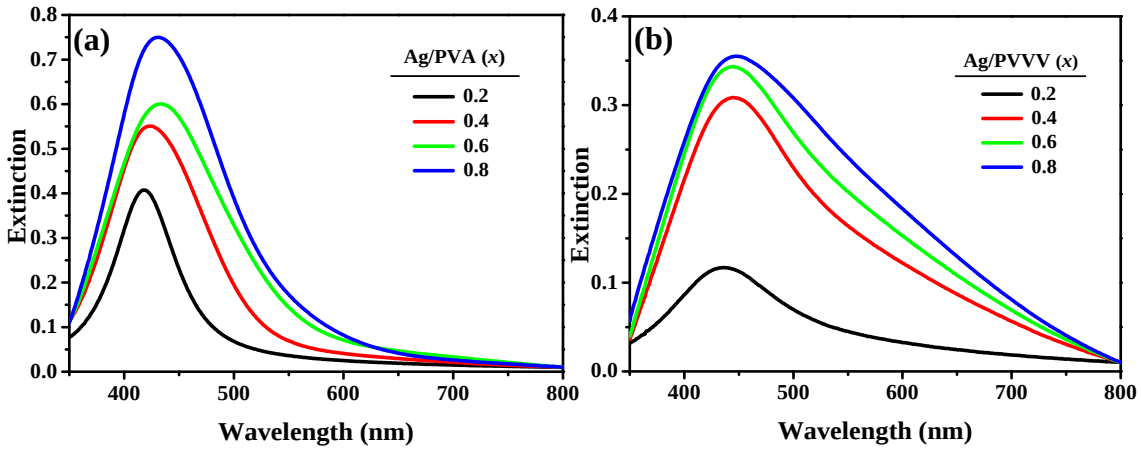

Figure 4.1. *LSPR extinction spectra of* ***(a)*** *Ag-PVA* ***(b)*** *Ag-PVVV thin films with different weight ratios, x.*

The Ag-PVA and Ag-PVVV films with x = 0.4, fabricated under the optimal spin-coating conditions are found to have thickness of ~110 ± 8 nm and ~270 ± 60 nm respectively. AFM images of these films on Si wafer are shown in Fig. 4.2. Ag-PVA film surface is extremely smooth with an average surface roughness of 0.7 ± 0.1 nm, whereas the Ag-PVVV surface has a roughness of the order of 8.0 ± 2.3 nm. The higher roughness is likely to be an advantage for the use of Ag-PVVV as a SERS substrate. TEM image of the free-standing film of Ag-PVA (Fig. 4.3a) shows a homogeneous distribution of nearly spherical nanoparticles, ~9-12 nm in diameter. FESEM image of

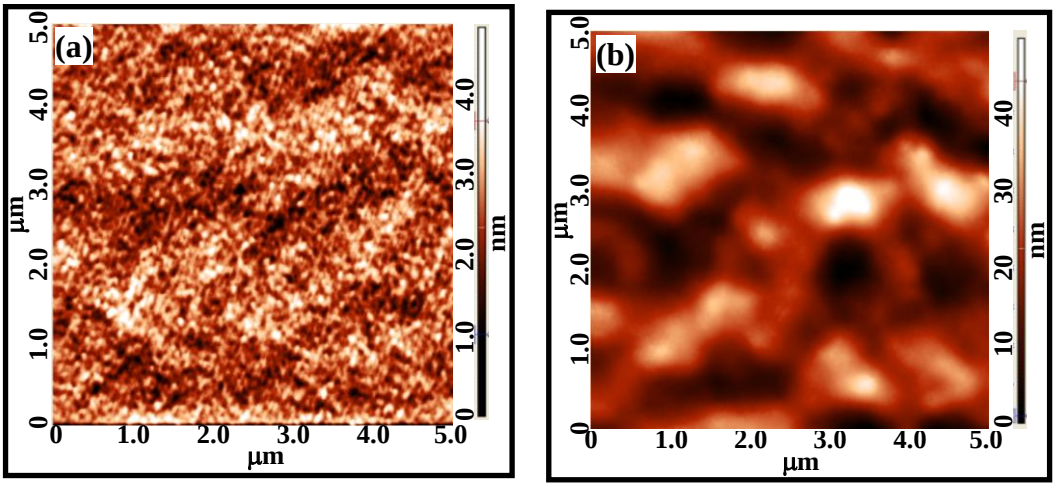

Figure 4.2. *AFM image (5 μm × 5 μm) of* ***(a)*** *Ag-PVA (x = 0.4) and* ***(b)*** *Ag-PVVV (x = 0.4) thin films.*

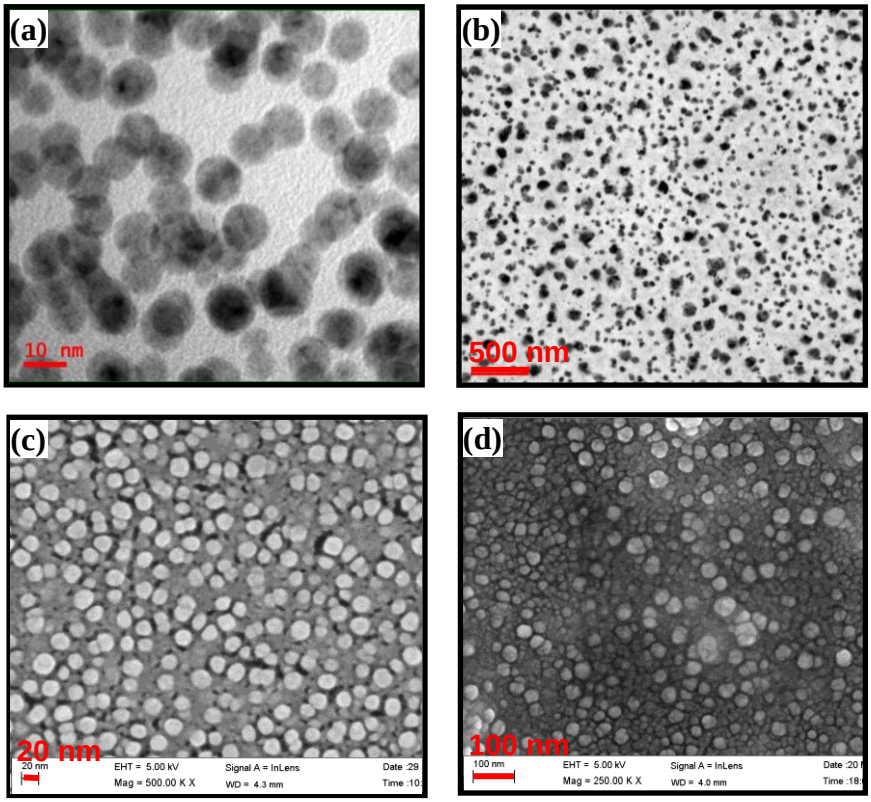

Figure 4.3. TEM *image of* ***(a)*** *Ag-PVA (x = 0.4),* ***(b)*** *Ag-PVVV (x = 0.4) and FESEM image of* ***(c)*** *Ag-PVA (x = 0.4),* ***(d)*** *Ag-PVVV (x = 0.4).*

the film directly coated on a Si wafer showed Ag nanoparticles of ~15-20 nm in diameter (Fig. 4.3c); change in the size distribution is likely to be due to the difference in the substrate. TEM image of the Ag-PVVV film with $x = 0.4$ shows Ag nanoparticles with two different size distributions, 2-5 nm and 25-100 nm (Fig. 4.3b). FESEM image (Fig. 4.3d) is broadly consistent with this observation, showing the larger particles clearly. The particle morphologies range from nearly spherical to plate-like.

4.4 SERS Experiments

4-Aminothiophenol (4ATP) and Rhodamine 6G (R6G) recrystallized from methanol solutions were used as the probe molecules. Choice of these standard probe molecules was prompted by the fact that the former is capable of engaging in strong chemical interactions with the silver nanoparticles through the thiol group and the

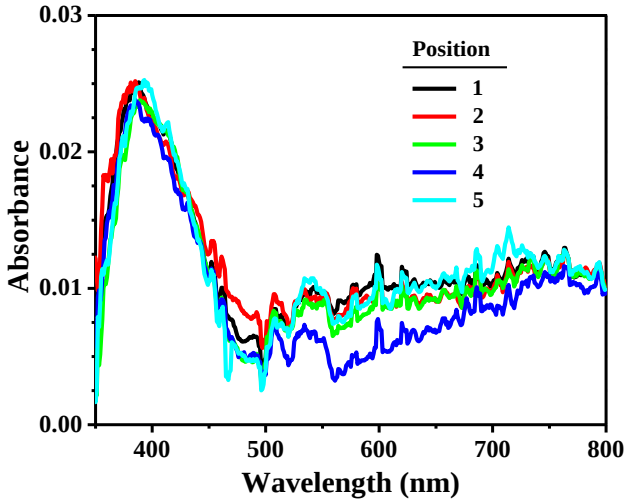

Figure 4.4. *Electronic absorption spectra of R6G adsorbed Ag-PVA thin film collected in DRS mode at different positions of substrate.*

latter is not. Typically 1-100 µM solutions of the probe molecules were prepared in HPLC grade methanol. 10 µL of the solution was spread homogeneously on the substrate and allowed to dry for 30 min. Homogeneous spreading of the solution was confirmed by recording the electronic absorption spectra at different points on the film in the case of R6G (Fig. 4.4); spectra recorded in the diffuse reflectance mode were converted into absorbance spectra using the Kubelka-Munk function.

Raman spectra were recorded with a 0.5 s integration time and 10 accumulations, through a 50× aperture (NA = 0.8). The laser intensity was maintained constant in all measurements and a 25 µm detecting fiber was used to collect the spectra. Excitation wavelengths of 633 nm and 488 nm were used for 4ATP and R6G, respectively. Wavelengths away from and close to the LSPR extinction peak of the silver nanoparticles were chosen so as to test the efficiency of our SERS substrate without and with strong contribution from the local electromagnetic field effects. We believe that both electromagnetic field and chemical interactions could play a role in the SERS of 4ATP, whereas it is likely to be mostly the former effect with R6G. It may also be noted that the electromagnetic field contribution may not be very high when the excitation wavelength is away from the LSPR peak. Raman spectra corresponding to the bulk material (reference) was collected using a microcrystal placed on a silicon wafer; identity and purity of the crystal was confirmed by X-ray diffraction analysis.

Special care has to be exercised to employ sufficiently low laser power in the case of 4ATP, in order to avoid photochemical processes (dimerization). Several earlier studies with 4ATP have shown that the enhanced Raman signals can arise from 4,4'-dimercaptoazobenzene photogenerated during the experiment.[37,38] We have recorded the spectra using different laser powers (Fig. 4.5); with the present substrates it was found that the peaks at ~1140, ~1390 and 1440 cm^{-1}, attributed to the dimer,[38] do not appear up to a laser power of ~100 kW/cm^2. Therefore, we have carried out all the SERS studies with 4ATP using a laser power of 50.0 kW/cm^2, precluding the possibility of 4ATP undergoing the photochemical change. The spectra of 4ATP on the nanocomposite thin film show the small, but characteristic red shifts of the peaks (1075, 1583 cm^{-1}) relative to those of the bulk crystals (1086, 1590 cm^{-1}). This is commonly attributed to the impact of chemical interaction between the silver nanoparticle surface and the adsorbed thio compound.[39]

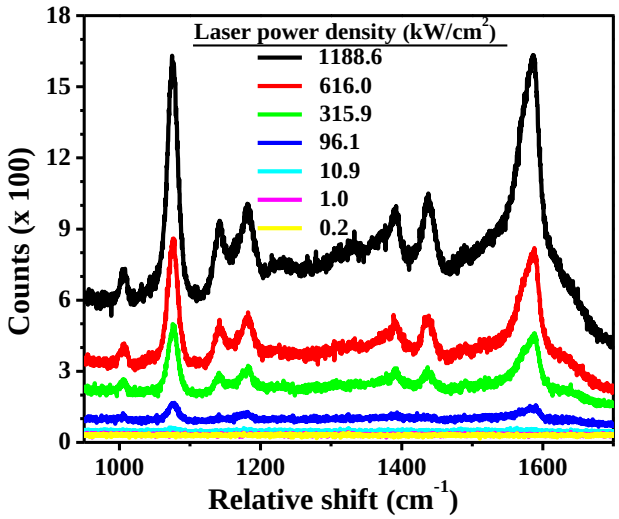

Figure 4.5. *Raman spectra recorded for 4ATP on Ag-PVA using different laser powers; peaks at ~1140, ~1390 and ~1440 cm^{-1} which are attributed to the dimer appear when laser power above 90 kW/cm^2 is used.*

4.4.1 *Calculation of Enhancement Factors*

The SERS EF was estimated using the approach discussed in earlier studies[40,41] adapted for the current experimental protocol. EF is given by the general expression:

$$\mathrm{EF} = \frac{I_{\mathrm{SERS}}}{I_{\mathrm{bulk}}} \times \frac{N_{\mathrm{bulk}}}{N_{\mathrm{SERS}}}$$

where I is the intensity of a Raman signal and N is the number of molecules within the laser spot (giving rise to the signal), in the focal volume of the beam in the solutions adsorbed on the SERS substrate (SERS) and in a single crystal of the analyte (bulk). For the current experiment, the ratio of the number of molecules in the two cases can be shown to be:

$$\frac{N_{\mathrm{bulk}}}{N_{\mathrm{SERS}}} = \frac{2344\lambda}{NA^2} \times A \times \frac{\rho}{w}$$

where λ is the wavelength of the laser light (nm), *NA* is the numerical aperture, *A* is the total area over which the analyte solution is spread on the SERS substrate (cm^2), ρ is the density of the analyte crystal (g cm^{-3}) and *w* is the weight of the analyte in the solution spread on the film (ng). Derivation of the equation with details is shown in Box 4.1.

Box 4.1

Laser spot diameter, $W_o \frac{1.22\lambda}{NA}$ ~~$\frac{0.61\lambda}{\text{N.A.}}$~~ ~~$\frac{1.22\lambda}{\text{N.A.}}$~~

Focal depth: $Z_o = \left(\frac{2\pi}{\lambda}\right) W_o^2$ $\quad Z_o = \left(\frac{2\pi}{\lambda}\right) w_o{}^2$

Focal volume: $\tau = \left(\frac{\pi}{2}\right)^{1.5} W_o^2 Z_o$ $\quad \tau = \left(\frac{\pi}{2}\right)^{1.5} * w_o{}^2 * Z_o$

N_{bulk} = ((Focal volume × Density)/ (Molecular weight)) ×N_A

N_{SERS} = (Laser spot area/Substrate area) × (N_A × Volume × Concentration)

$$\frac{N_{bulk}}{N_{SERS}} = \frac{\left(\frac{\pi}{2}\right)^{1.5} W_o^2 \left(\frac{2\pi}{\lambda}\right) W_o^2 \frac{\rho}{M} N_A}{\frac{\pi}{4} W_o^2 \frac{N_A VC}{A}} = \left(\frac{\pi}{2}\right)^{1.5} \left(\frac{8}{\lambda}\right) W_o^2 \frac{\rho}{M} \frac{A}{VC} = \frac{(2\pi)^{1.5}}{\lambda} W_o^2 A \frac{\rho}{w}$$

$$\frac{N_{bulk}}{N_{SERS}} = \frac{(2\pi)^{1.5}}{\lambda} \left(\frac{1.22\lambda}{NA}\right)^2 A \frac{\rho}{w} = 100 \times (2\pi)^{1.5} \times (1.22)^2 \frac{\lambda}{NA^2} \times A \times \frac{\rho}{w} = \frac{2344\lambda}{NA^2} \times A \times \frac{\rho}{w}$$

N_{bulk}/N_{SERS} was estimated for the probe molecules by substituting the values given in Table 4.1 in the above equation. The value obtained for N_{bulk}/N_{SERS} is ~7.5×10^5 and ~4.5×10^5 for 4ATP and R6G, respectively.

Table 4.1. *Experimental parameter values used for the estimation of N_{bulk}/N_{SERS}.*

	4-ATP	**R6G**
λ (nm)	633	488
ρ (g cm^{-3})	1.19	1.26
***w*(ng)**	11.02 (10 μL of 8.8 μM solution)	14.85 (10 μL of 3.1 μM solution)
NA (50x)	0.8	
A (cm^2)	3	

4.4.2 *Efficiency of the Polymer-Ag Thin Film Substrates*

Initially a series of experiments were carried out using Ag-PVA thin films fabricated with different Ag/PVA weight ratio, (*x*), and spin-coating conditions. The SERS efficiency determined for the different combinations, with the two probe molecules are collected in Table 4.2. The optimal thickness is achieved for spin-coating speed of 10 krpm. EF increased significantly when *x* was increased from 0.2 to 0.4, but less prominently at still higher loadings of silver. This possibly reflects the deleterious effect of particle aggregation at higher *x*. Since the Ag-PVA films contain Ag nanoparticles with dimensions that are relatively small compared to the film thickness and the film surface is very smooth, it appears that the access of the nanoparticle to the analyte molecules is limited leading to moderate EF values of the order of 10^6. This led us to explore thin films containing relatively larger Ag nanoparticles and having a higher surface roughness. As PVA and the thermal annealing protocol did not appear to be ideally suited for this, we explored related polymers and modifications in the *in situ* fabrication method to prepare novel polymer-silver nanocomposite thin films.

Enhancement factors achieved for the Ag-PSAA (PSAA = poly(styrene–*co*–allyl alcohol)) and Ag-PVVV substrates are collected in Table 4.3 and Table 4.4. Ag-PVVV

Table 4.2. *Enhancement factor (EF) for the probe molecules 4ATP and R6G on Ag-PVA thin films with different composition (Ag/PVA weight ratio, x) fabricated at different spin-coating speeds (S). The values are estimated using the 1075 cm^{-1} peak for 4ATP and the 1648 cm^{-1} peak for R6G.*

x	**EF (10^6)**					
	S = 8 krpm		**S = 10 krpm**		**S = 12 krpm**	
	4ATP	**R6G**	**4ATP**	**R6G**	**4ATP**	**R6G**
0.2	0.5	4.2	1.3	11.9	1.4	1.1
0.4	6.1	5.1	1.8	18.8	2.6	5.7
0.6	7.9	6.7	2.6	16.8	2.9	6.8
0.8	9.1	8.3	2.9	18.5	3.5	7.3

Table 4.3. *Enhancement factor (EF) for the probe molecules 4ATP and R6G on Ag-PSAA thin films with different composition (Ag/PSAA weight ratio, x) fabricated at different spin-coating speeds (S). The values are estimated using the 1075 cm^{-1} peak for 4ATP and the 1648 cm^{-1} peak for R6G.*

x	**EF (10^6)**			
	S = 4 krpm		**S = 8 krpm**	
	4ATP	**R6G**	**4ATP**	**R6G**
0.2	1.9	0.4	3.5	0.5
0.4	3.9	0.6	4.2	1.0
0.6	4.2	0.7	4.3	1.1
0.8	4.3	0.7	4.7	1.2

substrates show significantly higher EF values compared to Ag-PVA and Ag-PSAA. Dependence of the EF on *x* is similar to that observed with Ag-PVA; the increase in EF is significant on increasing *x* from 0.2 to 0.4, but less prominent on further increase. The LSPR extinction spectra of Ag-PVVV thin film (Fig. 4.1b) in particular provide a

useful insight into this. Increase in the density of nanoparticles when *x* increases from 0.2 to 0.4 promotes the SERS enhancement due to the increased surface area available,but their aggregation when *x* increases further, affects it adversely.

Table 4.4. *Enhancement factor (EF) for the probe molecules 4ATP and R6G on Ag-PVVV thin films with different composition (Ag/PVVV weight ratio, x) fabricated at different spin-coating speeds (S). The values are estimated using the 1075 cm^{-1} peak for 4ATP and the 1648 cm^{-1} peak for R6G.*

x	EF (10^6)			
	S = 4 krpm		S = 8 krpm	
	4ATP	R6G	4ATP	R6G
0.2	6.8	3.5	7.1	37.3
0.4	12.9	5.9	15.3	63.0
0.6	17.3	6.6	20.0	73.5
0.8	18.8	7.1	20.7	78.2

The Raman spectra recorded for the bulk crystalline samples of the analytes and for the solutions containing few picomols of the analyte spread uniformly on the Ag-PVVV (x = 0.4) thin film are shown in Fig. 4.6. The EF estimated for the 4ATP and R6G molecules on the Ag-PVVV film with different spectral peaks as markers are collected in Tables 4.5 and 4.6. In both cases (4ATP and R6G) the EF's are found to be ~10^7. The values estimated for the different vibrational transitions fall within a narrow range. Similar enhancement observed in the case of the two different probe molecules

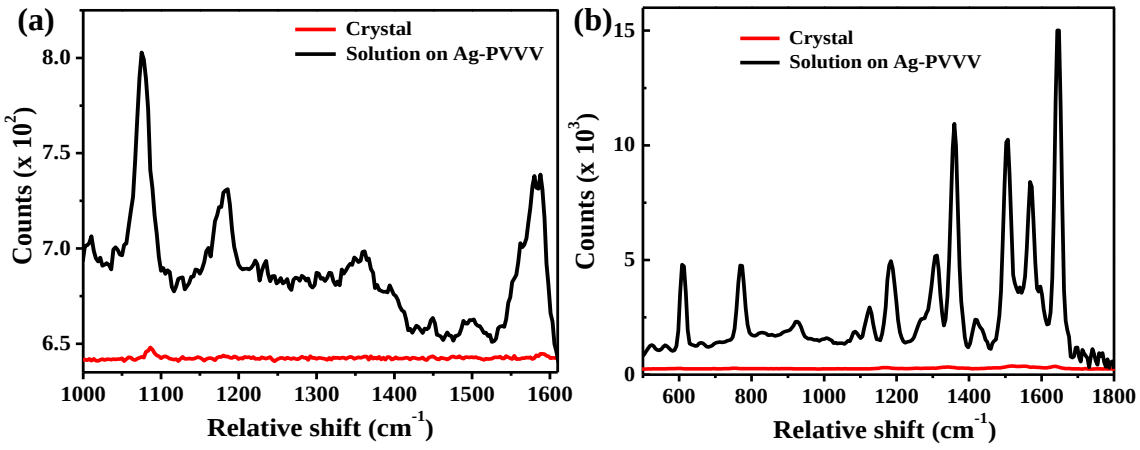

Figure 4.6. *Raman spectra of **(a)** 4ATP crystal and 4ATP solution adsorbed on Ag-PVVV (x = 0.4) thin film substrate, **(b)** R6G crystal and R6G solution adsorbed on Ag-PVVV (x = 0.4) thin film substrate (corrected for fluorescence background).*

indicates that Ag-PVVV is an efficient SERS substrate irrespective of the mechanism of Raman signal enhancement and excitation wavelengths. It also shows that potential problems such as photochemical process in the case of 4ATP can be ruled out in the present study. Repeated experiments on Ag-PVVV substrates fabricated in several different batches showed a high level of reproducibility of the surface enhanced Raman spectra and the EF values. The EF observed with these easily fabricated, cheap and durable SERS substrates are quite high. This factor coupled with the good reproducibility of the spectra demonstrates the high utility of the *in situ* synthesized polymer-metal nanocomposite thin films for analytical applications. The Ag-PVVV films can be stored under normal atmosphere and ambient conditions for several months without any significant loss of the original LSPR characteristics and SERS efficiency.

Table 4.5. *Intensity of the Raman spectral peaks (I) of a crystal of 4ATP and a solution of 4ATP (containing ~90 pmol) on Ag-PVVV (x = 0.4) as the substrate (Fig. 4.6a), along with the enhancement factor (EF) in each case.*

Bulk		**SERS**		**EF (10^7)**
Peak (cm^{-1})	**I**	**Peak (cm^{-1})**	**I**	
1086	5.6	1075	115	1.3
1590	2.8	1583	88	2.0

Table 4.6. *Intensity of the Raman spectral peaks of a crystal of R6G (I_{bulk}) and a solution of R6G (containing ~30 pmol) on Ag-PVVV (x = 0.4) as the substrate (I_{SERS}) (Fig. 4.6b), along with the enhancement factor (EF) in each case.*

Peak (cm^{-1})	**I_{bulk}**	**I_{SERS}**	**EF (10^7)**
608	17.4	3487.6	9.1
768	16.0	2931.4	8.3
1194	29.0	2433.9	3.8
1364	28.0	7939.0	12.9
1573	31.4	3248.5	4.7

1648	78.2	10779.7	6.3

.

In addition to the EF values, the limit of detection (LOD) is an important signature of the sensitivity of the SERS materials: LOD is commonly defined as $3\sigma_{blank}/m$ where σ_{blank} is the standard deviation for blank measurements and m is the slope for the calibration plot.[42,43] σ_{blank} on the Ag-PVVV substrate (without probe molecules) was determined by recording the Raman spectra 7-10 times. The value was estimated to be 30.5 counts for the intensity at 1075 cm^{-1} (excitation at 633 nm) and 24.8 counts for the intensity at 1648 cm^{-1} (excitation at 488 nm); these corresponds to the Raman peaks of interest and the excitation wavelength for the probe molecules 4-ATP and R6G respectively. The slope m was determined from the calibration plot of signal intensity versus concentration; the plots for 4ATP and R6G are shown in Fig. 4.7. The LOD estimated for 4ATP and R6G on Ag-PVVV are respectively 86 and 55 pmol. These values are based on the total solution spread on the substrate; the values would be much smaller if only those in the focal volume are considered.

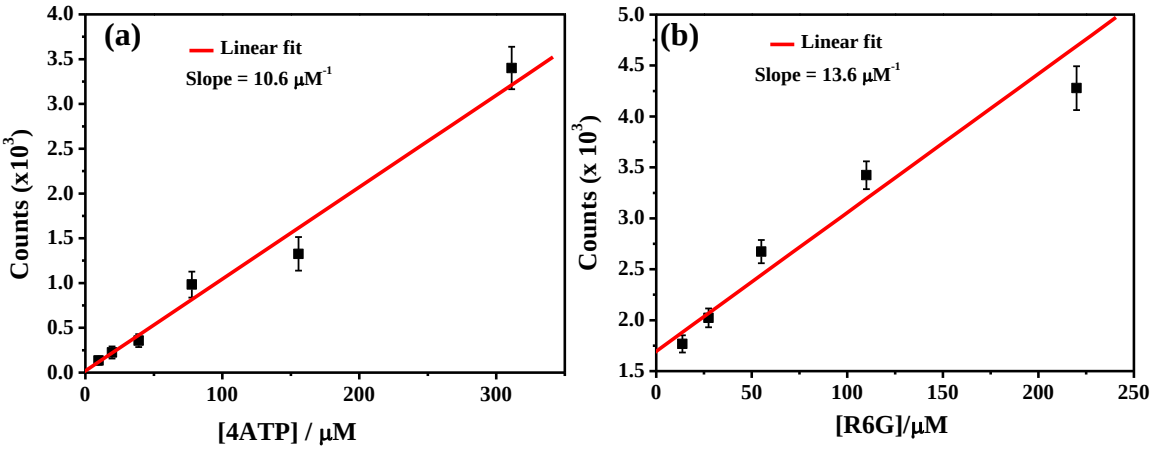

Figure 4.7. ***(a)*** *Plot of the intensity at 1075 cm^{-1} peak for solutions of 4ATP with different concentrations spread on Ag-PVVV (x = 0.4).* ***(b)*** *Plot of the intensity of 1648 cm^{-1} peak for solutions of R6G with different concentrations spread on Ag-PVVV (x = 0.4).*

4.4.3 *Capillary Substrates*

We have probed a unique advantage of the *in situ* fabricated nanocomposite thin films as SERS substrate by forming it on the inner walls of a glass capillary. Mixture of the solutions of $AgNO_3$ and PVA/PVVV were prepared and a very small volume

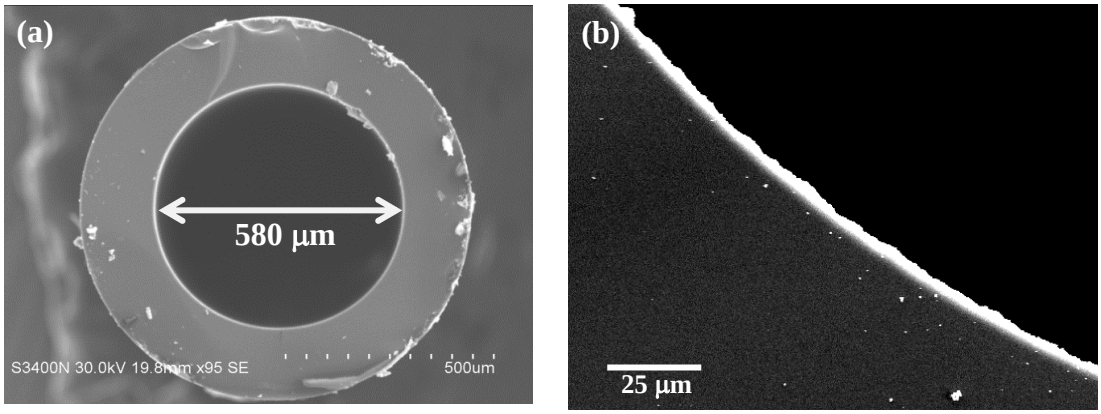

Figure 4.8. ***(a)*** *SEM image of the cross-section of the capillary, with an inner lining of Ag-PVA thin film,* ***(b)*** *magnified view of the inner wall showing the film coating.*

(typically 0.5-1.0 μL) was sucked into a glass capillary (inner diameter ~600 μm). After removing traces of the solution that may be sticking on the outside wall, the capillary was heated inside a hot air oven at 130 ^{o}C (Ag-PVA) or UV irradiated (Ag-PVVV) for 3 h. The solution dries and the *in situ* reduction of the silver ions to silver nanoparticles imparts a deep yellow color to the film coated on the inner wall of the capillary. The SEM images in Fig. 4.8 show the cross-section of the glass capillary and the thin film coating; the coating is estimated to be ~4 μm thick. EDX spectra recorded at several positions on the cross section of the capillary coated with Ag-PVA (Fig. 4.9) reveal the presence of the silver nanoparticles in the thin film coating on the inner wall.

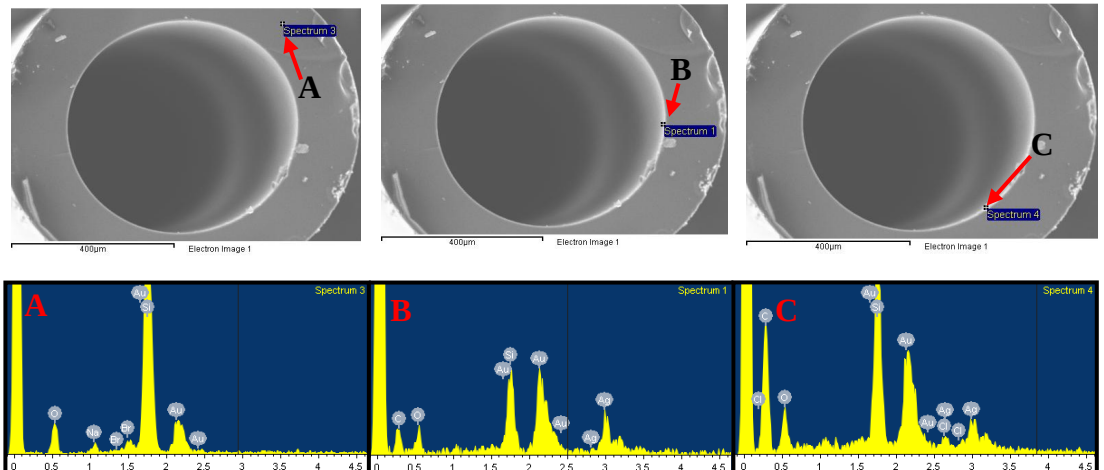

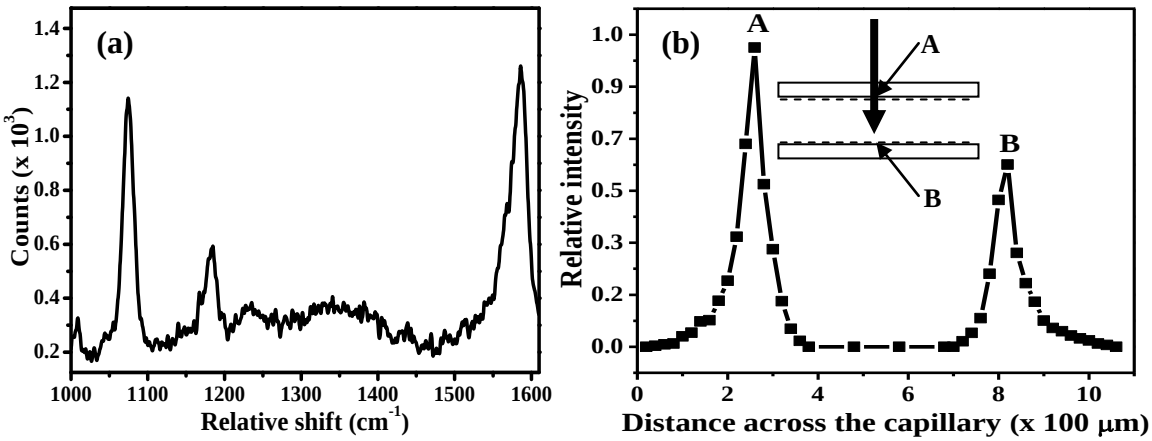

Figure 4.10. ***(a)*** *A typical SERS spectrum of 4ATP adsorbed on the Ag-PVA film coating inside the capillary, and* ***(b)*** *plot of the signal intensity of the 1075 cm^{-1} peak of 4ATP as a function of the point of focus across the diameter of the capillary (the schematic diagram shows the orientation of the capillary, the laser beam and the points where the beam meets the Ag-PVA film coating containing 4ATP).*

In order to test the analyte, ~0.5 μL of an 8.8 μM solution of 4ATP was sucked into the capillary and allowed to get absorbed on the polymer coating lining. After drying, the capillary was placed directly in the Raman microscope so that the laser beam can be directed across the diameter. The beam was focused at different levels across the capillary and the spectra recorded (10× objective (NA = 0.25) was used). When the focal spot is in the region of the polymer film, clear spectra could be recorded; a typical spectrum is shown in Fig. 4.10a. It is important to note that the molecular content sucked into the capillary is as low as 5 pmol and that the exact amount of molecules which come under the laser spot will be even smaller. Intensity of the 1075 cm^{-1} peak

of 4ATP is plotted against the focal position across the diameter of the capillary (Fig. 4.10b). The two peaks separated by ~560 μm correspond to the beam focusing on the coatings across the inner diameter at positions A and B. Peak B is relatively weaker, possibly because of the losses in the Raman scattered beam while traversing back across A. Width of the peaks is consistent with the focal depth (~95 μm) of the laser beam. The maximum EF observed is ~10^7.

Silver nanowires deposited on the inner walls of a capillary as SERS substrate has been reported[12] earlier involved a multi-step procedure for the synthesis followed by a flow protocol for assembling them inside the capillary, the latter step requiring relatively large amounts of silver nanowires. The present study illustrates the feasibility of fabricating cheap, easily deployable and disposable SERS substrates based on *in situ* generated polymer-metal nanocomposites, and a simple and convenient approach to the detection of extremely small amounts of analytes using them.

4.5 Conclusions

Polymer-metal nanocomposite thin films formed through our *in situ* generation protocol have been used in a wide range of applications as demonstrated in earlier studies in our laboratory, and in the previous chapters. The study presented in this chapter demonstrates the utility of these easily fabricated materials as cheap and convenient SERS substrates for a highly sensitive detection of molecules. A new Ag-polymer nanocomposite thin film is developed by photoirradiation based *in situ* fabrication of the nanoparticles inside the PVVV film. Raman scattering experiments with analyte molecules such as 4-aminothiophenol and Rhodamine 6G indicate that these nanocomposite thin films can routinely produce SERS with EF ~10^7 and LOD in the picomols range. The unique utility of these materials as SERS substrates is demonstrated by fabricating glass capillaries with their inner walls coated with the nanocomposite thin film that can be used to pick up tiny volumes of highly dilute analyte solutions and directly record their Raman spectra. The ease of fabrication and

use, coupled with the low cost of the materials and processes involved, make these SERS substrates of considerable value in analytical applications.

References

1. Sharma, B.; Frontiera, R. R.; Henry, A.; Ringe, E.; Van Duyne, R. P. *Mater. Today* **2012**, *15*, 16.
2. Graham, D. *Angew. Chem. Int. Ed.* **2010**, *49*, 9325.
3. Lombardi, J. R.; Birke, R. L. *Acc. Chem. Res.* **2009**, *42*, 734.
4. Fan, M.; Andrade, G. F. S.; Brolo, A. G. *Anal. Chim. Acta* **2011**, *693*, 7.
5. Jiang, Z. Y.; Jiang, X. X.; Su, S.; Wei, X. P.; Lee, S. T.; He, Y. *Appl. Phys. Lett.* **2012**, *100*, 203104.
6. Freeman, R. G.; Grabar, K. C.; Allison, K. J.; Bright, R. M.; Davis, J. A.; Guthrie, A. P.; Hommer, M. B.; Jackson, M. A.; Smith, P. C.; et al *Science* **1995**, *267*, 1629.
7. Guo, H.; Jiang, D.; Li, H.; Xu, S.; Xu, W. *J. Phys. Chem. C* **2013**, *117*, 564.
8. Lu, Y.; Liu, G. L.; Lee, L. P. *Nano Lett.* **2005**, *5*, 5.
9. Qian, K.; Liu, H.; Yang, L.; Liu, J. *Nanoscale* **2012**, *4*, 6449.
10. Xu, W.; Ling, X.; Xiao, J.; Dresselhaus, M. S.; Kong, J.; Xu, H.; Liu, Z.; Zhang, J. *Proc. Nat. Acad. Sci. USA* **2012**, *109*, 9281.
11. Cui, Y.; Wang, T.; Zhou, D.; Cheng, Q.; Zhang, C.; Sun, S.; Liu, W.; Han, B. *J. Phys. Chem. C* **2012**, *116*, 17698.
12. Jian-Wei, L.; Jin-Long, W.; Wei-Ran, H.; Le, Y.; Xi-Feng, R.; Wu-Cheng, W.; Shu-Hong, Y. *Sci. Rep.* **2012**, *2*, 987.
13. Schmidt, M. S.; Huebner, J.; Boisen, A. *Adv. Mater.* **2012**, *24*, OP11.
14. An, Q.; Zhang, P.; Li, J.; Ma, W.; Guo, J.; Hu, J.; Wang, C. *Nanoscale* **2012**, *4*, 5210.
15. Kodiyath, R.; Papadopoulos, T. A.; Wang, J.; Combs, Z. A.; Li, H.; Brown, R. J. C.; Bredas, J.; Tsukruk, V. V. *J. Phys. Chem. C* **2012**, *116*, 13917.
16. Cheng, M.; Tsai, B.; Yang, J. *Anal. Chim. Acta* **2011**, *708*, 89.

17. Yu, W.; White, I. M. *Anal. Chem.* **2010**, *82*, 9626.

18. Gutes, A.; Carraro, C.; Maboudian, R. *J. Am. Chem. Soc.* **2010**, *132*, 1476.

19. Im, H.; Bantz, K. C.; Lindquist, N. C.; Haynes, C. L.; Oh, S. *Nano Lett.* **2010**, *10*, 2231.

20. Oh, Y.; Jeong, K. *Adv. Mater.* **2012**, *24*, 2234.

21. Wu, H.; Choi, C. J.; Cunningham, B. T. *Small* **2012**, *8*, 2878.

22. Siddhanta, S.; Thakur, V.; Narayana, C.; Shivaprasad, S. M. *ACS Appl. Mater. Interfaces* **2012**, *4*, 5807.

23. Kahraman, M.; Cakmakyapan, S.; Ozbay, E.; Culha, M. *Ann. Phys.* **2012**, *524*, 663.

24. Yang, L.; Liu, H.; Wang, J.; Zhou, F.; Tian, Z.; Liu, J. *Chem. Commun.* **2011**, *47*, 3583.

25. Yu, D.; Lin, W.; Lin, C; Chang, L.; Yang, M. *Mater. Chem. Phys.* **2007**, *101*, 93.

26. Karabicak, S.; Kaya, M.; Vo-Dinh, T.; Volkan, M. *J. Nanosci. Nanotech.* **2008**, *8*, 955.

27. He, D.; Hu, B.; Yao, Q.; Wang, K.; Yu, Sh. *ACS Nano* **2009**, *3*, 3993.

28. Porel, S.; Singh, S.; Harsha, S. S.; Rao, D. N.; Radhakrishnan, T. P. *Chem. Mater.* **2005**, *17*, 9.

29. Ramesh, G. V.; Porel, S.; Radhakrishnan, T. P. *Chem. Soc. Rev.* **2009**, *38*, 2646.

30. Porel, S.; Hebalkar, N.; Sreedhar, B.; Radhakrishnan, T. P. *Adv. Func. Mater.* **2007**, *17*, 2550.

31. Ramesh, G. V.; Sreedhar, B.; Radhakrishnan, T. P. *Phys. Chem. Chem. Phys.* **2009**, *11*, 10059.

32. Porel, S.; Venkatram, N.; Rao, D. N.; Radhakrishnan, T. P. *J. App. Phys.* **2007**, *102*, 033107.

33. Porel, S.; Ramakrishna, D.; Hariprasad, E.; Dutta Gupta, A.; Radhakrishnan, T. P. *Curr. Sci.* **2011**, *101*, 927.

34. Ramesh, G. V.; Radhakrishnan, T. P. *ACS Appl. Mater. Interfaces* **2011**, *3*, 988.

35. Hariprasad, E.; Radhakrishnan, T. P. *Chem. Eur. J.* **2010**, *16*, 14378.

36. Hariprasad, E.; Radhakrishnan, T. P. *ACS Catal.* **2012**, *2*, 1179.

37. Huang, Y.; Wu, D.; Zhu, H.; Zhao, L.; Liu, G.; Ren, B.; Tian, Z. *Phys. Chem. Chem. Phys.* **2012**, *14*, 8485.

38. Choi, H.; Shon, H. K.; Yu, H.; Lee, T. G.; Kim, Z. H. *J. Phys. Chem. Lett.* **2013**, *4*, 1079.

39. Osawa, M.; Matsuda, N.; Yoshii, K.; Uchida, I. *J. Phys. Chem.* **1994**, *98*, 12702.

40. Le Ru, E. C.; Blackie, E.; Meyer, M.; Etchegoin, P. G. *J. Phys. Chem. C* **2007**, *111*, 13794.

41. Lin, X-M.; Cui, Y.; Xu, Y-H.; Ren, B.; Tian, Z-Q. *Anal. Bioanal. Chem.* **2009**, *394*, 1729.

42. El-Safty, S. A.; Ismail, A. A.; Matsunaga, H.; Nanjo, H.; Mizukami, F. *J. Phys. Chem. C* **2008**, *112*, 4825.

43. Christian, G. D. *Analytical Chemistry*, 6th ed.; John Wiley & Sons Inc.: New York, **2003**.

CHAPTER 5

Overview of the Present Work, New Directions and Future Prospects

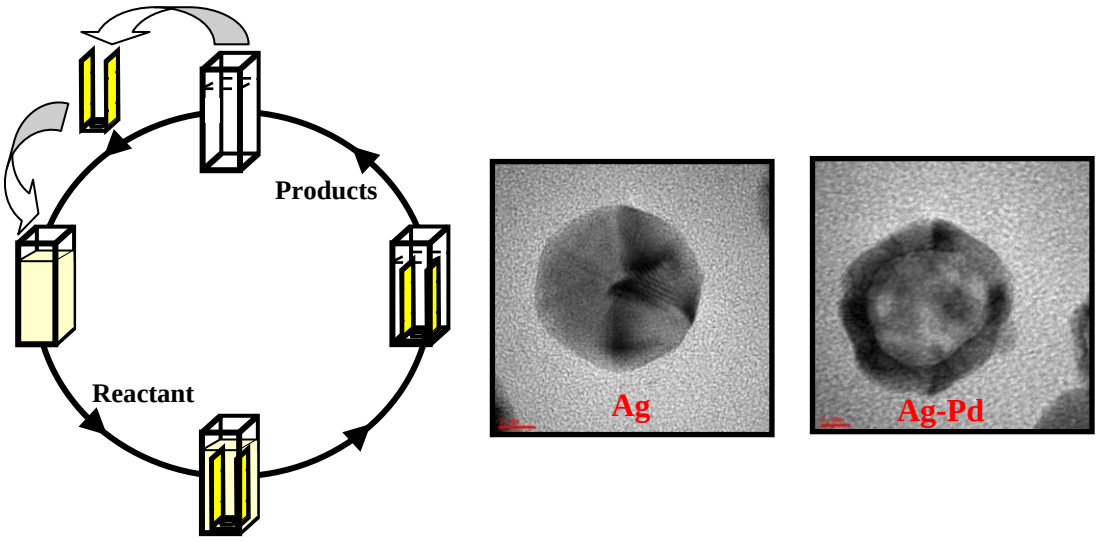

Overview of the development of new fabrication methods and application of polymer-metal nanocomposite thin films presented in this thesis and new directions for further work in this area.

5.1 Overview of the Present Work

Design and development of efficient fabrication protocols, exploration of novel functions and demonstration of new applications are contemporary issues in the research on nanomaterials. Even though there are innumerable reports on each of these aspects, considerable interest and extensive activity continues because of the uniqueness of these materials and the promise they hold for future technologies. Thin films and coatings are of special interest from an application perspective. Towards this end, *in situ* fabrication protocols are very popular, since they provide significant advantages over other methods in terms of simplicity, ease of implementation and the production of a homogeneous distribution of the nanoparticles. The *in situ* methodology developed in our laboratory, for the fabrication of polymer-metal nanocomposite thin films, is a simple, convenient and environmentally benign approach that enables control of size, shape and distribution of the particles.[1,2] We have now made relevant modifications in the fabrication protocol for special and unique situations and explored novel applications of these *in situ* synthesized polymer-metal nanocomposite thin films in the important area of catalysis and the emerging analytical technique based on surface enhanced Raman scattering (SERS).

Earlier work in our laboratory has demonstrated the appreciable optical limiting capability,[3,4] effective antibacterial property,[5] efficient microwave absorption[6] and sensitive detection of mercury[7] using the *in situ* fabricated polymer-metal nanocomposite thin films, and their unique advantages in these applications. In this thesis we have explored further, new directions for the applications of these thin films in chemical catalysis and SERS. Low cost, ease of fabrication, amenability to large area coating and chemical/thermal stability of these films are significant advantages and highly relevant from the point of view of developing novel materials and application protocols.

Poly(vinyl alcohol) (PVA) is an optimal choice for the polymer component in the *in situ* fabrication of the polymer-metal nanocomposite thin films. The hydroxy groups are used as the reducing agent in the formation of noble metal nanoparticles and

their stabilization. The fabrication is made convenient because of the solubility in water and the application is facilitated by the fact that it gets cross-linked and hence insoluble during the *in situ* fabrication process. The hydrogel characteristic of PVA is also uniquely important. We have used PVA extensively in the various studies described in this thesis. We have explored further, the utility of other polymers, especially poly(vinyl butyral - *co* - vinyl alcohol - *co* - vinyl acetate) (PVVV). The latter polymer, together with the novel approach of photoirradiation (in place of thermal annealing) for the *in situ* generation of nanoparticles, yielded optimal substrates for the SERS application. We have developed a novel multilayer design for the catalyst film to facilitate reversible swelling in the reaction medium, ensuring the easy passage of reactants to the catalyst embedded in the polymer matrix without leaching or degradation of the catalyst. The efficiency of polymer-metal nanocomposite thin film as a catalyst is demonstrated by using the well-studied and industrially important reactions, the reduction of 4-nitrophenol by sodium borohydride and carbon-carbon coupling. The multilayer film, M–PVA/PVA/M–PVA (M = Ag, Pd) is shown to provide robust free-standing films with excellent catalytic efficiency. We have demonstrated the switching on or off of the reaction by simple insertion/removal of the catalyst film. This experiment provides a vivid illustration of a novel concept in catalyst design; we have named it a 'dip catalyst'. The crucial significance of the 'dip catalyst' is the ease and facility of reuse, a fundamental aspect of catalysis. In addition, we realize the critical advantage of convenient monitoring of the catalyst between the reuses. The M‑PVA multilayer film was examined at regular intervals through the reuse cycles by microscopy and spectroscopy which provided very useful insight into the status of the catalyst nanoparticles. The crucial role of the polymer matrix in channeling the reactants to the nanoparticles and the products away could also be modeled using a variety of experiments. The cheap materials and simple methods used in the catalyst fabrication, in combination with the large TON achieved through a large number (typically ~30) of reuses, establish the cost effectiveness of the 'dip catalyst' approach. Embedding the metal nanoparticles inside the polymer film effectively precludes

aggregation, and enables long-term storage of these nanocomposite films, an aspect of considerable practical relevance.

One of the unique advantages of the *in situ* nanoparticle generation protocol developed in our laboratory is that, it enables the facile fabrication of the nanocomposite thin film as a coating on curved and irregular surfaces. We have explored the use of polymer-silver nanocomposite thin film coated on flat substrates and the inner walls of capillaries as SERS substrates. Analyte molecules such as 4-aminothiophenol and Rhodamine 6G were used in the Raman scattering experiments. In the case of Ag-PVA film, we were able to achieve enhancement factors of ~10^6, through optimization of the metal nanoparticle concentration and the thin film characteristics. Ag-PVVV films with larger surface roughness were found to be capable of providing SERS with enhancement factor of ~10^7. The unique utility of these nanocomposite thin films as SERS substrates was demonstrated by fabricating glass capillaries with their inner walls coated with the film having *in situ* generated nanoparticles. These capillaries were used to pick up tiny volumes of highly dilute analyte solutions and record their Raman spectra. We could record clear Raman signals with typically ~5 pmol of the probe molecules. The ease of fabrication and use, coupled with the low cost of the materials and processes involved, make these SERS substrates of considerable value in analytical applications.

We believe that the fabrication, characterization and applications of *in situ* fabricated polymer-metal nanocomposite thin films presented in this thesis represent a new direction in the field of nanocomposite materials. Further optimization of the methodologies we have developed, is likely to improve the desired features and functions of these novel materials.

5.2 New Directions of Research

Wide range of polymers and metal precursors are available for the fabrication of different nanostructure-embedded polymer thin films, using the general strategies we

have developed. The *in situ* method can be extended to fabricate polymer thin films with nanoparticles of other metals such as ruthenium and platinum embedded within. The reduction potentials of these materials are appropriate for fabrication with polymers such as PVA; this is confirmed by some preliminary experiments that we have carried out. The kinetics of formation and the dependence of particle size, shape and distribution on the nature of precursor and polymer and their compositions need to be investigated. Fabrication of metal nanoparticles in polymer films described in this thesis involved only thermal treatment and photoirradiation. Alternate methods that use microwave heating, electron beam irradiation/electron beam lithography and focused ion beams to generate metal nanoparticles *in situ* inside the polymer films need to be explored. The reduction process can have significant effect on the particle size and shape distribution through the modification of the nucleation and growth mechanism.

Another interesting avenue to investigate is the synthesis of bimetallic nanostructures inside polymer thin films. Explorations in this direction have been initiated recently in our laboratory, through the fabrication of silver-palladium bimetallic nanoparticles.[8] The general protocol involved a Galvanic displacement process carried out under ambient conditions, on the *in situ* generated nanoparticles of the first metal acting as sacrificial template. This opens up a wide range of possibilities in terms of the metal combinations, their composition and structures. These bimetallic nanoparticles have higher application potential over monometallic nanocomposite thin films as the amount of the precious metal component can be considerably reduced, and a wider range of nanostructures can be explored. The general protocol can be easily extended to multimetallic systems.

Another important aspect to be explored is the organization of nanoparticles and nanostructures inside the polymer films. Simple approaches would involve the use of chemical linkers and external constraints such as electrical and magnetic fields. Preliminary studies in our laboratory suggest that mechanical force employed on the film causes the ordering of the nanoparticles in the direction of force employed; systematic investigations are in progress. Electrical and mechanical properties of these

polymer-metal nanocomposite thin films remain to be investigated in detail. Initial observations suggest that the conductivity of these films depends on the metal nanoparticle loading and thickness of the film. Use of conjugated polymers as the matrix and the *in situ* generation of nanoparticles to form the nanocomposite thin films need careful investigations. The optical and electronic properties of these thin films are likely to be fascinating.

Catalytic applications in other industrially important reactions remain to be explored. New dip catalysts based on a range of metals and semiconducting nanostructures and their activity in photocatalytic applications is under investigation. Asymmetric catalysts can be developed by including chiral auxiliaries in the polymer-metal nanocomposite thin film or by generating chiral nanostructures. The polymer-metal nanocomposites thin films can be developed as coatings for catalytic flow reactors. Test experiments show great promise. Development of chemical and biological sensors based on various polymer-metal combinations would be interesting. Polymer-metal and polymer-metal oxide nanocomposite thin films are likely to have immense potential in areas such as sensing, catalysis and photovoltaics.

The development and applications of polymer-metal nanocomposite thin films presented in this thesis and the exploration of the proposed ideas and new directions outlined above will open up new avenues for promising and exciting research in future.

References

1. Porel, S.; Singh, S.; Radhakrishnan, T. P. *Chem. Commun.* **2005**, 2387.
2. Porel, S.; Hebalkar, N.; Sreedhar, B.; Radhakrishnan, T. P. *Adv. Funct. Mater.* **2007**, *17*, 2550.
3. Porel, S.; Singh, S.; Harsha, S. S.; Rao, D. N.; Radhakrishnan, T. P. *Chem. Mater.* **2005**, *17*, 9.
4. Porel, S.; Venkatram, N.; Rao, D. N.; Radhakrishnan, T. P. *J. Appl. Phys.* **2007**, *102*, 033107.
5. Porel, S.; Ramakrishna, D.; Hariprasad, E.; Gupta, A. D.; Radhakrishnan, T. P. *Curr. Sci.* **2011**, *101*, 927.
6. Ramesh, G. V.; Sudheendran, K.; Raju, K. C. J.; Sreedhar, B.; Radhakrishnan, T. P. *J. Nanosci. Nanotechnol.* **2009**, *9*, 261.
7. Ramesh, G. V.; Radhakrishnan, T. P. *ACS Appl. Mater. Interfaces* **2011**, *3*, 988.
8. Rao, V. K.; Radhakrishnan, T. P. *J. Mater. Chem. A* **2013,** *1*, 13612.

Appendix

APPENDIX

Materials

Silver nitrate	:	Aldrich, 99+%
Potassium tetrachloropalladate	:	Aldrich, 99.99%
4-nitrophenol	:	Loba chemie, 98%
Sodium borohydride	:	Merck, ≥ 95%
Iodobenzene	:	Aldrich, 98%
Phenylboronic acid	:	Aldrich, 95%
4-aminothiophenol	:	Aldrich, 97%
Rhodamine-6g	:	Loba
PS	:	Aldrich, M_w = 280 kDa
PVA	:	Aldrich, M_w = 87-146 kDa, % hydrolysis = 99+
PVVV	:	Aldrich, M_w = 70-100 kDa
PSAA	:	Aldrich, average M_w = 2200
Nitric acid	:	Merck, ≥69%
Ultrapure water	:	Millipore MilliQ (resistivity = 18.2 MΩ cm)

Instrumentation

Spin-coating

Laurell Technologies Corporation Model WS-400B-6NPP/LITE/8K or WS-650HZ-23NPP/LITE photoresist spinner was used for the fabrication of thin polymer films.

Film thickness measurement

Thickness of the films was measured using an Ambios Technology XP-1 profilometer.

Absorption spectroscopy

Absorption spectra were recorded on a Cary 100 UV-Visible spectrophotometer. The spectra recorded in diffuse reflectance mode using the DRA-CA-30I accessory were converted to absorption spectra using the Kubelka-Munk function. Measurements for kinetic studies involving temperature variation were carried out on a Cary 100 Bio UV-Visible spectrophotometer.

Atomic force microscopy

AFM images were recorded on a Solver Pro M (NT-MDT) atomic force microscope in contact and semi-contact modes. A tip having a force constant of 12 N/m was used in semi-contact mode. Images were analyzed using the NOVA (version 1.0.26) software supplied by the microscope manufacturer.

Scanning electron microscopy

Zeiss Ultra 55 FESEM was used. Energy dispersive X-ray spectra were recorded using an Oxford INCA X-Act EDS System. The samples were coated with gold or gold-palladium.

Transmission electron microscopy

TEM images were recorded on a FEI TECNAI G^2 S-Twin 200 kV TEM at an accelerating voltage of 200 kV.

Ultramicrotome

A Leica ultramicrotome was used. Cross section samples were prepared by fixing the free standing polymer-metal nanocomposite thin film in Araldite resin and cutting into 50 nm thin sections.

Inductively coupled plasma-optical emission spectrometer

A Varian Model Liberty Series ICP-OES was used. Samples dissolved in 69% aqueous nitric acid and diluted to required concentrations were used.

Gas chromatograph-mass spectrometer

GCMS analysis was carried out on Shimadzu model QP2010 Gas chromatograph-Mass spectrometer.

Photoreactor

Scientific Aids & Instruments Corporation model MLR-8 was used to photoirradiate the polymer thin film.

Confocal Raman microscope

WITec model Alpha300 R equipped with an AFM was used the Raman spectral studies. The AFM with a 100 µm scanner was used for some of the imaging work. Its optical microscope with 10x objective was used for photographing the thin film samples.

Publications and Presentations

PUBLICATIONS

1. **Hariprasad, E.;** Radhakrishnan, T. P. *Chem. Eur. J.* **2010**, *16*, 14378.
   A Highly Efficient and Extensively Reusable "Dip Catalyst" Based on a Silver Nanoparticle-Embedded Polymer Thin Film.

2. Porel, S.; Ramakrishna, D.; **Hariprasad, E.;** Gupta, A. D.; Radhakrishnan, T. P. *Curr. Sci.* **2011**, *101*, 927.
   Polymer Thin Film With *In Situ* Synthesized Silver Nanoparticles as a Potent Reusable Bactericide.

3. **Hariprasad, E.;** Radhakrishnan, T. P. *ACS Catal.* **2012,** *2*, 1179.
   Palladium Nanoparticle-Embedded Polymer Thin Film "Dip Catalyst" for Suzuki−Miyaura Reaction.

4. **Hariprasad, E.;** Radhakrishnan, T. P. Nanocompsites: In Situ Synthesis of Polymer-Embedded Nanostructures. Eds. G. Carotenuto, L. Nicolais; *John Wiley & Sons* **2013**, (in press).
   Chemistry Inside a Polymer Thin Film: In Situ Soft Chemical Synthesis of Metal Nanoparticles and Applications.

5. **Hariprasad, E.;** Radhakrishnan, T. P. *Langmuir*, (DOI: 10.1021/la402594j)
   In situ Fabricated Polymer-Silver Nanocomposite Thin Film as an Inexpensive and Efficient Substrate for Surface Enhanced Raman Scattering.

PRESENTATIONS

1. Oral presentation: National Review and Coordination Meeting on Nanoscience and Nanotechnology, S. N. Bose National Centre for Basic Sciences, Kolkata, India, March 12-14, **2009**.
   Metal Nanoparticles Formed *In Situ* inside Polymer Film: Fabrication and Application in Catalysis.

2. Oral presentation: 5th International workshop on Polymer/Metal nanocomposites, University of Bari, Bari, Italy, September 20-22, **2011**.
   Palladium Nanoparticles-Embedded Polymer Films: An Efficient and Reusable 'Dip Catalyst' for Suzuki Coupling Reaction.

3. Poster presentation: Modern Trends in Inorganic Chemistry (MTIC-XIV), University of Hyderabad, Hyderabad, India, December 10-13, **2011**.
   Metal Nanoparticles-Embedded Polymer Films: An Efficient and Reusable 'Dip Catalyst'.

4. Poster presentation: International Conference on Nanoscience and Technology, Hyderabad, India, January 20-23, **2012**.
   Metal Nanoparticle-Embedded Polymer Thin Film: An Efficient and Reusable 'Dip Catalyst'.

5. Oral presentation: Chemfest-2012, University of Hyderabad, Hyderabad, India, February 24-25, **2012**.
   Metal Nanoparticle-Embedded Polymer Film: An Efficient and Reusable 'Dip Catalyst'. (**selected as best presentation**)